

A Characterization of Scale Invariant Responses in Enzymatic Networks

Maja Skataric¹, Eduardo D. Sontag^{2*}

1 Department of Electrical Engineering, Rutgers University, Piscataway, New Jersey, United States of America, **2** Department of Mathematics, Rutgers University, Piscataway, New Jersey, United States of America

Abstract

An ubiquitous property of biological sensory systems is adaptation: a step increase in stimulus triggers an initial change in a biochemical or physiological response, followed by a more gradual relaxation toward a basal, pre-stimulus level. Adaptation helps maintain essential variables within acceptable bounds and allows organisms to readjust themselves to an optimum and non-saturating sensitivity range when faced with a prolonged change in their environment. Recently, it was shown theoretically and experimentally that many adapting systems, both at the organism and single-cell level, enjoy a remarkable additional feature: scale invariance, meaning that the initial, transient behavior remains (approximately) the same even when the background signal level is scaled. In this work, we set out to investigate under what conditions a broadly used model of biochemical enzymatic networks will exhibit scale-invariant behavior. An exhaustive computational study led us to discover a new property of surprising simplicity and generality, uniform linearizations with fast output (ULFO), whose validity we show is both *necessary and sufficient* for scale invariance of three-node enzymatic networks (and sufficient for any number of nodes). Based on this study, we go on to develop a mathematical explanation of how ULFO results in scale invariance. Our work provides a surprisingly consistent, simple, and general framework for understanding this phenomenon, and results in concrete experimental predictions.

Citation: Skataric M, Sontag ED (2012) A Characterization of Scale Invariant Responses in Enzymatic Networks. *PLoS Comput Biol* 8(11): e1002748. doi:10.1371/journal.pcbi.1002748

Editor: Mark S. Alber, University of Notre Dame, United States of America

Received: February 19, 2012; **Accepted:** August 13, 2012; **Published:** November 1, 2012

Copyright: © 2012 Skataric, Sontag. This is an open-access article distributed under the terms of the Creative Commons Attribution License, which permits unrestricted use, distribution, and reproduction in any medium, provided the original author and source are credited.

Funding: This work was funded by AFOSR FA9550-11-1-0247, NIH 1R01GM100473, and NIH 1R01GM086881. The funders had no role in study design, data collection and analysis, decision to publish, or preparation of the manuscript.

Competing Interests: The authors have declared that no competing interests exist.

* E-mail: sontag@math.rutgers.edu

Introduction

The survival of organisms depends critically upon their capacity to formulate appropriate responses to sensed chemical and physical environmental cues. These responses manifest themselves at multiple levels, from human sight, hearing, taste, touch, and smell, to individual cells in which signal transduction and gene regulatory networks mediate the processing of measured external chemical concentrations and physical conditions, such as ligand concentrations or stresses, eventually leading to regulatory changes in metabolism and gene expression.

An ubiquitous property of biological sensory systems at all levels is that of *adaptation*: a step increase in stimulus triggers an initial, and often rapid, change in a biochemical or physiological response, followed by a more gradual relaxation toward a basal, pre-stimulus level [1]. Adaptation plays a role in ensuring that essential variables stay within acceptable bounds, and it also allows organisms to readjust themselves to an optimum and non-saturating sensitivity range even when faced with a prolonged change in their operating environment, thus making them capable of detecting changes in signals while ignoring background information.

Physiological examples of adaptation in higher organisms include phenomena such as the control of the amount of light entering eyes through the contraction and relaxation of the pupil by the nervous system, which brings intensities of illumination within the retinal working range, or the regulation of key metabolites in the

face of environmental variations [2]. At the single-cell level, one of the best understood examples of adaptation is exhibited by the *E. coli* chemotaxis sensory system, which responds to gradients of nutrient and ignores constant (and thus uninformative) concentrations [3,4]. The term “exact” or “perfect” adaptation is employed to describe processes which, after a transient, return with very high accuracy to the same input-independent level. In practice, however, an approximate adaptation property is usually adequate for proper physiological response [5].

By definition, neither the concepts of perfect nor approximate adaptation address the characteristics of the transient signaling which occurs prior to a return to steady state. The amplitude and other characteristics of transient behaviors, however, are physiologically relevant. In this more general context, a remarkable phenomenon exhibited by several human and animal sensory systems is *scale invariance* or logarithmic sensing [2,6,7]. This means that responses are functions of ratios (in contrast to actual magnitudes), of a stimulus relative to the background. There is evidence for this phenomenon at an intracellular level as well. It appears in bacterial chemotaxis [8,9], in the sensitivity of *S. cerevisiae* to fractional rather than absolute pheromone gradients [10], and in two mammalian signaling systems: transcriptional as well as embryonic phenotype responses to β -catenin levels in Wnt signaling pathways [11], and nuclear ERK localization in response to EGF signaling [12]. Scale invariance allows systems to react to inputs ranging over several orders of magnitude, and is speculated

Author Summary

Sensory systems often adapt, meaning that certain measured variables return to their basal levels after a transient response to a stimulus. An additional property that many adapting systems enjoy is that of scale invariance: the transient response remains the same when a stimulus is scaled. This work presents a mathematical study of biochemical enzymatic networks that exhibit scale-invariant behavior.

to help make behaviors robust to external noise as well as to stochastic variations in total expressed concentrations of signaling proteins [13].

Mathematically, scale invariance is defined by the following property of transient behaviors [13]: if a stimulus changes from a background level u_0 to a new level u , then the entire time response of the system is the same as if the stimulus had changed, instead, from a background level pu_0 to pu . In other words, only the ratio (or “fold-change”) $pu/pu_0 = u/u_0$ is relevant to the response; the “scale” p is irrelevant. For this reason, the term “fold change detection” is interchangeably used instead of scale-invariance. Scale invariance implies adaptation, but not every adaptive system is scale invariant [13]. A mathematical analysis of scale-invariance was initiated in [13,14]. Predictions regarding scale-invariance of *E. coli* chemotaxis were subsequently experimentally verified [15]. While adaptation can be often understood in terms of control-theoretic tools based on linearizations [16,17,18,19,20], scale invariance is a genuinely **nonlinear** property; as a matter of fact, a linear system can never display scale-invariance, since the response to an input scaled by p will also be scaled by this same factor p .

In this work, we focus on enzymatic signal transduction systems, which involve the activation/deactivation cycles that typically mediate transmission of external signals to transcription factors and other effectors. Networks involving such enzymatic cycles are involved in signal transduction networks from bacterial two-component systems and phosphorelays [21,22] to actin treadmilling [23], guanosine triphosphatase cycles [24], glucose mobilization [25], metabolic control [26], cell division and apoptosis [27], cell-cycle checkpoint control [28], and the eukaryotic Mitogen-Activated Protein Kinase (MAPK) cascades which mediate growth factor inputs and determine proliferation, differentiation, and apoptosis [29,30,31,32,33].

Given the biological importance of these processes, and the already observed scale-invariance in some of these pathways [11,12], we pose here the following question: which enzymatic networks do not merely adapt, but also display scale invariance? In order to answer this question, we performed an exhaustive computational study of all 3-node networks, finely sampled in parameter space. Only about 0.01% of these networks are capable of (approximate) adaptation. Testing which of these adapting networks also display scale-invariant behavior, we found that only about 0.15% of them did. Once that this small subclass was identified, we turned to the problem of determining what network characteristics would explain the results of these numerical experiments. We discovered a surprisingly simple and general property, which we call uniform linearizations with fast output (ULFO), that is displayed by all the networks in this subclass, and here we provide a theoretical framework that explains conceptually why this property is both *necessary and sufficient* for scale invariance of such three-node enzymatic networks. The condition is also sufficient for networks with larger numbers of nodes. As an application (with more than three nodes), we consider a recently

published model [34] of an eukaryotic enzymatic system, specifically the pathway involved in the social amoeba *Dictyostelium discoideum*'s chemotactic response to cAMP, and show that our conditions are satisfied in appropriate ranges of cAMP input.

Characterizations of this sort allow one to understand which networks are robust to scale uncertainty, and constitute a powerful tool in allowing one to discard putative mechanisms that are not consistent with experimentally observed scale-invariant behaviors [14,15].

Results

Three-node enzymatic networks

We consider networks consisting of three types of enzymes, denoted respectively as A , B , and C . Each of these enzymes can be in one of two states, active or inactive. The fractional concentration of active enzyme A is represented by a variable $x_A = x_A(t)$, so $\tilde{x}_A = 1 - x_A$ is the fraction of inactive enzyme A . Similar notations are used for B and C . Only enzyme A is directly activated by an external input signal, and the response of the network is reported by the fraction of active C . Enzyme B acts as an auxiliary element. Each enzyme may potentially act upon each other through activation (positive regulation), deactivation (negative regulation), or not at all. If a given enzyme is not deactivated by any of the remaining two, we assume that it is constitutively deactivated by a specific enzyme; similarly, if a given enzyme is not activated by any other, there is a constitutively activating enzyme for it. One represents networks by 3-node directed graphs, with nodes labeled A , B , C , and with edges between two nodes labeled $+$ and $-$ (or “ \rightarrow ” and “ \leftarrow ”) to denote positive or negative regulation respectively; no edge is drawn if there is no action. There are $3^2 = 9$ potential directed edges among the three nodes (A to A , A to B , etc.), each of whose labels may be $+$, $-$, or “none” if there is no edge. This gives a total of $3^9 = 19,683$ possible graphs. One calls each of these possible graphs a *topology*. Discarding the 3,645 topologies that have no direct or indirect links from the input to the output, there remain 16,038 topologies.

The restriction to three-node networks is made for both practical and biological reasons. As argued in several papers that use a similar approach [20,35,36], even though adaptation (as well as scale-invariant) behaviors can, and do, arise in larger networks, the coarse-graining involved in restricting the computational search to minimal networks leads to a tractable search problem, and allows also one to intuitively understand the basic principles. The same motifs are observed in larger networks, in which several nodes may represent a single node in the three-node networks that we study. In fact, the necessary property that we discover for three-node networks turns out to be sufficient, as well, for networks with arbitrary numbers of nodes. The discussion section elaborates further on this point, and an illustration of this reduction is given by an example discussed below of a 6-variable model published in [34] to represent the adaptation kinetics of a chemotaxis signaling pathway in *Dictyostelium discoideum*.

Specification of a dynamic model

We quantify the effects of each existing regulatory interaction by a Michaelis-Menten term and write a three-variable ordinary differential equation (ODE) that describes the time evolution of $x_A(t)$, $x_B(t)$, and $x_C(t)$:

$$\dot{x}_A = \sum_i \frac{k_{V_i A} v_i \tilde{x}_A}{\tilde{x}_A + K_{V_i A}} - \sum_i \frac{k_{W_i A} w_i x_A}{x_A + K_{W_i A}} \quad (1a)$$

$$\dot{x}_B = \sum_i \frac{k_{V_i B} v_i \tilde{x}_B}{\tilde{x}_B + K_{V_i B}} - \sum_i \frac{k_{W_i B} w_i x_B}{x_B + K_{W_i B}} \quad (1b)$$

$$\dot{x}_C = \sum_i \frac{k_{V_i C} v_i \tilde{x}_C}{\tilde{x}_C + K_{V_i C}} - \sum_i \frac{k_{W_i C} w_i x_C}{x_C + K_{W_i C}} \quad (1c)$$

The K 's denote Michaelis-Menten, and the k 's catalytic, rate constants associated to each regulatory interaction. All the summations range over $i = 1, \dots, 6$. Each “ V_i ” represents one of A, B, C, E_A, E_B, E_C , the activating enzymes in the respective equations, and each “ W_i ” one of A, B, C, F_A, F_B, F_C , the deactivating enzymes; E and F are the constitutively activating and deactivation enzymes, buffered at constant concentrations. (Lower-case variables $v_i, w_i = x_A, \dots, x_{F_C}$ denote active fractions) As an exception, the equation for node A does not include an E_A term, but instead includes a term $k_{UA}u \frac{\tilde{x}_A}{\tilde{x}_A + K_{UA}}$ that models activation of A by an external input whose strength at time t is given by $u = u(t)$ and whose values $u(t)$ stay within a range $[\underline{u}, \bar{u}]$. No enzyme appears both an activator and as a deactivator of any given component, that is, $k_{X_i A} k_{Y_i A} = 0$, $k_{X_i B} k_{Y_i B} = 0$, and $k_{X_i C} k_{Y_i C} = 0$, and constitutive enzymes are included only if the reaction would be otherwise irreversible. For example, the topology shown in Fig. 1 is described by the following set of ODE's:

$$\dot{x}_A = \frac{k_{UA}u \tilde{x}_A}{\tilde{x}_A + K_{UA}} - \frac{k_{BA}x_B x_A}{x_A + K_{BA}} - \frac{k_{CA}x_C x_A}{x_A + K_{CA}} \quad (2a)$$

$$\dot{x}_B = \frac{k_{AB}x_A \tilde{x}_B}{\tilde{x}_B + K_{AB}} - \frac{k_{FB}x_F x_B}{x_B + K_{FB}} \quad (2b)$$

$$\dot{x}_C = \frac{k_{AC}x_A \tilde{x}_C}{\tilde{x}_C + K_{AC}} - \frac{k_{BC}x_B x_C}{x_C + K_{BC}} - \frac{k_{CC}x_C x_C}{x_C + K_{CC}} \quad (2c)$$

The term *circuit* is used to refer to a given topology together with a particular choice of the K and k parameters. The three-node model in Eq.1 was employed by Ma et al. [20], in order to classify the minimal enzymatic circuits that adapt. (With the model in [20] that we adopted, there is no direct connection from the input to the output node, and two-node networks are not sufficient for adaptation, while larger adapting networks contain these three-node networks [20]. If one allows direct connections from input to outputs, then two-node networks are able to display adaptation.) The same paradigm has since been used to investigate other network characteristics as well [35,36].

Adaptation

Following [37], we define adaptation behavior in terms of two functional metrics. The first metric quantifies the following effect: if we start at steady state, and then step the input at time $t = 0$ from a value u_0 to a different constant value u_1 , then the system's output, as reported by a response variable $y(t)$ (where $y(t) = x_C(t)$ in Eq.1), should return asymptotically to a value that is close to the original value $y(0)$. The relative difference in initial and final response $\Delta_y^\infty = |y(+\infty) - y(0)|$ provides a measure of adaptation precision. We say that a system is (approximately) adaptive provided that, for

all inputs in the valid range, $\Delta_y^\infty / \Delta_u < 0.1$, where $\Delta_u = |u_1 - u_0| / |u_0|$ is the relative change in input. In particular, exact or perfect adaptation means that $\Delta_y^\infty = 0$. The 10% error tolerance is natural in applications, and the qualitative conclusions are not changed by picking a smaller cutoff [20]. A second metric relies upon the maximal transient difference in output, normalized by the steady-state output, $\Delta_y^{\max} = \max |y(t) - y(0)| / |y(0)|$. A *signal-detection* property for adaptation [18,38], should be imposed in order to rule out the trivial situation $\Delta_y^{\max} \approx 0$ in which a system's output is independent of the input. To avoid having to pick an arbitrary threshold, in this study we follow the convention in [20] of requiring the *sensitivity* $\Delta_y^{\max} / \Delta_u$ to be greater than one.

Scale invariance

Scale invariance is the property that if a system starts from a steady state that was pre-adapted ($t < 0$) to a certain background level u_0 , and the input is subsequently set to a new level u at $t = 0$, then the entire time response of the system $y_{u_0, u}(t)$ is the same as the response $y_{pu_0, pu}(t)$ that would result if the stimulus had changed, instead, from pu_0 to pu . This property should hold for scale changes $p > 0$ that respect the bounds $\underline{u} \leq u \leq \bar{u}$ on inputs. For example, recent microfluidics and FRET experimental work [15] verified scale-invariance predictions that had been made in [13] for bacterial chemotaxis under the nonmetabolizable attractant α -methylaspartate (MeAsp) as an input. In these experiments, *E. coli* bacteria were pre-adapted to input concentrations and then tested in new nutrient gradients, and it was found experimentally that there were two different ranges of inputs $[\underline{u}_1, \bar{u}_1]$ and $[\underline{u}_2, \bar{u}_2]$ in which scale-invariance holds, the “FCD1” and “FCD2” regimes, respectively. (The term fold-change detection, or FCD, is used to reflect the fact that only the ratio or fold-change $pu/pu_0 = u/u_0$ can be detected by the response $y(t)$.) More generally, the mathematical definition of (perfect) scale invariance [14] imposes the ideal requirement that the same response invariance property is exhibited if $u = u(t)$, $t \geq 0$ is any time-varying input. The experiments in [15] included excitation by certain oscillatory inputs, for example. In practice, however, this property will always break down for high-frequency inputs, since there are limits to the speed of response of biological systems.

Adaptive systems need not be scale-invariant

As an illustration of a (perfectly) adaptive yet not scale-invariant system, consider the following equations:

$$\dot{x}_A = k_1 u - k_2 x_B \quad (3a)$$

$$\dot{x}_B = k_3 x_A - k_4 x_B \quad (3b)$$

$$\dot{x}_C = k_5 x_A - k_6 x_B x_C \quad (3c)$$

which is a limiting case of the system described by Eq.2 when $k_{CA}, k_{CC}, K_{UA}, K_{BA}, K_{AB}, K_{AC} \approx 0$, $k_{BC} = k_6 K_{BC}$, $K_{BC} \gg 1$ (so $-k_{BC} x_B x_C / (x_C + K_{BC}) \approx -k_6 x_B x_C$), and $k_{FB} x_F x_B = k_2 K_{FB}$ and $K_{FB} \gg 1$. This network perfectly adapts, since at steady state the output is $x_C = \bar{x}_C = k_4 k_5 / (k_3 k_6)$, no matter what is the magnitude of the constant input u , and in fact the system returns to steady state after a step change in input u , with $x_C(t) \rightarrow \bar{x}_C$ as $t \rightarrow \infty$ (general stability properties of feedforward circuits shown in [39]). On the other hand, the example in Eq.3 does not display scale invariance. Indeed, consider the solution from an initial state

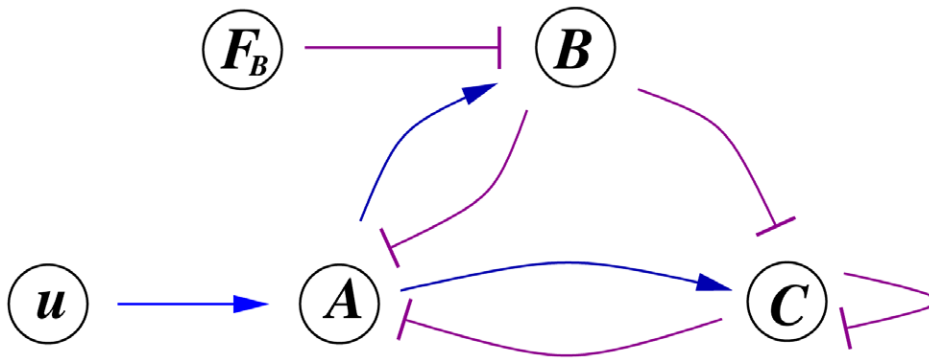


Figure 1. Topology 2293. An example of a topology.
doi:10.1371/journal.pcbi.1002748.g001

pre-adapted to an input level u_0 , that is $x_A(0) = k_1 k_4 u_0 / (k_2 k_3)$, $x_B(0) = k_1 u_0 / k_2$, and $x_C(0) = k_4 k_5 / (k_3 k_6)$, and the input $u(t) \equiv u_1$ for $t \geq 0$. Then, $x_C(t) = k_4 k_5 / (k_3 k_6) + k_1 k_5 (u_1 - u_0) t^2 / 2 + O(t^3)$ for small $t \geq 0$. Since the t^2 coefficient in this Taylor expansion gets multiplied by p when u_0 is replaced by pu_0 and u_1 is replaced by pu_1 , it follows that the transient behavior of the output $x_C(t)$ depends on p . Interestingly, if the equation for the third node is replaced by $\dot{x}_C = k_5 x_A / x_B - k_6 x_C$, that is to say the activation of C is repressed by B , instead of its de-activation being enhanced by

A , then scale invariance does hold true, because $x_A(t)$ and $x_B(t)$ both scale by p when $u_0 \mapsto pu_0$, $u_1 \mapsto pu_1$, and $x_C(t)$ depends on the ratio of these two functions (in particular, the $t^2/2$ term is $k_2 k_5 (u_1 - u_0) / u_0$). Such a repression is typical of genetic interaction networks, but is not natural in enzymatic reactions.

It turns out that the example described by Eq.3 is typical: no enzymatic network described by Eq.1 can display perfect scale-invariant behavior. This fact is a consequence of the equivariance theorem proved in [14] (see *Materials and Methods*). Thus, a

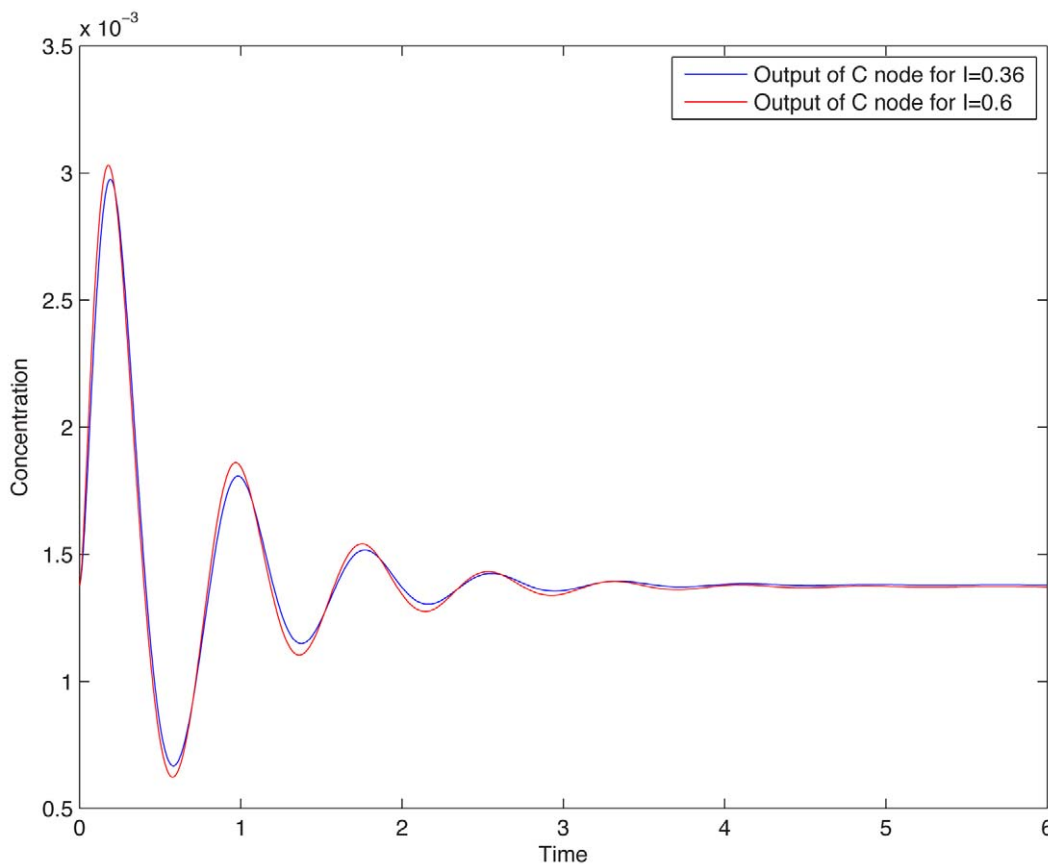


Figure 2. Scale-invariance. Plots overlap, for responses to steps $3 \rightarrow 1.2 * 3$ and $5 \rightarrow 1.2 * 5$. Network is the one described by Eq.2. Random parameter set: $K_{UA} = 0.093918$ $k_{UA} = 11.447219$, $K_{BA} = 0.001688$ $k_{BA} = 44.802268$, $K_{CA} = 90.209027$ $k_{CA} = 96.671843$, $K_{AB} = 0.001191$ $k_{AB} = 1.466561$, $K_{FB} = 9.424319$ $k_{FB} = 22.745736$, $K_{AC} = 0.113697$ $k_{AC} = 1.211993$, $K_{BC} = 0.009891$ $k_{BC} = 7.239357$, $K_{CC} = 0.189125$ $k_{CC} = 17.910182$.
doi:10.1371/journal.pcbi.1002748.g002

meaningful study of enzymatic networks, even for perfectly adaptive ones, must rely upon a test of approximate scale invariance. Instead of asking that $y_{u_0,u}(t) = y_{pu_0,pu}(t)$, as was the case in the theory developed in [13,14], one should require only that the difference be small. To investigate this issue, we computationally screened all 3-node topologies through a high-throughput random parameter scan, testing for small differences in responses to scaled steps. We found that approximately 0.01% of the samples showed adaptation, but of them, only about 0.15% passed the additional criterion of approximate scale invariance (see *Materials and Methods*). These samples belonged to 21 (out of 16,038 possible) topologies. As an example of the behavior of one of these, Fig. 2 shows a response resulting from a 20% step, from 3 to 3.6, compared to the response obtained when stepping from 5 to 6; the graphs are almost indistinguishable. (See *Text S1* for an enumeration of circuits and corresponding plots). In the following discussion, we will refer to these surviving circuits, and their topologies, as being “approximately scale invariant” (ASI).

We found that all ASI networks possess a feedforward motif, meaning that there are connections (positively or negatively signed) $A \rightarrow B \rightarrow C$ and as well as $A \rightarrow C$. Such feedforward motifs have been the subject of extensive analysis in the systems biology literature [1] and are often involved in detecting changes in signals [40]. They appear in pathways as varied as *E. coli* carbohydrate uptake via the carbohydrate phosphotransferase system [41], control mechanisms in mammalian cells [42], nitric oxide to NF- κ B activation [43,44], EGF to ERK activation [45,46], glucose to insulin release [47,48], ATP to intracellular calcium release [49], and microRNA regulation [50]. The feedforward motifs in all ASI

networks are incoherent, meaning such that the direct effect $A \rightarrow C$ has an opposite sign to the net indirect effect through B . An example of an incoherent feedforward connection is provided by the simple system described by Eq.3, where the direct effect of A on C is positive, but the indirect effect is negative: A activates B which in turn deactivates C . (Not every incoherent feedforward network provides scale invariance; a classification of those that provide exact scale invariance is known [14].)

It is noteworthy that all ASI circuits have a positive regulation from A to B and a negative regulation from B to A . Thus, they all include a negative feedback loop which is nested inside the incoherent feedforward loop. In addition, as discussed below, all ASI circuits and have only a weak (or no) self-loop on the response node C .

We then discovered another surprising common feature among all ASI circuits. This feature can best be explained by a further examination of the example in Eq.3.

Approximate scale invariance

Continuing with example in Eq.3, let us suppose that $k_1, k_2, k_3, k_4 \ll k_5, k_6$, so that the output variable $y = x_C$ reaches its steady state much faster than x_A and x_B do. Then, we may approximate the original system by the planar linear system represented by the differential equations for x_A and x_B together with the new output variable $\tilde{y}(t) = h(x_A(t), x_B(t)) = kx_A(t)/x_B(t)$, where $k = k_5/k_6$. This reduced planar system, obtained by a quasi-steady state approximation, has a perfect scale-invariance property: replacing the input u by pu results in the solution $(px_A(t), px_B(t))$, and thus the output is the same: $h(x_A(t), x_B(t)) = h(px_A(t), px_B(t))$. The exact

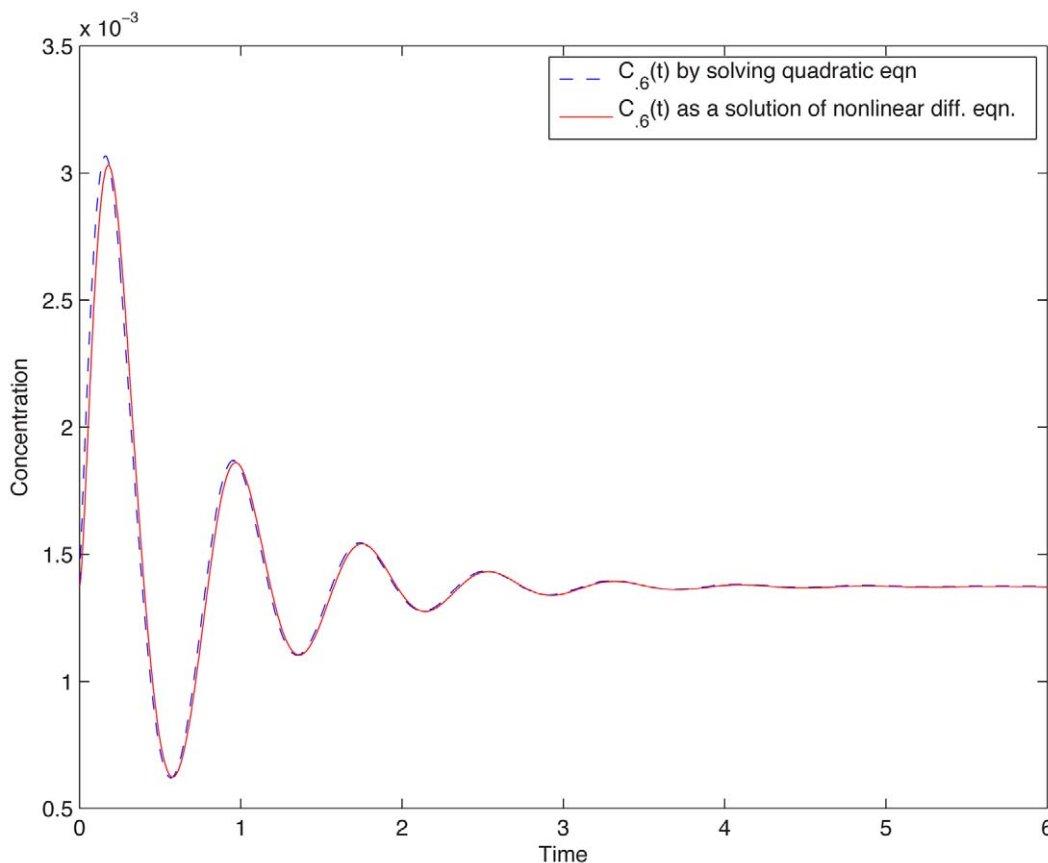


Figure 3. QSS quadratic approximation. Network is the one described by Eq.2. Random parameter set is as in Fig. 2. doi:10.1371/journal.pcbi.1002748.g003

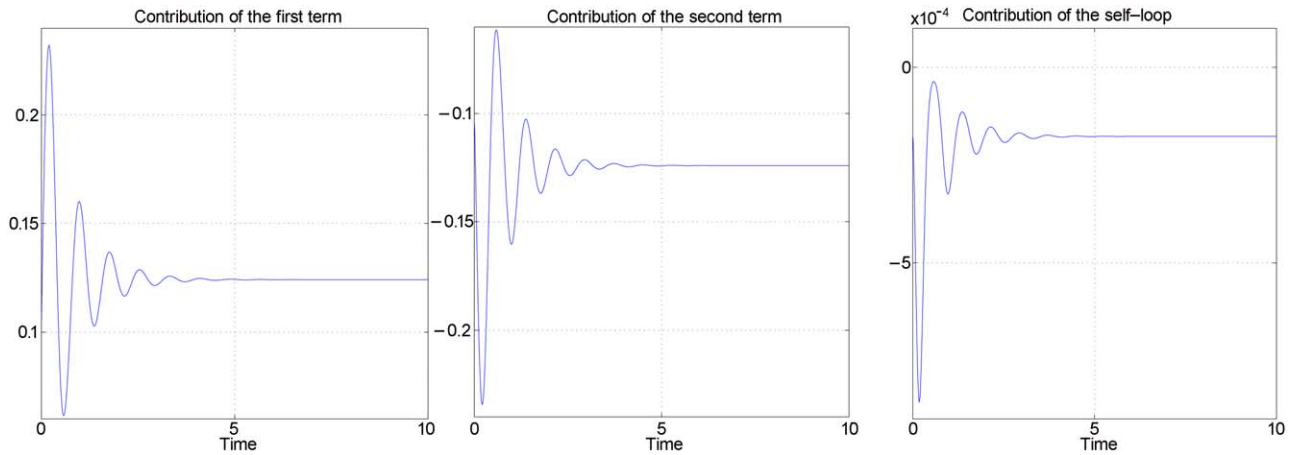


Figure 4. Relative contribution of terms in the equation for node C. The first two terms range in $[-0.25, 0.25]$ but self-loop magnitude is always less than 10^{-3} , i.e. contribution of self-loop to \dot{x}_C is less than 1%. Similar results hold for all ASI circuits. Network is the one described by Eq.2. Random parameter set is as in Fig. 2 . Similar results are available for all ASI circuits. doi:10.1371/journal.pcbi.1002748.g004

invariance of the reduced system translates into an approximate scale invariance property for the original three-dimensional system because, except for a short boundary-layer behavior (the relatively short time for x_C to reach equilibrium), the outputs of both systems are essentially the same, $y(t) \approx \tilde{y}(t)$. The assumption $k_1, k_2, k_3, k_4 \ll k_5, k_6$ is often written symbolically as $\dot{x}_A = k_1 u - k_2 x_B$, $\dot{x}_B = k_3 x_A - k_4 x_B$, $\varepsilon \dot{x}_C = k_5 x_A - k_6 x_B x_C$, where $0 < \varepsilon \ll 1$ and where k_5, k_6 are now the original k_5, k_6

multiplied by ε . The quality of approximate scale invariance will depend on how small “ ε ” is.

Generality of the planar reduction

We found that, just as in the example in Eq.3 when $k_1, k_2, k_3, k_4 \ll k_5, k_6$, in every ASI circuits the time scale of node C is much shorter than that of A and B. Therefore, the same

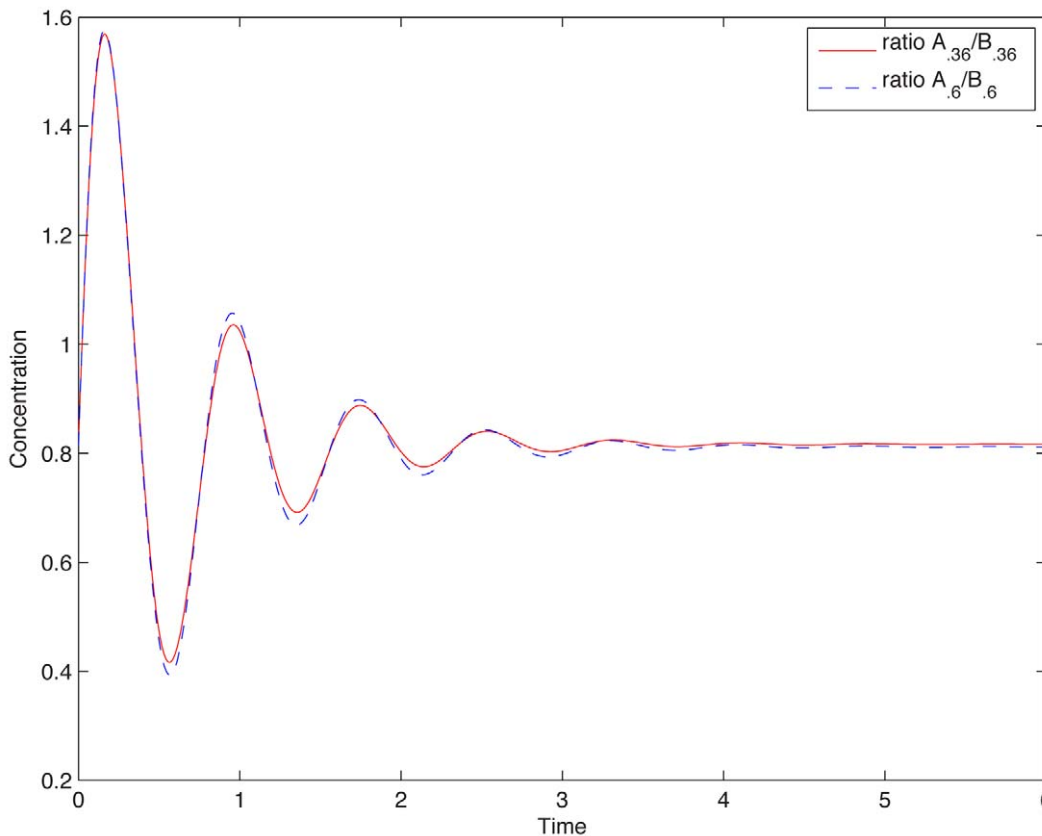


Figure 5. Constant A/B ratio in responses to $3 \rightarrow 1.2 * 3$ and $5 \rightarrow 1.2 * 5$. Network is the one described by Eq.2. Random parameter set is as in Fig. 2. Similar results are available for all ASI circuits (see Text S1). doi:10.1371/journal.pcbi.1002748.g005

two-dimensional reduction is always valid. It follows that one can drop the last equation, approximating these circuits by planar systems that are described by only the two state variables x_A and x_B , where every occurrence of x_C in the first two equations of the right-hand side of Eq.1 is replaced by $h(x_A, x_B)$, the function obtained by setting the right-hand side of the third equation in Eq.1 to zero and solving for the unique root in the interval $[0,1]$ of the quadratic equation. This reduced system, with $\tilde{y}(t) = h(x_A(t), x_B(t))$ as an output, provides an excellent approximation of the original dynamics. Fig. 3 compares the true response with the response obtained by the quasi-steady state approximation, for one ASI circuit (see *Text SI* for all comparisons).

Generality of dependence on x_A/x_B

In the example given by Eq.3, there were two additional key mathematical properties that made the planar reduction scale-invariant (and hence the original system approximately so). The first property was that, at equilibrium, the variable x_C must be a function of the ratio x_A/x_B , and the second one was that each of x_A and x_B must scale by the same factor when the input scales by p . Neither of these two properties need to hold, even approximately, for general networks. Surprisingly, however, we discovered that both are valid with very high accuracy for every ASI circuit. The equilibrium value of x_C is obtained from setting the last right-hand side of Eq.1 to zero and solving for x_C . A solution $x_C = h(x_A, x_B)$ in the interval $[0,1]$ always exists, because at $x_C = 0$ one has $\tilde{x}_C = 1$ and thus the term is positive, and at $x_C = 1$ one has $\tilde{x}_C = 0$ and so the term is negative. This right-hand side has the general form $x_A\phi(x_C) + x_B\gamma(x_C) + \kappa(x_C, x_{E_C}, x_{F_C})$, where ϕ and γ are increasing functions, each a constant multiple of a function of the form $\tilde{x}_C/(\tilde{x}_C + K)$ or $-x_C/(x_C + K)$. If the term κ is negligible, then $x_A\phi(x_C) + x_B\gamma(x_C) = 0$ means that also $(x_A/x_B)\phi(x_C) + \gamma(x_C) = 0$, and therefore x_C at equilibrium is a (generally nonlinear) function of the ratio x_A/x_B . There is no a priori reason for the term κ to be negligible. However, we discovered that in every ASI circuit, $\kappa \approx 0$. More precisely, there is no dependence on the constitutive enzymes, and this “self-loop” link, when it exists, contributes to the derivative \tilde{x}_C much less than the x_A and x_B terms, see Fig. 4.

Generality of homogeneity of x_A, x_B

The last ingredient of the example given by Eq.3 that plays a role in approximate scale invariance is that each of x_A and x_B must scale proportionately when the input is scaled. In that example, the property holds simply because the equations for these two variables are linear. In general, however, the dynamics of (x_A, x_B) are described by nonlinear equations. Thus it is remarkable that, in all ASI circuits, the property holds. We tested the property by plotting $x_A(t)/x_B(t)$ in a set of experiments in which a system was pre-adapted to an input value u_0 and the input was subsequently set to a new level u at $t=0$. When going from pu_0 to pu , we found that the new value $x_A(t)/x_B(t)$ was almost the same, meaning that x_A and x_B scaled in the same fashion. A representative plot is shown in Fig. 5.

A new property: uniform linearizations with fast output

The (approximate) independence of $x_A(t)/x_B(t)$ on input scalings is not due to linearity of the differential equations for x_A and $x_B(t)$. Instead, the analysis of this question led us to postulate a new property, which we call *uniform linearizations with fast output (ULFO)*. To define this property, we again drop the last equation, and approximate circuits by the planar system that has only the state variables x_A and x_B , where every occurrence of x_C in their differential equations shown in Eq.1 is replaced by $h(x_A, x_B)$. We denote by $f(x_A, x_B, u)$

$= (f_1(x_A, x_B, u), f_2(x_A, x_B, u))$ the result of these substitutions, so that the reduced system is described in vector form by $\dot{x} = f(x, u)$, $x = (x_A, x_B)$. We denote by $\sigma(u)$ the unique steady state corresponding to a constant input u , that is, the solution of the algebraic equation $f(\sigma(u), u) = 0$. We denote by $\mathcal{A}(u) = (\partial f / \partial x)(\sigma(u), u)$ the Jacobian matrix of f with respect to x , and by $\mathcal{B}(u) = (\partial f / \partial u)(\sigma(u), u)$ the Jacobian vector of f with respect to u .

The property ULFO is then defined by requiring the following properties:

1. time-scale separation for x_C ;
2. $h(x_A, x_B)$ depends only on the ratio x_A/x_B ;
3. for every u, v , and p such that u, v , and pu are in the range $[\underline{u}, \bar{u}]$:

$$\sigma(pu) = p\sigma(u), \quad \mathcal{A}(u) = \mathcal{A}(v), \quad \mathcal{B}(u) = \mathcal{B}(v) \quad (4)$$

Notice that we are not imposing the far stronger property that the Jacobian matrices should be constant. We are only requiring the same matrix at every steady state.

The first condition in Eq.4 means that the vector $\sigma(u)/u$ should be constant. We verified that this requirement holds with very high accuracy in every one of the ASI circuits. With $\underline{u} = 0.3$ and $\bar{u} = 0.6$, we have the following $\sigma(u)/u$ values, rounded to 3 decimal digits: (0.195, 0.239), (0.193, 0.237), (0.192, 0.236), (0.191, 0.235) when $u = 0.3, 0.4, 0.5$, and 0.6 respectively, for the network described by Eq.2 and the random parameter set in Fig. 2. Similar results are available for all ASI circuits (see *Text SI*).

The Jacobian requirements in Eq.10 are also verified with high accuracy for all the ASI circuits. We illustrate this with the same network and parameter set. Let us we compute the linearizations $\mathcal{A}_{0.3} = \mathcal{A}(0.3)$, $\mathcal{A}_{0.4} = \mathcal{A}(0.4)$, ..., $\mathcal{B}_{0.6} = \mathcal{B}(0.6)$ and the average relative differences

$$\mathcal{A}_{ij}^{\text{err}} = \sum_{u=0.3,0.4,0.5,0.6} \frac{|(\mathcal{A}_u)_{ij} - (\mathcal{A}_{0.45})_{ij}|}{|(\mathcal{A}_{0.45})_{ij}|}$$

and we define similarly \mathcal{B}^{err} . These relative differences are very small (shown to 3 decimal digits):

$$\mathcal{A}^{\text{err}} = \begin{pmatrix} 0.069 & 0.004 \\ 0 & 0.005 \end{pmatrix}, \quad \mathcal{B}^{\text{err}} = \begin{pmatrix} 0.002 \\ 0 \end{pmatrix},$$

thus justifying the claim that the Jacobians are practically constant. Similar results are available for all ASI circuits (see *Text SI*).

The key theoretical fact is that the property ULFO implies approximate scale-invariance, see *Materials and Methods*.

Intuitively, the conditions in Eq.4 mean that the “memory” of past inputs, represented by the activity level (phosphorylation, methylation, etc.) of the pre-adapted steady state, is proportional to the input, indicating an integration mechanism, and that the small-signal behavior from different pre-adapted levels is the same. The term “uniform” refers to the fact that the linearizations at every steady state are the same. If the linearizations are not all the same, it is easy to see that scale invariance does not hold. The uniformity of linearizations provides a “global” way to tie together behaviors at different scales. The conditions give us the approximate homogeneity property $f(px, pu) \approx pf(x, u)$ when near steady states, because, for $u \approx u^*$ and $x \approx \sigma(u^*)$:

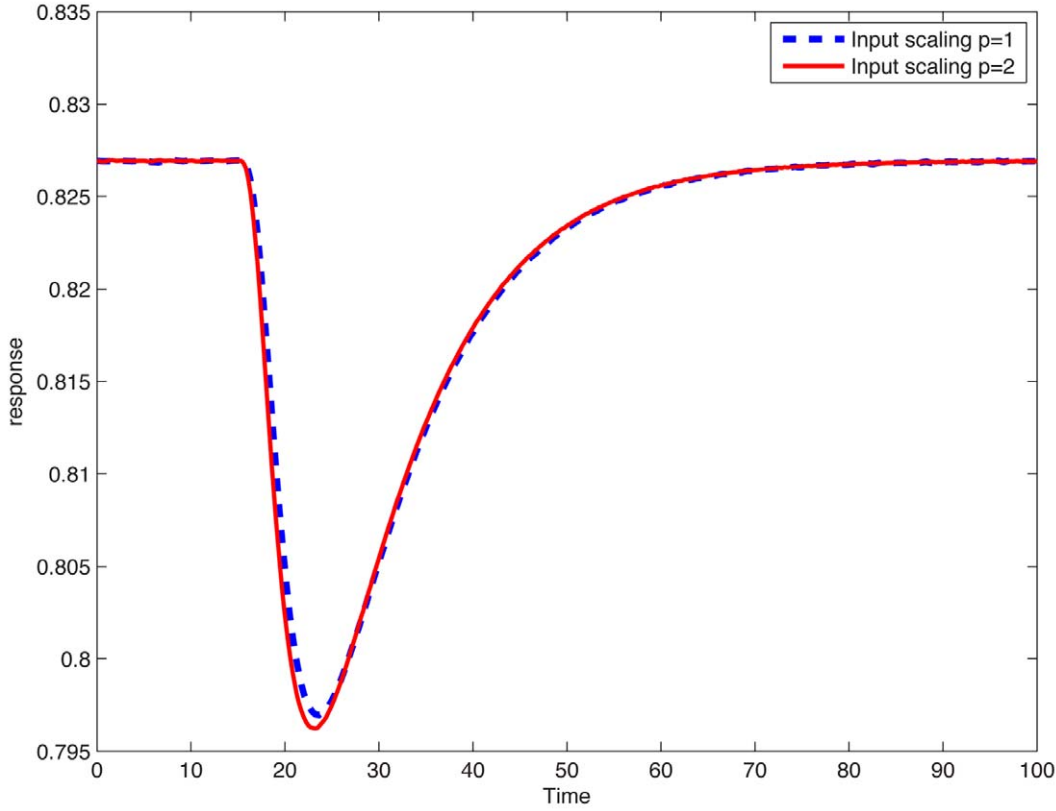


Figure 6. Scale-invariance computed when using the model in [34]: Responses to steps 1→2 and 2→4 coincide.
doi:10.1371/journal.pcbi.1002748.g006

$$\begin{aligned} f(px, pu) &\approx A(pu^*)(px - \sigma(pu^*)) + B(pu^*)(pu - pu^*) \\ &= A(u^*)(px - p\sigma(u^*)) + B(u^*)(pu - pu^*) \\ &\approx pf(x, u). \end{aligned}$$

These conditions are satisfied in various combinations of parameter regimes. As a purely theoretical example, consider the following system (denoting $x = x_A$, $y = x_B$, $z = x_C$):

$$\dot{x} = -\frac{x}{1+x/K}z + u$$

$$\dot{y} = x - y$$

$$\dot{z} = x - zy,$$

which can be viewed as a limiting case of the system described by Eq.2 when

$$k_{UA} = 1, k_{AB} = 1, k_{CC}, K_{UA}, k_{BA}, K_{AB}, K_{AC} \approx 0, k_{BC} = K_{BC}, K_{BC} \gg 1,$$

$$k_{AC} = 1, k_{F_B B} x_{F_B} = K_{F_B B}, K_{F_B B} \gg 1, K_{BA} \approx 0, k_{CA}/K_{CA} = 1.$$

Substituting $z = x/y$ in the first equation, we have:

$$\dot{x} = f_1(x, y, u) = -\frac{x^2}{y + xy/K} + u$$

The linearization of the system evaluated at a steady state corresponding to a constant input u has

$$A(u) = \begin{pmatrix} -2 + 3u/K - u^2/K^2 & 0 \\ 1 & -1 \end{pmatrix}$$

(and $B(u)$ constant), and is therefore approximately constant provided that K is large or that the input u is small in relative magnitude. Similarly, if we use $\sigma(pu)$ as initial state and pu as inputs, we get a similar expression (with $o(pu)$ instead of $o(u)$ and the p 's in the fraction canceling out).

A concrete biological model

In a recent paper [34] Takeda and collaborators studied the adaptation kinetics of a eukaryotic chemotaxis signaling pathway, employing a microfluidic device to expose *Dictyostelium discoideum* to changes in chemoeffector cyclic adenosine monophosphate (cAMP). Specifically, they focused on the dynamics of activated Ras (Ras-GTP), which was in turn reported by RBD-GFP (the Ras binding domain of fluorescently tagged human Raf1), and showed almost perfect adaptation of previously unstimulated cells to cAMP concentrations ranging from 10^{-2} nM to 1μ M. Furthermore, inspired by [20], the authors proposed alternative models

for adaptation, and concluded that the best fit was obtained by using an incoherent feedforward structure. The model that they identified is given by the following system of 6 differential equations:

$$\frac{dR_1}{dt} = k_{R_1}(v + r_1)(R_1^{\text{tot}} - R_1) - k_{-R_1}R_1$$

$$\frac{dR_2}{dt} = k_{R_2}(v + r_2)(R_2^{\text{tot}} - R_2) - k_{-R_2}R_2$$

$$u = R_1 + R_2$$

$$\frac{dGEF}{dt} = k_{GEF}u - k_{-GEF}GEF$$

$$\frac{dGAP}{dt} = k_{GAP}u - k_{-GAP}GAP$$

$$\frac{dRas^{GTP}}{dt} = k_{RAS}GEF(RAS^{\text{tot}} - Ras^{GTP}) - k_{-RAS}GAPRas^{GTP}$$

$$\frac{dRBD^{\text{cyt}}}{dt} = k_{RBD}^{\text{off}}(RBD^{\text{tot}} - RBD^{\text{cyt}}) - k_{RBD}^{\text{on}}Ras^{GTP}RBD^{\text{cyt}}.$$

The symbol v stands for the chemoeffector cAMP, and the authors assumed the existence of two different receptor populations (R_1 and R_2 , with very different K_d 's) which when bound pool their signals to downstream components (through u). The constants r_1 and r_2 represent levels of constitutive activation. The variables GEF and GAP represent activation and deactivation of RasGEF and RasGAP, Ras^{GTP} represents the activated Ras, and RBD^{cyt} describes the cytosolic reporter molecule RBD-GFP.

The best-fit parameters obtained in [34] are as follows: $R_1^{\text{tot}} = 0.1$, $R_2^{\text{tot}} = 0.9$, $r_1 = 0.012\text{nM}$, $r_2 = 0.115\text{nM}$, $k_{R_1} = 0.00267\text{nM}^{-1}\text{sec}^{-1}$, $k_{-R_1} = 0.16\text{sec}^{-1}$, $k_{R_2} = 0.00244\text{nM}^{-1}\text{sec}^{-1}$, $k_{-R_2} = 1.1\text{sec}^{-1}$, $k_{GEF} = 0.04\text{sec}^{-1}$, $k_{-GEF} = 0.4\text{sec}^{-1}$, $k_{GAP} = 0.01\text{sec}^{-1}$, $k_{-GAP} = 0.1\text{sec}^{-1}$, $RAS^{\text{tot}} = 1$, $k_{RAS} = 390\text{sec}^{-1}$, $k_{-RAS} = 3126\text{sec}^{-1}$, $RBD^{\text{tot}} = 1$, $k_{RBD}^{\text{off}} = 0.53\text{sec}^{-1}$, $k_{RBD}^{\text{on}} = 1.0\text{sec}^{-1}$. With these parameters, and cAMP concentrations which are small yet also satisfy $r_1 \ll v(t)$ and $r_2 \ll v(t)$, it follows that $\dot{R}_1 \approx k_{R_1}R_1^{\text{tot}}v - k_{-R_1}R_1$ and $\dot{R}_2 \approx k_{R_2}R_2^{\text{tot}}v - k_{-R_2}R_2$, so we may view $u(t)$ as an input (linearly dependent on the external $v(t)$) to the three-variable system described by $x_A = GEF$, $x_B = GAP$, $x_C = Ras^{GTP}$. Since RBD^{cyt} depends only on x_C , we may view x_C as the output. This three-variable system (interpreted as having limiting values of Michaelis-Menten constants) has the ULFO property provided that the dynamics of x_C are fast compared to x_A and x_B , which the identified parameters insure. So, we expect scale-invariant behavior. Indeed, Fig. 6 shows a simulation of the entire six-dimensional system (not merely of our 3-dimensional reduction) when using a step from 1 to 2 nM of cAMP, and shows that essentially the same response is obtained when stepping from 2 to 4 nM. This prediction of scale-invariant behavior is yet to be tested experimentally.

Discussion

Work in molecular systems biology seeks to unravel the basic dynamic processes, feedback control loops, and signal processing mechanisms in single cells and entire organisms, both for basic scientific understanding and for guiding drug design. One of the key questions is: how can one relate phenotype (function) to interaction maps (gene networks, protein graphs, and so forth) derived from experimentation, especially those obtained from high-throughput tools? Answers to this question provide powerful tools for guiding the reverse-engineering of networks, by focusing on mechanisms that are consistent with experimentally observed behaviors, and, conversely, from a synthesis viewpoint, allow one to design artificial biological systems that are capable of adaptation [51] and other objectives. In particular, scale-invariance, a property that has been observed in various systems [11,12], can play a key role in this context, helping to discard putative mechanisms that are not consistent with experimentally observed scale-invariant behaviors [15]. Through a computational study, we identified a set of simple mathematical conditions that are used to characterize three-node scale invariant enzymatic networks.

The conditions that we obtained for three-node networks are also sufficient for an arbitrary number of nodes, in the following sense. Suppose that we consider a set of $n+1$ nodes, where n nodes are described by variables $x = (x_1, \dots, x_n)$ and an additional node is described by a variable z . Suppose that the z variable evolves at a faster time scale than the x variables. Then, the ULFO property implies approximate scale invariance (see *Materials and Methods*). A variation of this situation is that in which a three-node network already displays scale invariance through an output node x_C , and this output feeds into an additional node x_D which evolves in a linear mode; then the entire four-node network will display scale invariance as well. Yet another variation is that in which an input is processed linearly before being fed into a three-node network. The discussed example of a published chemotaxis pathway in *Dityostelium discoideum* combines these variations. One could ask, of course, whether there exist large networks that are scale invariant yet are not built in this fashion. We carried out a limited computational search with four-node networks and have found none so far, leading us to conjecture that the ULFO mechanism is indeed necessary as well as sufficient in larger networks. However, a complete proof of necessity for arbitrary networks is outside the scope of this paper, and is most likely a very difficult if not impossible problem. A full computational screen as performed for three-node networks is already infeasible for four-node networks, due to the combinatorial explosion in the number of possible networks and of parameters to be randomly tested. A theoretical proof is also very difficult to envision, because (a) exact scale invariance is impossible for enzymatic networks, as shown in this paper, and (b) approximate adaptation and scale invariance are mathematically very hard to formalize in such a manner that impossibility can be rigorously proved for systems that do not satisfy our characterizations. In any event, as has been argued in other recent papers dealing with biological adaptation by enzymatic networks [20,35,36], a restriction to three-node networks is biologically reasonable, both as a coarse-graining of the problem and because many eukaryotic biological pathways, such as MAPK pathways, have at their core a three-component architecture.

Materials and Methods

Computational screen

We generalized and extended the computational protocol developed for adaptation in [20] to an investigation of approx-

imate scale invariance. MATLAB scripts were used, in conjunction with the software developed in [20]. In order to test inputs in ranges of the form $a \leq u(t) \leq 2a$, redefining the constant k_{UA} if needed, we take simply $\underline{u}=0.3$ and $\bar{u}=0.6$. We considered 160,380,000 circuits, obtained from the 16,038 nontrivial 3-node topologies, each one with 10,000 parameters sampled in logarithmic scale using the Latin hypercube method [52]. (We picked the ranges $k_{cat}=0.1-10$ and $K_m=0.001-100$. A finer sampling does not affect conclusions in any significant way [20].) Of these, 0.01% (16,304) circuits showed adaptation, meaning that, as in [20], when making a 20% step from $u_0=0.5$ to $u_1=0.6$ the precision is 10% or better, and the sensitivity is at least unity. Approximate scale invariance (ASI) was then tested by also performing a 20% step experiment from $u_0=0.3$ to $u_1=0.36$ and requiring that the relative difference between the responses be at most 10%: $\max_t \{|y_{0.6}(t) - y_{3.6}(t)| / \max(y_{0.6}(t) - y_{3.6}(t))\} < 0.1$

Of the adapting circuits, about 0.15% (25 circuits, classified into 21 different topologies) were determined to be ASI.

ULFO implies approximate scale invariance, for any number of nodes

Consider a system of n differential equations with input signal u ,

$$\dot{x} = f(x, u)$$

with the variables x evolving on some closed bounded set and f differentiable, and suppose that for each constant input \bar{u}^* there is a unique steady state $\bar{x}^* = \sigma(\bar{u}^*)$ with the conditions in Eq.10 and an output

$$y(t) = h(x(t))$$

such that h is differentiable and homogeneous of degree zero ($h(px) = h(x)$ for nonzero p). We view 3-node enzymatic networks as obtained from a set of $n+1$ equations

$$\dot{x} = F(x, z, u)$$

$$\varepsilon \dot{z} = G(x, z)$$

with $n=2$, $x=(x_A, x_B)$, and $z=x_C$ ($0 < \varepsilon \ll 1$ represents the faster time scale for x_C), and we are studying the reduced system $\dot{x} = f(x, u) = F(x, \alpha(x), u)$ obtained by solving $G(x, z) = 0$ for $z = \alpha(x)$ and substituting in F . Consider a time interval $[0, T]$, a constant input \bar{u}^* , and a possibly time-varying input $u(t)$, $t \geq 0$, as well as a scaling $p > 0$, such that all values \bar{u}^* , $p\bar{u}^*$, $u(t)$, $pu(t)$ are in the input range $[\underline{u}, \bar{u}]$. The solutions of $\dot{x} = f(x, u)$ with initial condition $x(0) = \sigma(\bar{u}^*)$ and of $\dot{z} = f(z, pu)$ with initial condition $z(0) = \sigma(p\bar{u}^*)$ are denoted respectively by $x(t)$ and $z(t)$, and the respective outputs are $y(t) = h(x(t))$ and $y_p(t) = h(z(t))$. We wish to show that these two responses are approximately equal on $0 \leq t \leq T$.

More precisely, we will prove that the relative error

$$\frac{\sup_t |y_p(t) - y(t)|}{\sup_t |u(t) - \bar{u}^*|} \rightarrow 0$$

as a function of the input perturbation $u(t) - \bar{u}^*$.

Write $\delta(t) = u(t) - \bar{u}^*$. From Theorem 1 in [16] we know that

$$x(t) = x(0) + \xi(t) + o(\|\delta\|)$$

where $\|\delta\| = \sup_{0 \leq t \leq T} |\delta(t)|$ and ξ is the solution of the variational system

$$\dot{\xi}(t) = \mathcal{A}\xi(t) + \mathcal{B}\delta(t)$$

with $\xi(0) = 0$, and that

$$z(t) = z(0) + \zeta(t) + o(\|pu - p\bar{u}^*\|) = z(0) + \zeta(t) + o(\|\delta\|),$$

where

$$\dot{\zeta} = \mathcal{A}\zeta(t) + \mathcal{B}p\delta(t)$$

with $\zeta(0) = 0$. Recall that $\mathcal{A}(u) = (\partial f / \partial x)(\sigma(u), u)$ is the Jacobian matrix of f with respect to x , and $\mathcal{B}(u) = (\partial f / \partial u)(\sigma(u), u)$ is the Jacobian vector of f with respect to u , and the assumptions are that these matrices are in fact independent of u . By linearity, $\zeta = p\check{\zeta}$. Using $z(0) \equiv \sigma(p\bar{u}^*) = p\sigma(\bar{u}^*) = px(0)$, we have that $px(t) - z(t) = o(\|\delta\|)$. Thus,

$$y(t) = h(x(t)) = h(px(t)) = h(z(t) + o(\|\delta\|)).$$

If K is an upper bound on the gradient of h , then

$$|y_p(t) - y(t)| = |h(z(t)) - h(z(t) + o(\|\delta\|))| \leq Ko(\|\delta\|).$$

Thus, the relative error $\sup_t |y_p(t) - y(t)| / \sup_t |u(t) - \bar{u}^*|$ converges to zero as a function of the input perturbation $u(t) - \bar{u}^*$, as claimed.

As a numerical illustration, we consider again the the network described by Eq.2 and the random parameter set in Fig. 2 . We compare the relative error between the original nonlinear system, with initial state $\xi = (x_A, x_B)$ corresponding to $u = 0.3$, and applied input $u = 0.36$, and the approximation is $\xi + z(t)$, where the z solves the linear system with initial condition zero and constant input 0.06. The maximum approximation error is about 5% (to 3 decimal places, 0.055 for x_A and 0.01 for x_B). When stepping from $u = 0.5$ to $u = 0.6$, the error is less than 3% (0.028 and 0.005 respectively). Similar results are available for all ASI circuits (see *Text S1*).

Impossibility of perfect scale-invariance

Consider any system with state $x = (x_A, x_B, x_C)$, output x_C , and equations of the general form:

$$\dot{x}_A = f(x) + G(x_A)u$$

$$\dot{x}_B = g(x)$$

$$\dot{x}_C = h(x) = x_A a(x_C) + x_B b(x_C) + c(x_C).$$

It is assumed that $a(x_C) \neq 0$ for all x_C , $G(x_A) \neq 0$ for all x_A , $\bar{G} := \sup_x G(x) < \infty$, and the system is irreducible [14]. We now prove that such a system cannot be scale-invariant. Suppose by way of contradiction that it would be, and pick any fixed $p \neq 1$. The main theorem in [14] insures that there are two differentiable functions $\alpha(x)$ and $\beta(x)$ such that the algebraic identities:

$$\begin{aligned} \alpha_x(x)[f(x) + G(x_A)u] + \alpha_y(x)g(x) + \alpha_z(x)h(x) \\ = f(\alpha(x), \beta(x), x_C) + G(\alpha(x))pu, \end{aligned}$$

$$\beta_x(x)[f(x) + u] + \beta_y(x)g(x) + \beta_z(x)h(x) = g(\alpha(x), \beta(x), x_C)$$

$$\alpha(x)a(x_C) + \beta(x)b(x_C) + c(x_C) = x_A a(x_C) + x_B b(x_C) + c(x_C)$$

hold for all constant $x = (x_A, x_B, x_C)$ and u , and the vector function $x \mapsto (\alpha(x), \beta(x), z)$ is one-to-one and onto, which implies in particular that

$$\sup_x G(\alpha(x)) = \bar{G}.$$

Dividing by u and taking the limit as $u \rightarrow \infty$ in the first identity, we conclude that $\alpha_x(x)G(x_A) \equiv pG(\alpha(x))$. Doing the same in the second identity, we conclude that $\beta_x(x) \equiv 0$. Finally, taking partial derivatives with respect to x_A in the third identity:

$$a(x_C)pG(\alpha(x))/G(x_A) = \alpha_x(x)a(x_C) + \beta_x(x)b(x_C) = a(x_C)$$

References

- Alon U (2006) An Introduction to Systems Biology: Design Principles of Biological Circuits. Chapman & Hall.
- Keener J, Sneyd J (1998) Mathematical Physiology. New York: Springer.
- Block SM, Segall JE, Berg HC (1983) Adaptation kinetics in bacterial chemotaxis. *J Bacteriol* 154: 312–323.
- Shimizu TS, Tu Y, Berg HC (2010) A modular gradient-sensing network for chemotaxis in *Escherichia coli* revealed by responses to time-varying stimuli. *Mol Syst Biol* 6: 382.
- Mello BA, Tu Y (2003) Perfect and near-perfect adaptation in a model of bacterial chemotaxis. *Biophys J* 84: 2943–2956.
- Laming D (1986) Sensory Analysis. London: Academic Press.
- Thompson R (1967) Foundations of physiological psychology. New York: Harper and Row.
- Kalinin YV, Jiang LL, Tu YH, Wu M (2009) Logarithmic sensing in *Escherichia coli* bacterial chemotaxis. *Biophysical Journal* 96: 2439–2448.
- R Mesibov GWO, Adler J (1973) The range of attractant concentrations for bacterial chemotaxis and the threshold and size of response over this range. *J Gen Physiol* 62: 203–223.
- Paliwal S, Iglesias PA, Campbell K, Hilioti Z, Groisman A, et al. (2007) MAPK-mediated bimodal gene expression and adaptive gradient sensing in yeast. *Nature* 446: 46–51.
- Goentoro L, Kirschner MW (2009) Evidence that fold-change, and not absolute level, of β -catenin dictates Wnt signaling. *Molecular Cell* 36: 872–884.
- Cohen-Saidon C, Cohen AA, Sigal A, Liron Y, Alon U (2009) Dynamics and variability of ERK2 response to EGF in individual living cells. *Molecular Cell* 36: 885–893.
- Shoval O, Goentoro L, Hart Y, Mayo A, Sontag E, et al. (2010) Fold change detection and scalar symmetry of sensory input_elds. *Proc Natl Acad Sci U S A* 107: 15995–16000.
- Shoval O, Alon U, Sontag E (2011) Symmetry invariance for adapting biological systems. *SIAM Journal on Applied Dynamical Systems* 10: 857–886.
- Lazova MD, Ahmed T, Bellomo D, Stocker R, Shimizu TS (2011) Response-rescaling in bacterial chemotaxis. *Proc Natl Acad Sci U S A* 108: 13870–13875.
- Sontag E (1998) Mathematical Control Theory. Deterministic Finite-Dimensional Systems, volume 6 of Texts in Applied Mathematics, second edition. New York: Springer-Verlag. xvii+531 pp.
- Yi TM, Huang Y, Simon M, Doyle J (2000) Robust perfect adaptation in bacterial chemotaxis through integral feedback control. *Proc Natl Acad Sci U S A* 97: 4649–4653.
- Sontag E (2003) Adaptation and regulation with signal detection implies internal model. *Systems Control Lett* 50: 119–126.
- Iglesias P (2003) Feedback control in intracellular signaling pathways: Regulating chemotaxis in *dictyostelium discoideum*. *European J Control* 9: 216–225.
- Bijlsma J, Groisman E (2003) Making informed decisions: regulatory interactions between two-component systems. *Trends Microbiol* 11: 359–366.
- Grossman A (1995) Genetic networks controlling the initiation of sporulation and the development of genetic competence in *Bacillus subtilis*. *Annu Rev Genet* 29: 477–508.
- Chen H, Bernstein B, Bamberg J (2000) Regulating actin filament dynamics in vivo. *Trends Biochem Sci* 25: 19–23.
- Donovan S, Shannon K, Bollag G (2002) GTPase activating proteins: critical regulators of intracellular signaling. *Biochim Biophys Acta* 1602: 23–45.
- Karp G (2002) Cell and Molecular Biology. Wiley.
- Stryer L (1995) Biochemistry. Freeman.
- Sulis M, Parsons R (2003) PTEN: from pathology to biology. *Trends Cell Biol* 13: 478–483.
- Lew D, Burke D (2003) The spindle assembly and spindle position checkpoints. *Annu Rev Genet* 37: 251–282.
- Asthagiri A, Lauffenburger D (2001) A computational study of feedback effects on signal dynamics in a mitogen-activated protein kinase (mapk) pathway model. *Biotechnol Prog* 17: 227–239.
- Chang L, Karin M (2001) Mammalian MAP kinase signaling cascades. *Nature* 410: 37–40.
- Huang CY, Jr JF (1996) Ultrasensitivity in the mitogen-activated protein kinase cascade. *Proc Natl Acad Sci U S A* 93: 10078–10083.
- Widmann C, Spencer G, Jarpe M, Johnson G (1999) Mitogen-activated protein kinase: Conservation of a three-kinase module from yeast to human. *Physiol Rev* 79: 143–180.
- Angeli D, Ferrell JE, Sontag E (2004) Detection of multistability, bifurcations, and hysteresis in a large class of biological positive-feedback systems. *Proc Natl Acad Sci U S A* 101: 1822–1827.
- Takeda K, Shao D, Adler M, Charest P, Loomis W, et al. (2012) Incoherent feedforward control governs adaptation of activated Ras in a eukaryotic chemotaxis pathway. *Sci Signal* 5(205): ra2.

is true for all x . Since $a(x_C) \neq 0$, it follows that

$$pG(\alpha(x)) = G(x_A)$$

for all x . We consider two cases: (a) $p < 1$ and (b) $p > 1$. Suppose $p < 1$. Pick any sequence of points $x^{(i)}$ with $G(x^{(i)}) \rightarrow \bar{G}$ as $i \rightarrow \infty$. Then $G(\alpha(x^{(i)})) \rightarrow \bar{G}/p > \bar{G}$, contradicting $G(x) \leq \bar{G}$. If $p > 1$, picking a sequence such that $G(\alpha(x^{(i)})) \rightarrow \bar{G}$ as $i \rightarrow \infty$ gives the contradiction $G(x^{(i)}) \rightarrow p\bar{G} > \bar{G}$. This shows that the FCD property cannot hold.

Supporting Information

Text S1 Supplementary Text describes the dynamics of A and B nodes for the linearized models, as well as the ratio between $x_A(t)$ and $x_B(t)$. (PDF)

Acknowledgments

We are grateful to Wenzhe Ma for making available and explaining his software for generating and testing networks for adaptation.

Author Contributions

Conceived and designed the experiments: MS EDS. Performed the experiments: MS EDS. Analyzed the data: MS EDS. Contributed reagents/materials/analysis tools: MS EDS. Wrote the paper: MS EDS.

35. Shah NA, Sarkar CA (2011) Robust network topologies for generating switch-like cellular responses. *PLoS Comput Biol* 7: e1002085.
36. Yao G, Tan C, West M, Nevins JR, You L (2011) Origin of bistability underlying mammalian cell cycle entry. *Mol Syst Biol* 7: 485.
37. Francois P, Siggia ED (2008) A case study of evolutionary computation of biochemical adaptation. *Phys Biol* 5: 026009.
38. Andrews B, Sontag E, Iglesias P (2008) An approximate internal model principle: Applications to nonlinear models of biological systems. In: Proceedings of the 17th IFAC World Congress; 6–11 July 2008; Seoul, Korea. pp. Paper FrB25.3, 6 pages.
39. Sontag E (2010) Remarks on feedforward circuits, adaptation, and pulse memory. *IET Systems Biology* 4: 39–51.
40. Mangan S, Itzkovitz S, Zaslaver A, Alon U (2006) The incoherent feed-forward loop accelerates the response-time of the gal system of *Escherichia coli*. *J Mol Biol* 356: 1073–1081.
41. Kremling A, Bettenbrock K, Gilles ED (2008) A feed-forward loop guarantees robust behavior in *Escherichia coli* carbohydrate uptake. *Bioinformatics* 24: 704–710.
42. Ma'ayan A, Jenkins SL, Neves S, Hasseldine A, Grace E, et al. (2005) Formation of regulatory patterns during signal propagation in a Mammalian cellular network. *Science* 309: 1078–1083.
43. Mahaut-Smith MP, Ennion SJ, Rolf MG, Evans RJ (2000) ADP is not an agonist at P2X(1) receptors: evidence for separate receptors stimulated by ATP and ADP on human platelets. *Br J Pharmacol* 131: 108–114.
44. Marsigliante S, Elia MG, Di Jeso B, Greco S, Muscella A, et al. (2002) Increase of $[Ca^{2+}]_i$ via activation of ATP receptors in PC-Cl3 rat thyroid cell line. *Cell Signal* 14: 61–67.
45. Sasagawa S, Ozaki Y, Fujita K, Kuroda S (2005) Prediction and validation of the distinct dynamics of transient and sustained ERK activation. *Nat Cell Biol* 7: 365–373.
46. Nagashima T, Shimodaira H, Ide K, Nakakuki T, Tani Y, et al. (2007) Quantitative transcriptional control of ErbB receptor signaling undergoes graded to biphasic response for cell differentiation. *J Biol Chem* 282: 4045–4056.
47. Menè P, Pugliese G, Pricci F, Di Mario U, Cinotti GA, et al. (1997) High glucose level inhibits capacitative Ca^{2+} influx in cultured rat mesangial cells by a protein kinase C-dependent mechanism. *Diabetologia* 40: 521–527.
48. Nesher R, Cerasi E (2002) Modeling phasic insulin release: immediate and time-dependent effects of glucose. *Diabetes* 51 Suppl 1: S53–59.
49. Ridnour LA, Windhausen AN, Isenberg JS, Yeung N, Thomas DD, et al. (2007) Nitric oxide regulates matrix metalloproteinase-9 activity by guanylyl-cyclase-dependent and -independent pathways. *Proc Natl Acad Sci U S A* 104: 16898–16903.
50. Tsang J, Zhu J, van Oudenaarden A (2007) MicroRNA-mediated feedback and feed-forward loops are recurrent network motifs in mammals. *Mol Cell* 26: 753–767.
51. Bleris L, Xie Z, Glass D, Adadey A, Sontag E, et al. (2011) Synthetic incoherent feed-forward circuits show adaptation to the amount of their genetic template. *Nature Molecular Systems Biology* 7: 519–.
52. Iman RL (2001) Appendix A : Latin Hypercube Sampling 1. *Encyclopedia of Statistical Sciences*, Update 3: 408–411.

Supplementary Material

A characterization of scale invariant responses in enzymatic networks

1 Circuits that exhibit ASI

We list here the results of the computational screen as described in the Main Text. Equations and parameters for the 25 identified ASI circuits (21 topologies) are given. Firstly, we give graphical representation of the 25 circuits.

For each circuit, four plots are shown:

- (a) a comparison between the plots of $x_A(t)$ and $x_B(t)$ for the original nonlinear system and the respective plots for the linearized approximations,
- (b) the plots showing scale-invariant behavior for step inputs, and the comparison between the plots of $x_C(t)$ for the original nonlinear system and for the quasi-steady state approximation, for
- (c) step input change from 0.3 to 0.36 and
- (d) step input change from 0.5 to 0.6.

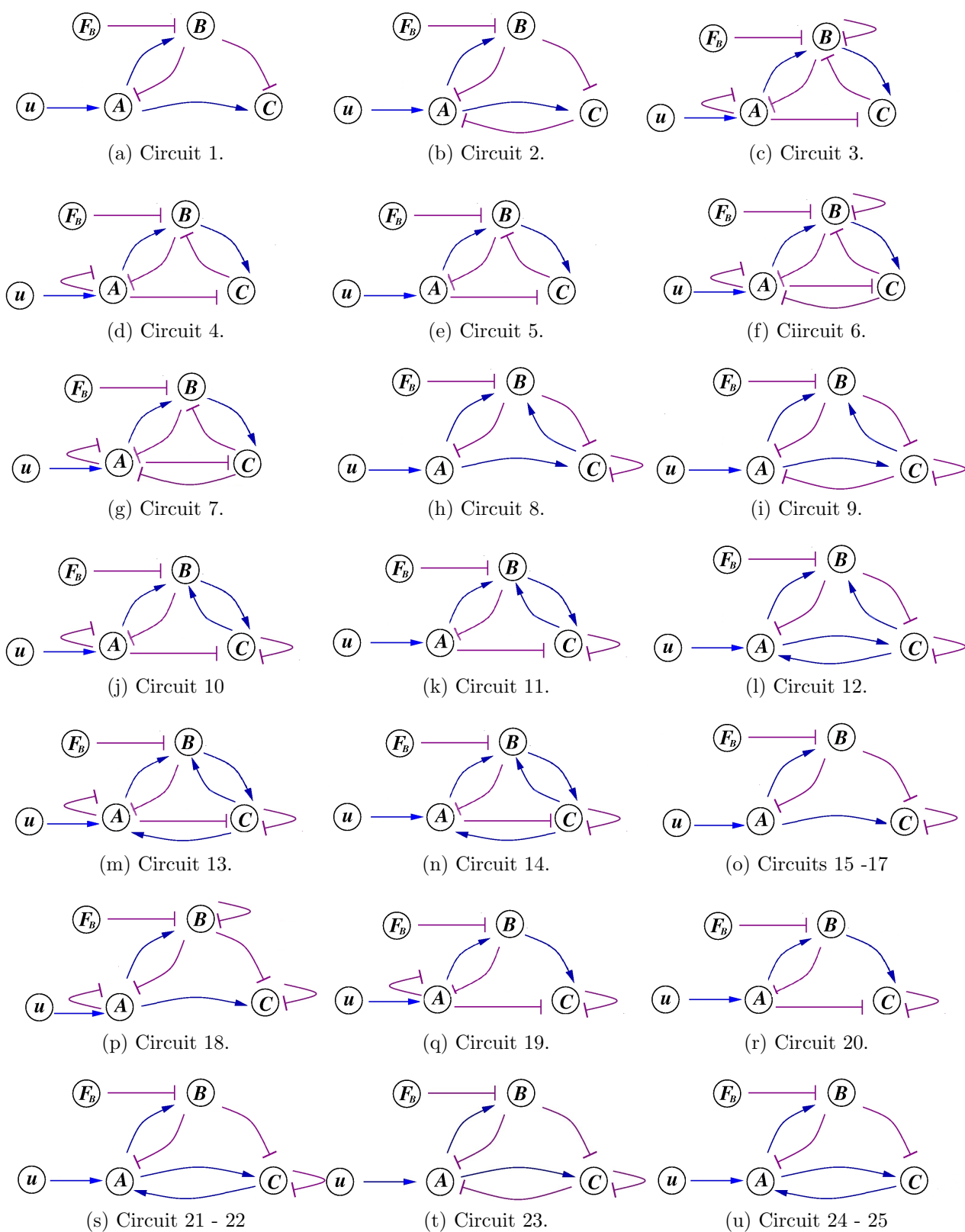
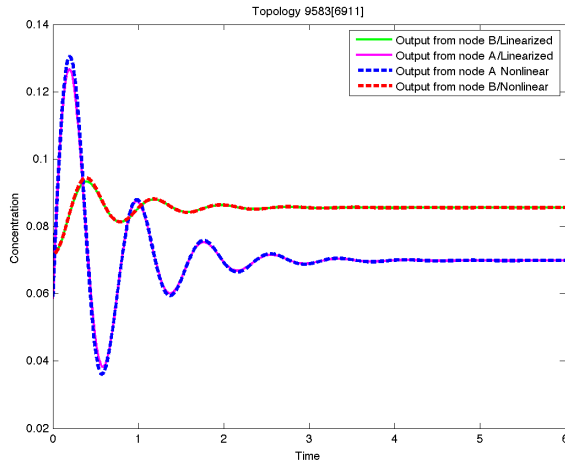


Figure S1. Identified ASI Circuits

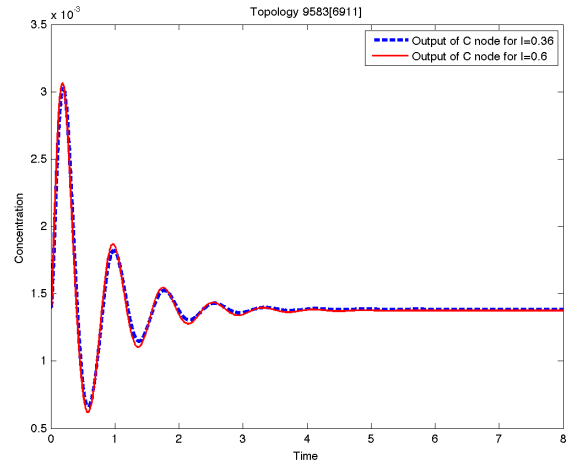
Circuit 1.

$$\begin{aligned}\dot{x}_A &= k_{uA}u\frac{\tilde{x}_A}{\tilde{x}_A + K_{uA}} - k_{BA}x_B\frac{x_A}{x_A + K_{BA}} \\ \dot{x}_B &= k_{AB}x_A\frac{\tilde{x}_B}{\tilde{x}_B + K_{AB}} - k_{F_B B}x_{F_B}\frac{x_B}{x_B + K_{F_B B}} \\ \dot{x}_C &= k_{AC}x_A\frac{\tilde{x}_C}{\tilde{x}_C + K_{AC}} - k_{BC}x_B\frac{x_C}{x_C + K_{BC}}\end{aligned}$$

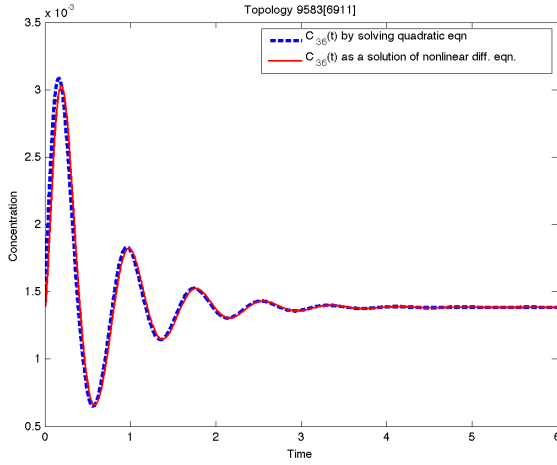
Parameters: $K_{AB} = 0.001191$; $k_{AB} = 1.466561$; $K_{AC} = 0.113697$; $k_{AC} = 1.211993$;
 $K_{BA} = 0.001688$; $k_{BA} = 44.802268$; $K_{BC} = 0.009891$; $k_{BC} = 7.239357$; $K_{uA} = 0.093918$;
 $k_{uA} = 11.447219$; $k_{AC} = 1.211993$; $K_{AC} = 0.1136927$; $K_{F_B} = 9.424319$; $k_{F_B} = 22.745736$



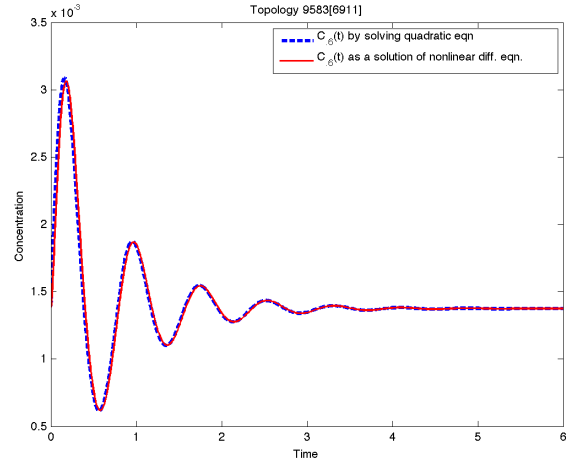
(a) Dynamics of A and B in linearized model



(b) Output from C nonlinear model



(c) Quadratic approx. and output of nonlinear system, I=0.36



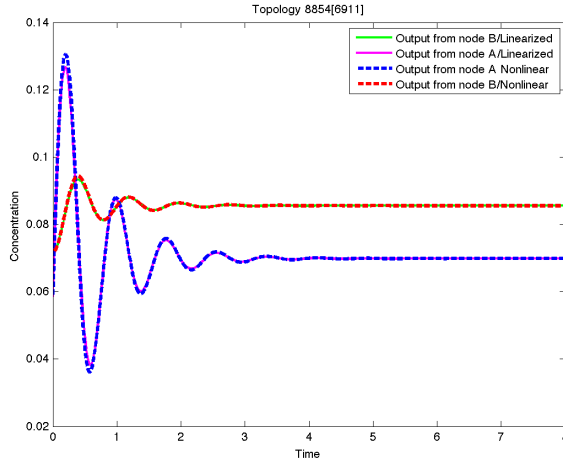
I=0.6

Figure S2. Circuit 1.

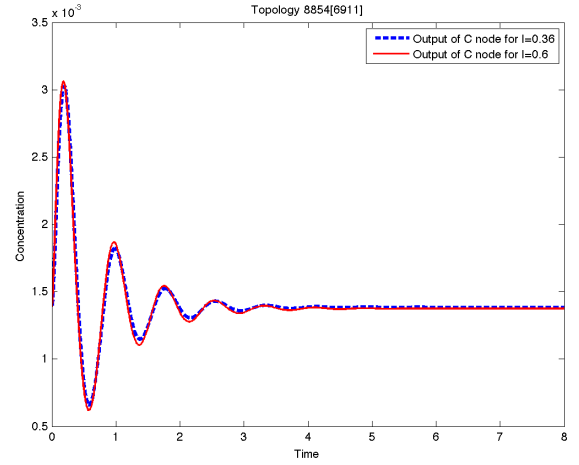
Circuit 2.

$$\begin{aligned}\dot{x}_A &= k_{uA}u\frac{\tilde{x}_A}{\tilde{x}_A + K_{uA}} - k_{BA}x_B\frac{x_A}{x_A + K_{BA}} - k_{CA}x_C\frac{x_A}{x_A + K_{CA}} \\ \dot{x}_B &= k_{AB}x_A\frac{\tilde{x}_B}{\tilde{x}_B + K_{AB}} - k_{F_B}Bx_{F_B}\frac{x_B}{x_B + K_{F_B}} \\ \dot{x}_C &= k_{AC}x_A\frac{\tilde{x}_C}{\tilde{x}_C + K_{AC}} - k_{BC}x_B\frac{x_C}{x_C + K_{BC}}\end{aligned}$$

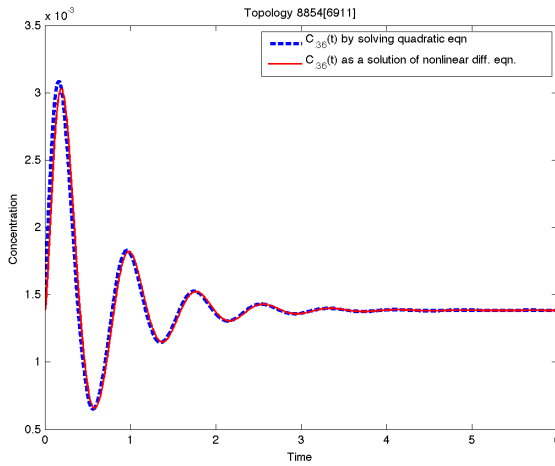
Parameters: $K_{uA} = 0.093918$; $k_{uA} = 11.447219$; $K_{BA} = 0.001688$; $k_{BA} = 44.802268$; $K_{CA} = 90.209027$; $k_{CA} = 96.671843$; $K_{AB} = 0.001191$; $k_{AB} = 1.466561$; $K_{F_B} = 9.424319$; $k_{F_B} = 22.745736$; $K_{AC} = 0.113697$; $k_{AC} = 1.211993$; $K_{BC} = 0.009891$; $k_{BC} = 7.239357$



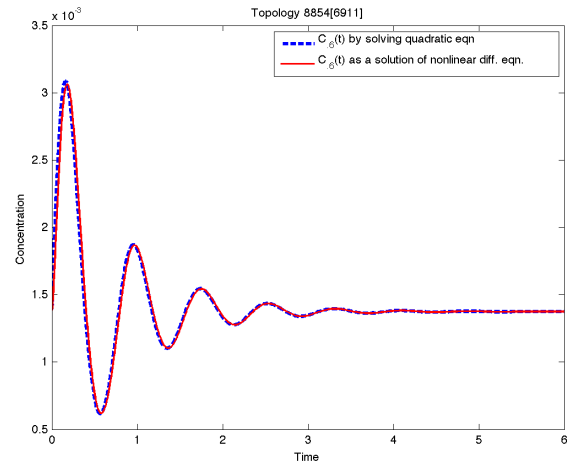
(a) Dynamics of A and B in linearized model



(b) Output from C nonlinear model



(c) Quadratic approx. and output of nonlinear system



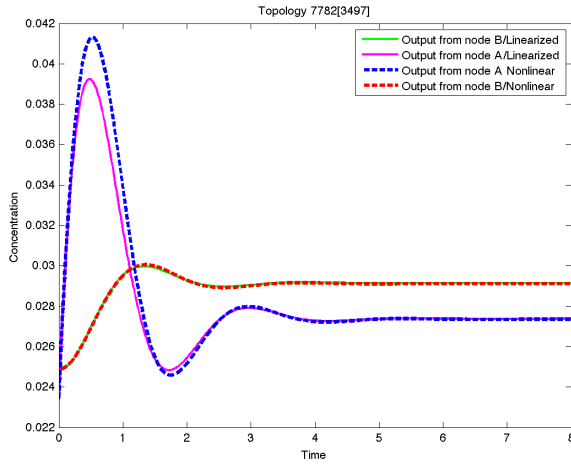
(d) Quadratic approx. and output of nonlinear system

Figure S3. Circuit 2.

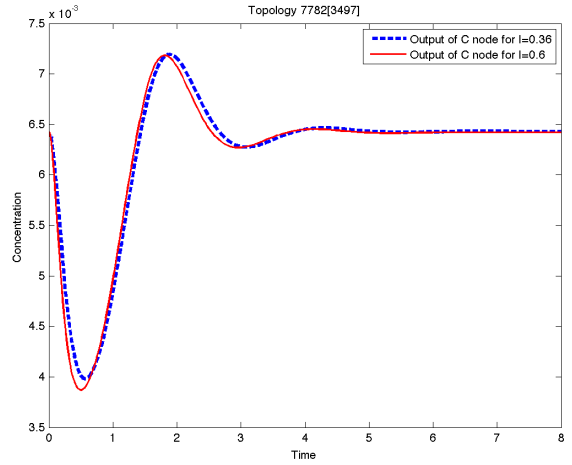
Circuit 3.

$$\begin{aligned}\dot{x}_A &= k_{uA}u\frac{\tilde{x}_A}{\tilde{x}_A + K_{uA}} - k_{BA}x_B\frac{x_A}{x_A + K_{BA}} - k_{AA}x_A\frac{x_A}{x_A + K_{AA}} \\ \dot{x}_B &= k_{AB}x_A\frac{\tilde{x}_B}{\tilde{x}_B + K_{AB}} - k_{CB}x_B\frac{x_B}{x_B + K_{CB}} - k_{BB}x_B\frac{x_B}{x_B + K_{BB}} \\ \dot{x}_C &= k_{BC}x_B\frac{\tilde{x}_C}{\tilde{x}_C + K_{BC}} - k_{AC}x_A\frac{x_C}{x_C + K_{AC}}\end{aligned}$$

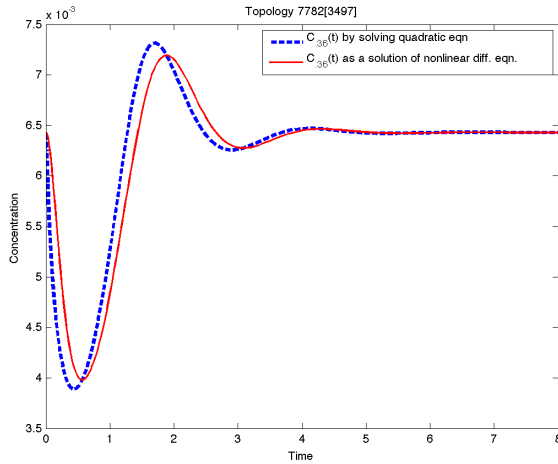
Parameters: $K_{AA} = 7.633962$; $k_{AA} = 86.238263$; $K_{AB} = 20.265158$; $k_{AB} = 5.428752$;
 $K_{AC} = 0.258375$; $k_{AC} = 62.416585$; $K_{BA} = 0.003960$; $k_{BA} = 17.705166$; $K_{BB} = 31.604578$;
 $k_{BB} = 3.692326$; $K_{BC} = 44.386408$; $k_{BC} = 65.027941$; $K_{CB} = 0.701052$; $k_{CB} = 26.091557$;
 $K_{uA} = 0.464248$; $k_{uA} = 1.882348$



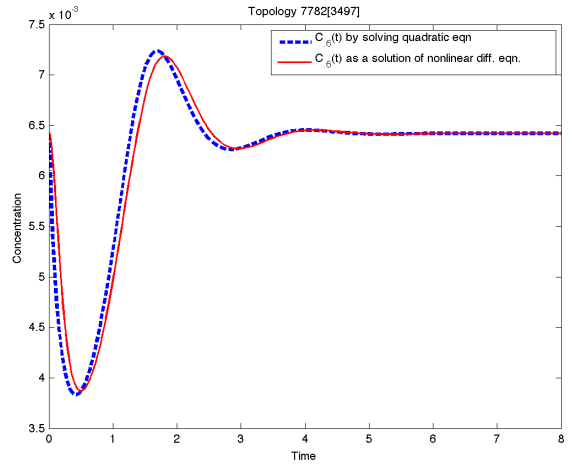
(a) Dynamics of A and B in linearized model



(b) Output from C nonlinear model



(c) Quadratic approx. and output of nonlinear system



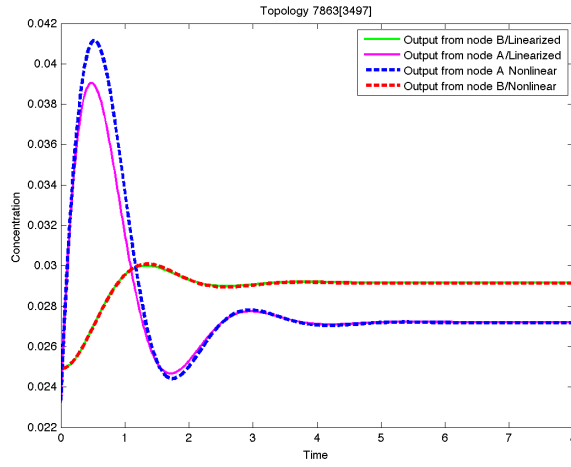
(d) Quadratic approx. and output of nonlinear system

Figure S4. Circuit 3.

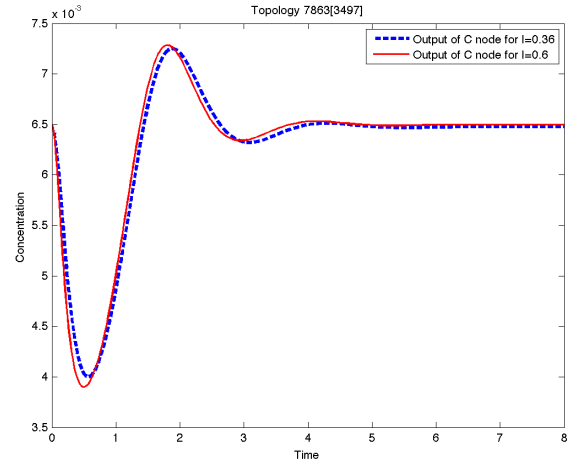
Circuit 4.

$$\begin{aligned}\dot{x}_A &= k_{uA}u\frac{\tilde{x}_A}{\tilde{x}_A + K_{uA}} - k_{BA}x_B\frac{x_A}{x_A + K_{BA}} - k_{AA}x_A\frac{x_A}{x_A + K_{AA}} \\ \dot{x}_B &= k_{AB}x_A\frac{\tilde{x}_B}{\tilde{x}_B + K_{AB}} - k_{CB}x_C\frac{x_B}{x_B + K_{CB}} \\ \dot{x}_C &= k_{BC}x_B\frac{\tilde{x}_C}{\tilde{x}_C + K_{BC}} - k_{AC}x_A\frac{x_C}{x_C + K_{AC}}\end{aligned}$$

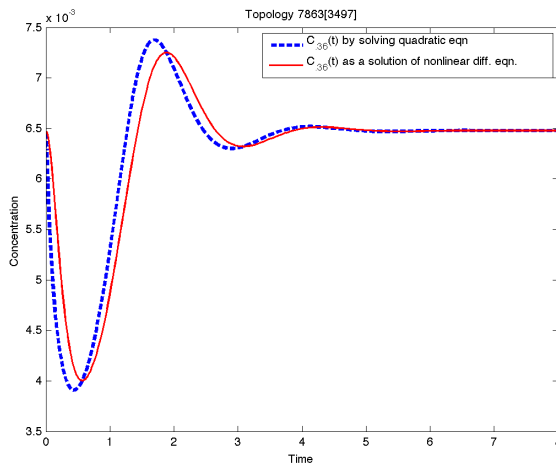
Parameters: $K_{AA} = 7.633962$; $k_{AA} = 86.238263$; $K_{AB} = 20.265158$; $k_{AB} = 5.428752$; $K_{AC} = 0.258375$; $k_{AC} = 62.416585$; $K_{BA} = 0.003960$; $k_{BA} = 17.705166$; $K_{BC} = 44.386408$; $k_{BC} = 65.027941$; $K_{CB} = 0.701052$; $k_{CB} = 26.091557$; $K_{uA} = 0.464248$; $k_{uA} = 1.882348$



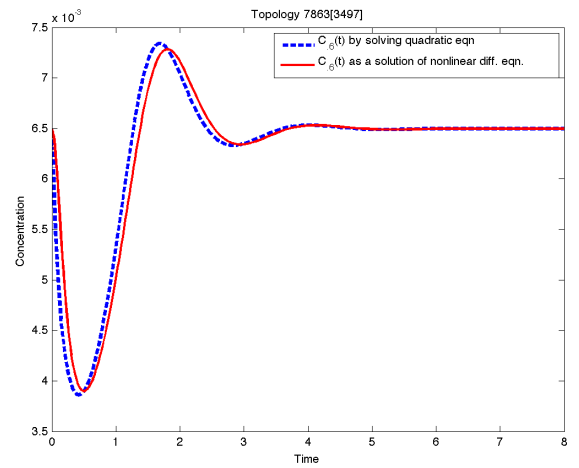
(a) Dynamics of A and B in linearized model



(b) Output from C nonlinear model



(c) Quadratic approx. and output of nonlinear system



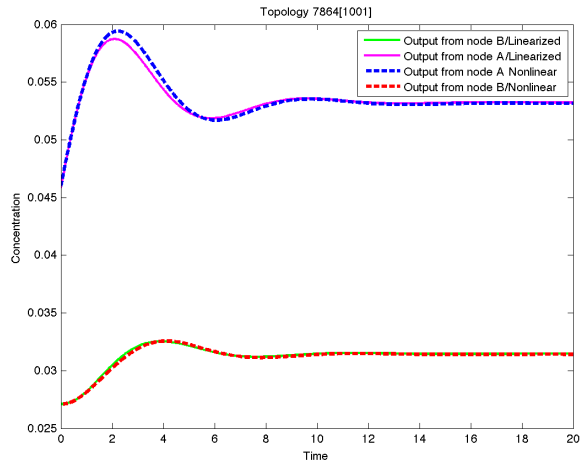
(d) Quadratic approx. and output of nonlinear system

Figure S5. Circuit 4.

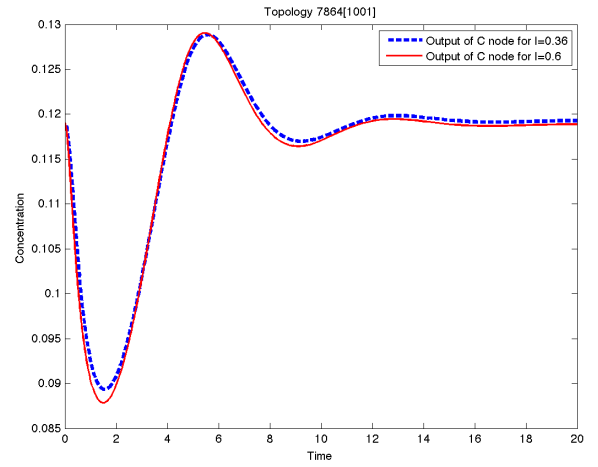
Circuit 5.

$$\begin{aligned}\dot{x}_A &= k_{uA}u\frac{\tilde{x}_A}{\tilde{x}_A + K_{uA}} - k_{BA}x_B\frac{x_A}{x_A + K_{BA}} \\ \dot{x}_B &= k_{AB}x_A\frac{\tilde{x}_B}{\tilde{x}_B + K_{AB}} - k_{CB}x_C\frac{x_B}{x_B + K_{CB}} \\ \dot{x}_C &= k_{BC}x_B\frac{\tilde{x}_C}{\tilde{x}_C + K_{BC}} - k_{AC}x_A\frac{x_C}{x_C + K_{AC}}\end{aligned}$$

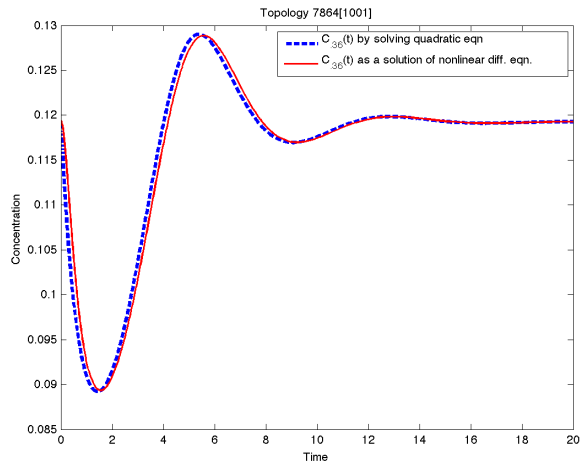
Parameters: $K_{AB} = 63.277600$; $k_{AB} = 6.638959$; $K_{AC} = 0.133429$; $k_{AC} = 55.731406$;
 $K_{BA} = 0.011188$; $k_{BA} = 2.749793$; $K_{BC} = 0.013374$; $k_{BC} = 45.175191$; $K_{CB} = 1.457975$;
 $k_{CB} = 2.114949$; $K_{uA} = 24.589517$; $k_{uA} = 5.346875$



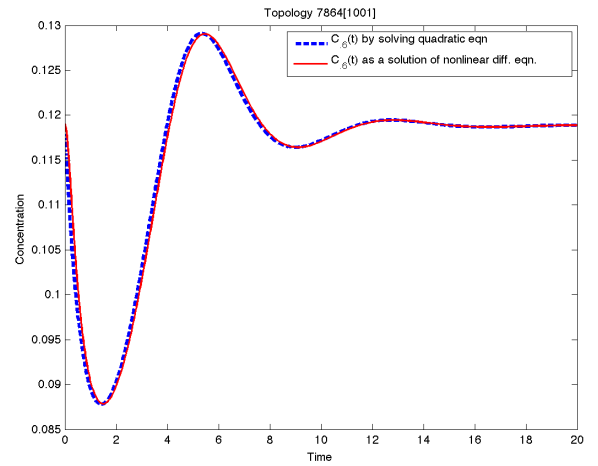
(a) Dynamics of A and B in linearized model



(b) Output from C nonlinear model



(c) Quadratic approx. and output of nonlinear system



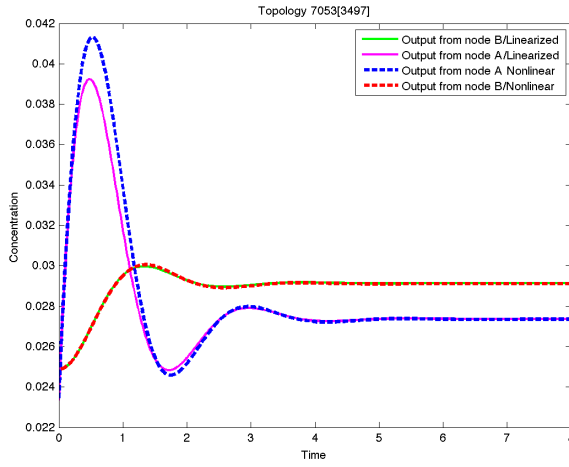
(d) Quadratic approx. and output of nonlinear system

Figure S6. Circuit 5.

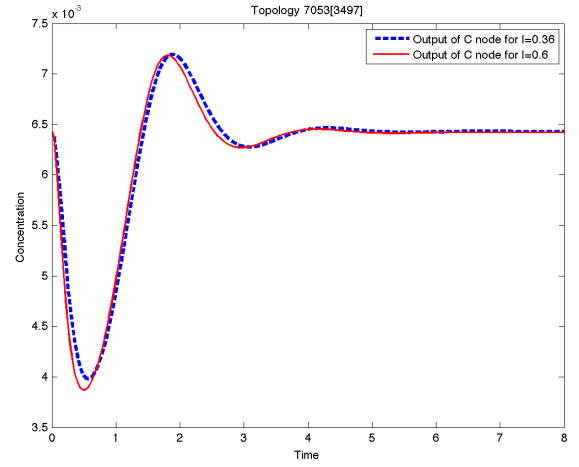
Circuit 6.

$$\begin{aligned}\dot{x}_A &= k_{uA}u\frac{\tilde{x}_A}{\tilde{x}_A + K_{uA}} - k_{BA}x_B\frac{x_A}{x_A + K_{BA}} - k_{AA}x_A\frac{x_A}{x_A + K_{AA}} - k_{CA}x_C\frac{x_A}{x_A + K_{CA}} \\ \dot{x}_B &= k_{AB}x_A\frac{\tilde{x}_B}{\tilde{x}_B + K_{AB}} - k_{CB}x_C\frac{x_B}{x_B + K_{CB}} - k_{BB}x_B\frac{x_B}{x_B + K_{BB}} \\ \dot{x}_C &= k_{BC}x_B\frac{\tilde{x}_C}{\tilde{x}_C + K_{BC}} - k_{AC}x_A\frac{x_C}{x_C + K_{AC}}\end{aligned}$$

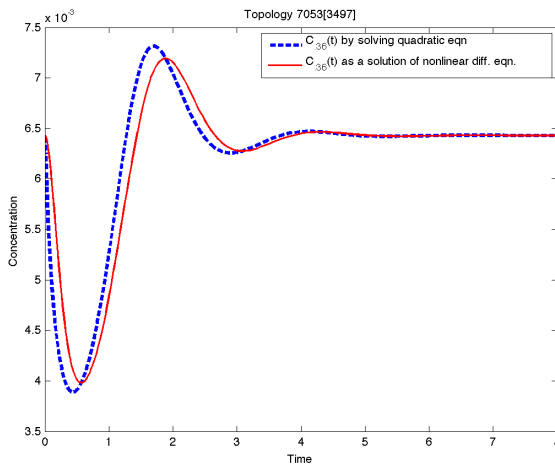
Parameters: $K_{AA} = 7.633962$; $k_{AA} = 86.238263$; $K_{AB} = 20.265158$; $k_{AB} = 5.428752$; $K_{AC} = 0.258375$; $k_{AC} = 62.416585$; $K_{BA} = 0.003960$; $k_{BA} = 17.705166$; $K_{BB} = 31.604578$; $k_{BB} = 3.692326$; $K_{BC} = 44.386408$; $k_{BC} = 65.027941$; $K_{CA} = 26.714681$; $k_{CA} = 2.806080$; $K_{CB} = 0.701052$; $k_{CB} = 26.091557$; $K_{uA} = 0.464248$; $k_{uA} = 1.882348$



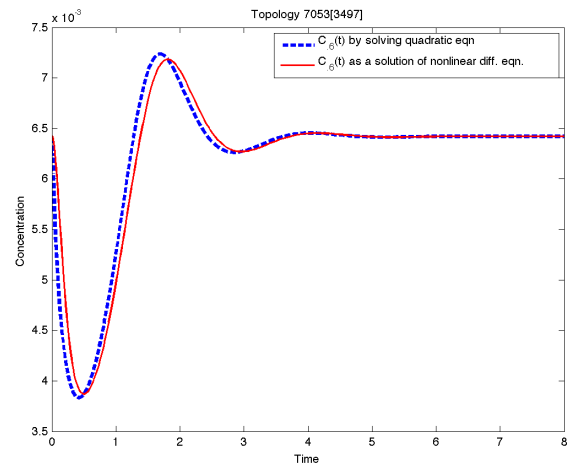
(a) Dynamics of A and B in linearized model



(b) Output from C nonlinear model



(c) Quadratic approx. and output of nonlinear system



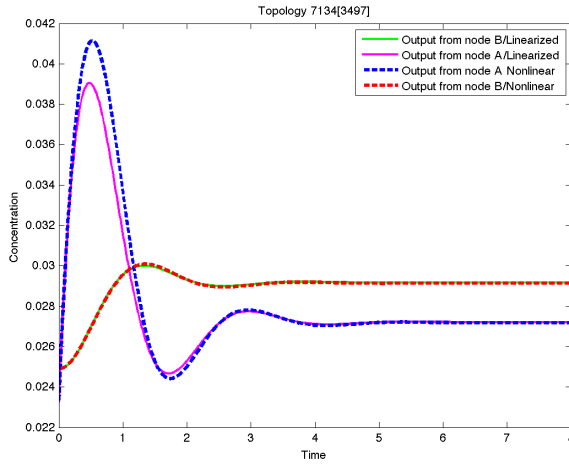
(d) Quadratic approx. and output of nonlinear system

Figure S7. Circuit 6.

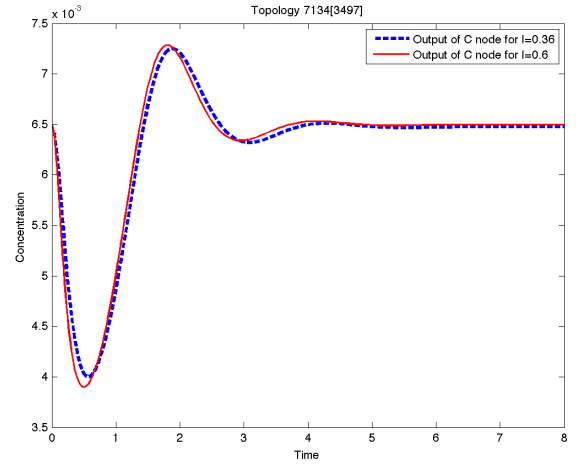
Circuit 7.

$$\begin{aligned}\dot{x}_A &= k_{uA}u\frac{\tilde{x}_A}{\tilde{x}_A + K_{uA}} - k_{BA}x_B\frac{x_A}{x_A + K_{BA}} - k_{AA}x_A\frac{x_A}{x_A + K_{AA}} - k_{CA}x_C\frac{x_A}{x_A + K_{CA}} \\ \dot{x}_B &= k_{AB}x_A\frac{\tilde{x}_B}{\tilde{x}_B + K_{AB}} - k_{CB}x_C\frac{x_B}{x_B + K_{CB}} \\ \dot{x}_C &= k_{BC}x_B\frac{\tilde{x}_C}{\tilde{x}_C + K_{BC}} - k_{AC}x_A\frac{x_C}{x_C + K_{AC}}\end{aligned}$$

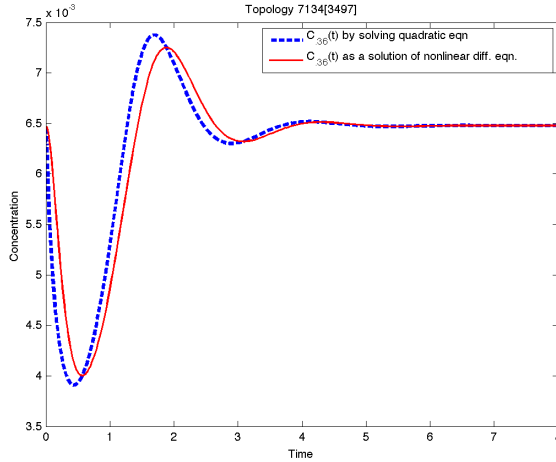
Parameters: $K_{AA} = 7.633962$; $k_{AA} = 86.238263$; $K_{AB} = 20.265158$; $k_{AB} = 5.428752$; $K_{AC} = 0.258375$; $k_{AC} = 62.416585$; $K_{BA} = 0.003960$; $k_{BA} = 17.705166$; $K_{BC} = 44.386408$; $k_{BC} = 65.027941$; $K_{CA} = 26.714681$; $k_{CA} = 2.806080$; $K_{CB} = 0.701052$; $k_{CB} = 26.091557$; $K_{uA} = 0.464248$; $k_{uA} = 1.882348$



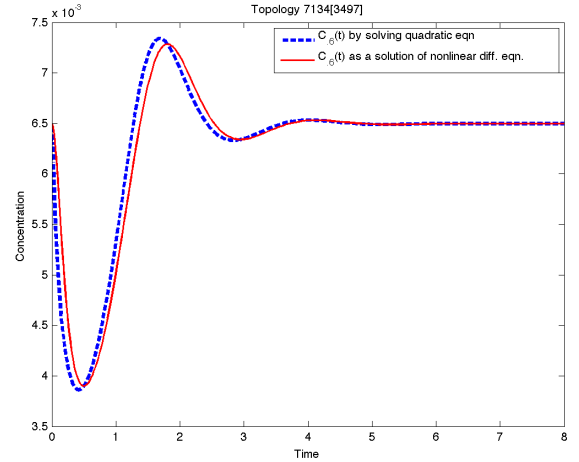
(a) Dynamics of A and B in linearized model



(b) Output from C nonlinear model



(c) Quadratic approx. and output of nonlinear system



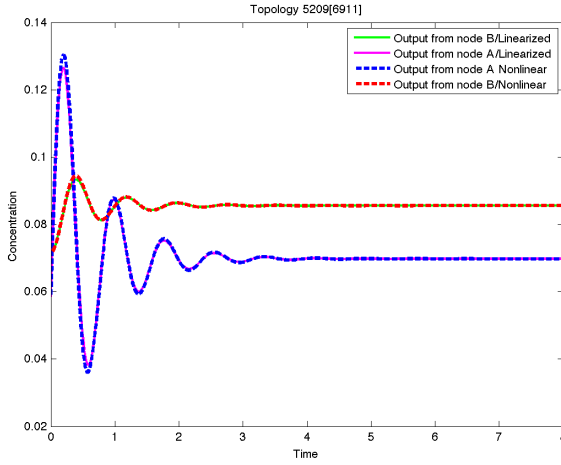
(d) Quadratic approx. and output of nonlinear system

Figure S8. Circuit 7.

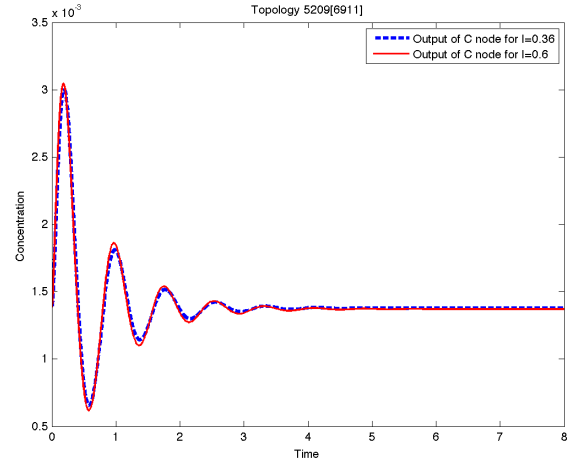
Circuit 8.

$$\begin{aligned}\dot{x}_A &= k_{uA}u\frac{\tilde{x}_A}{\tilde{x}_A + K_{uA}} - k_{BA}x_B\frac{x_A}{x_A + K_{BA}} \\ \dot{x}_B &= k_{AB}x_A\frac{\tilde{x}_B}{\tilde{x}_B + K_{AB}} - k_{F_B B}x_{F_B}\frac{x_B}{x_B + K_{F_B B}} + k_{CB}x_C\frac{\tilde{x}_B}{\tilde{x}_B + K_{CB}} \\ \dot{x}_C &= k_{AC}x_A\frac{\tilde{x}_C}{\tilde{x}_C + K_{AC}} - k_{BC}x_B\frac{x_C}{x_C + K_{BC}} - k_{CC}x_C\frac{x_C}{x_C + K_{CC}}\end{aligned}$$

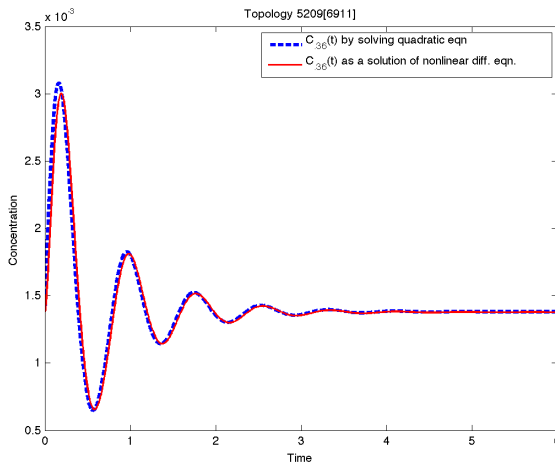
Parameters: $K_{uA} = 0.093918$; $k_{uA} = 11.447219$; $K_{BA} = 0.001688$; $k_{BA} = 44.802268$;
 $K_{AB} = 0.001191$; $k_{AB} = 1.466561$; $K_{F_B} = 9.424319$; $k_{F_B} = 22.745736$; $K_{AC} = 0.113697$;
 $k_{AC} = 1.211993$; $K_{BC} = 0.009891$; $k_{BC} = 7.239357$; $K_{CB} = 30.602013$; $k_{CB} = 3.811536$;
 $K_{CC} = 0.189125$; $k_{CC} = 17.910182$



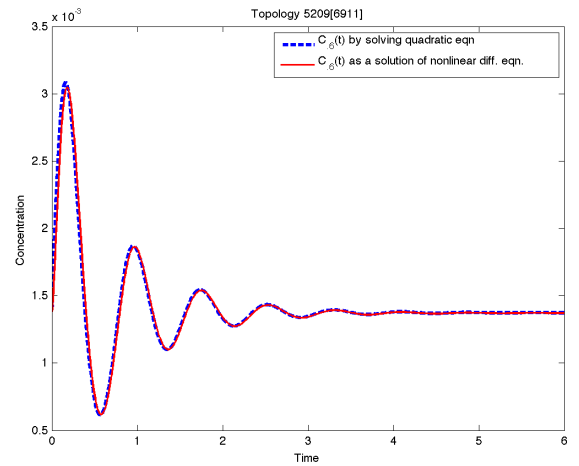
(a) Dynamics of A and B in linearized model



(b) Output from C nonlinear model



(c) Quadratic approx. and output of nonlinear system



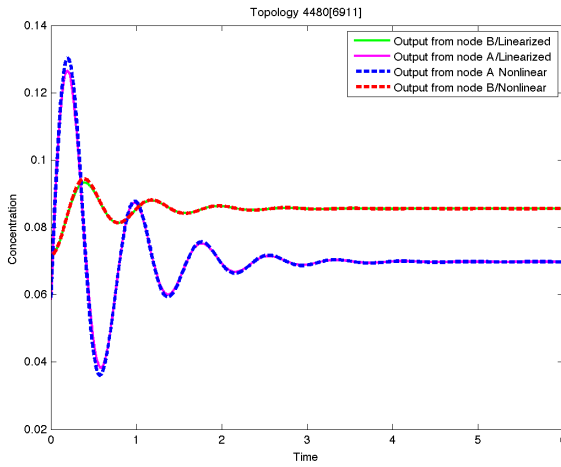
(d) Quadratic approx. and output of nonlinear system

Figure S9. Circuit 8.

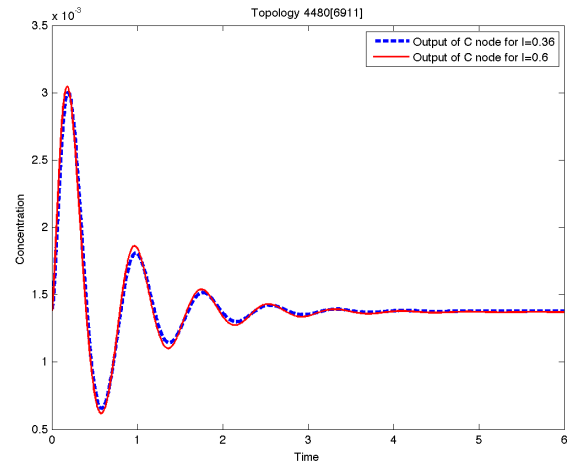
Circuit 9.

$$\begin{aligned}\dot{x}_A &= k_{uA}u\frac{\tilde{x}_A}{\tilde{x}_A + K_{uA}} - k_{BA}x_B\frac{x_A}{x_A + K_{BA}} - k_{CA}x_C\frac{x_A}{x_A + K_{CA}} \\ \dot{x}_B &= k_{AB}x_A\frac{\tilde{x}_B}{\tilde{x}_B + K_{AB}} + k_{CB}x_C\frac{\tilde{x}_B}{\tilde{x}_B + K_{CB}} - k_{F_B}Bx_{F_B}\frac{x_B}{x_B + K_{F_B}} \\ \dot{x}_C &= k_{AC}x_A\frac{\tilde{x}_C}{\tilde{x}_C + K_{AC}} - k_{BC}x_B\frac{x_C}{x_C + K_{BC}} - k_{CC}x_C\frac{x_C}{x_C + K_{CC}}\end{aligned}$$

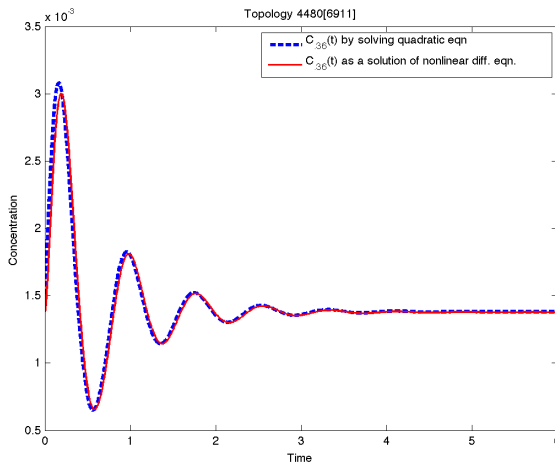
Parameters: $K_{uA} = 0.093918$; $k_{uA} = 11.447219$; $K_{BA} = 0.001688$; $k_{BA} = 44.802268$; $K_{CA} = 90.209027$; $k_{CA} = 96.671843$; $K_{AB} = 0.001191$; $k_{AB} = 1.466561$; $K_{F_B} = 9.424319$; $k_{F_B} = 22.745736$; $K_{Ac} = 0.113697$; $k_{AC} = 1.211993$; $K_{BC} = 0.009891$; $k_{BC} = 7.239357$; $K_{CB} = 30.602013$; $k_{CB} = 3.811536$; $K_{CC} = 0.189125$; $k_{CC} = 17.910182$



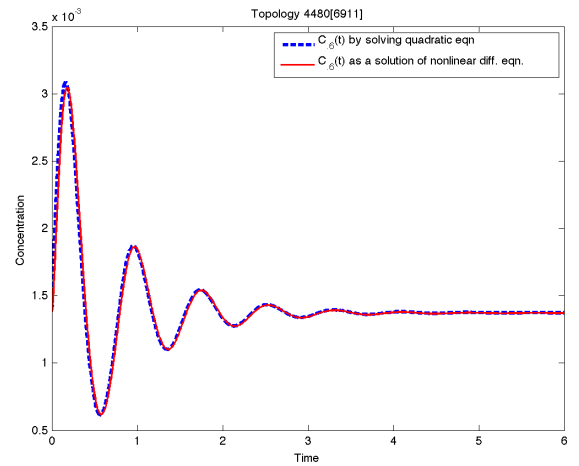
(a) Dynamics of A and B in linearized model



(b) Output from C nonlinear model



(c) Quadratic approx. and output of nonlinear system



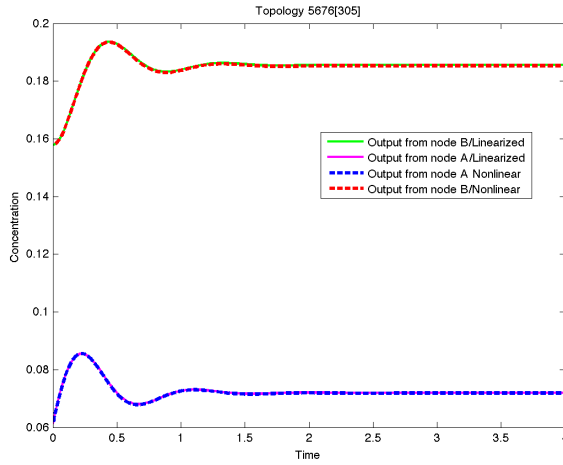
(d) Quadratic approx. and output of nonlinear system

Figure S10. Circuit 9.

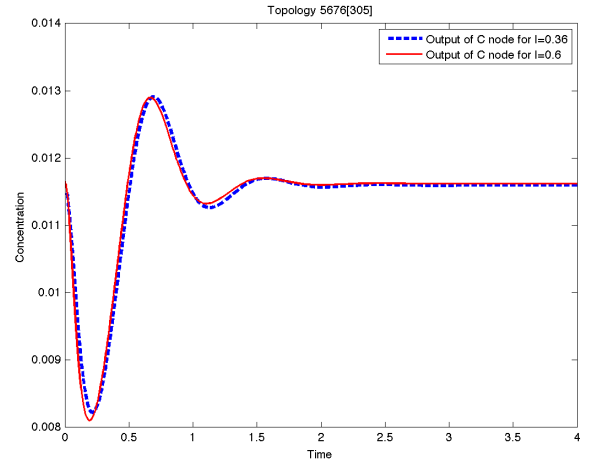
Circuit 10.

$$\begin{aligned}\dot{x}_A &= k_{uA}u\frac{\tilde{x}_A}{\tilde{x}_A + K_{uA}} - k_{BA}x_B\frac{x_A}{x_A + K_{BA}} - k_{AA}x_A\frac{x_A}{x_A + K_{AA}} \\ \dot{x}_B &= k_{AB}x_A\frac{\tilde{x}_B}{\tilde{x}_B + K_{AB}} + k_{CB}x_C\frac{\tilde{x}_B}{\tilde{x}_B + K_{CB}} - k_{F_B}Bx_{F_B}\frac{x_B}{x_B + K_{F_B}} \\ \dot{x}_C &= k_{BC}x_B\frac{\tilde{x}_C}{\tilde{x}_C + K_{BC}} - k_{AC}x_A\frac{x_C}{x_C + K_{AC}} - k_{CC}x_C\frac{x_C}{x_C + K_{CC}}\end{aligned}$$

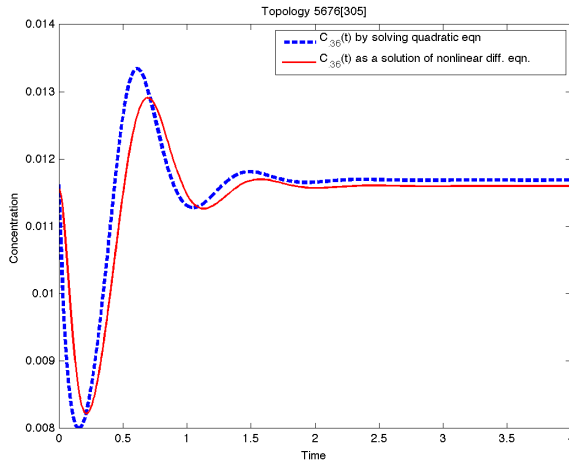
Parameters: $K_{AA} = 24.989065$; $k_{AA} = 53.174082$; $K_{AB} = 0.444375$; $k_{AB} = 12.053134$; $K_{F_B} = 1.716920$; $k_{F_B} = 11.601122$; $K_{AC} = 0.013988$; $k_{AC} = 8.521185$; $K_{BA} = 0.005461$; $k_{BA} = 7.103952$; $K_{BC} = 51.850148$; $k_{BC} = 80.408137$; $K_{CB} = 5.392001$; $k_{CB} = 3.086740$; $K_{CC} = 1.962230$; $k_{CC} = 17.382010$; $K_{uA} = 4.387832$; $k_{uA} = 19.638124$



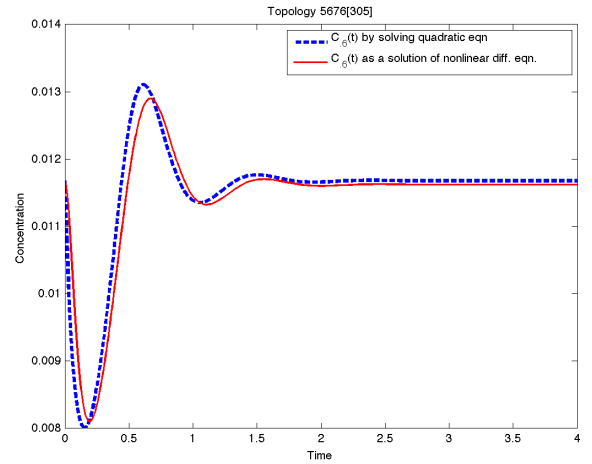
(a) Dynamics of A and B in linearized model



(b) Output from C nonlinear model



(c) Quadratic approx. and output of nonlinear system



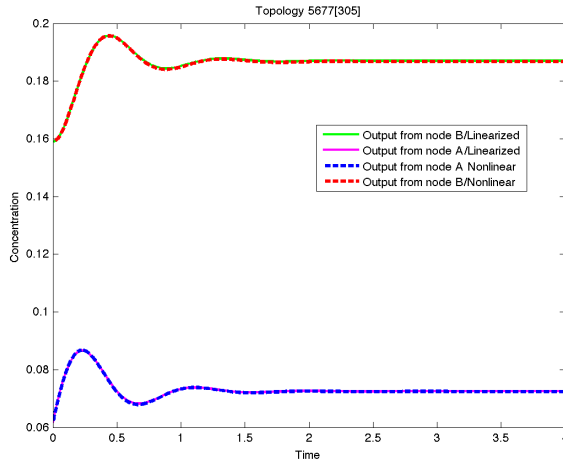
(d) Quadratic approx. and output of nonlinear system

Figure S11. Circuit 10.

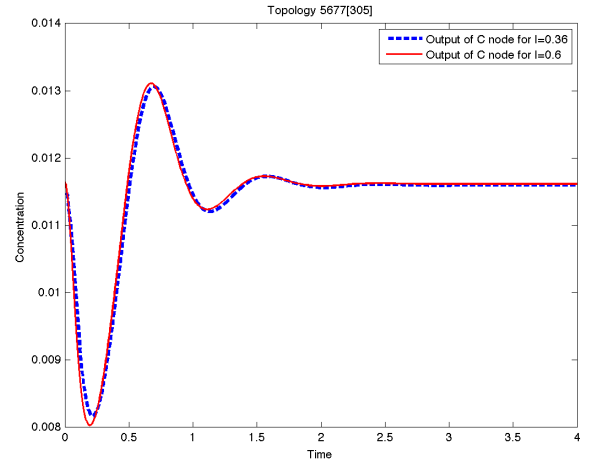
Circuit 11.

$$\begin{aligned}\dot{x}_A &= k_{uA}u\frac{\tilde{x}_A}{\tilde{x}_A + K_{uA}} - k_{BA}x_B\frac{x_A}{x_A + K_{BA}} \\ \dot{x}_B &= k_{AB}x_A\frac{\tilde{x}_B}{\tilde{x}_B + K_{AB}} + k_{CB}x_C\frac{\tilde{x}_B}{\tilde{x}_B + K_{CB}} - k_{F_B}Bx_{F_B}\frac{x_B}{x_B + K_{F_B}} \\ \dot{x}_C &= k_{BC}x_B\frac{\tilde{x}_C}{\tilde{x}_C + K_{BC}} - k_{AC}x_A\frac{x_C}{x_C + K_{AC}} - k_{CC}x_C\frac{x_C}{x_C + K_{CC}}\end{aligned}$$

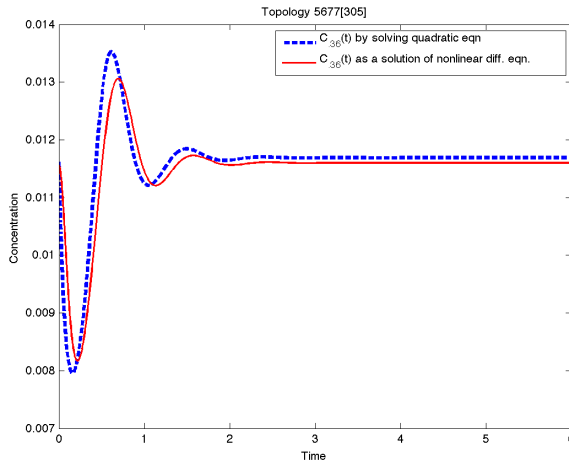
Parameters: $K_{AB} = 0.444375$; $k_{AB} = 12.053134$; $K_{F_B} = 1.716920$; $k_{F_B} = 11.601122$;
 $K_{AC} = 0.013988$; $k_{AC} = 8.521185$; $K_{BA} = 0.005461$; $k_{BA} = 7.103952$; $K_{BC} = 51.850148$;
 $k_{BC} = 80.408137$; $K_{CB} = 5.392001$; $k_{CB} = 3.086740$; $K_{CC} = 1.962230$; $k_{CC} = 17.382010$;
 $K_{uA} = 4.387832$; $k_{uA} = 19.638124$



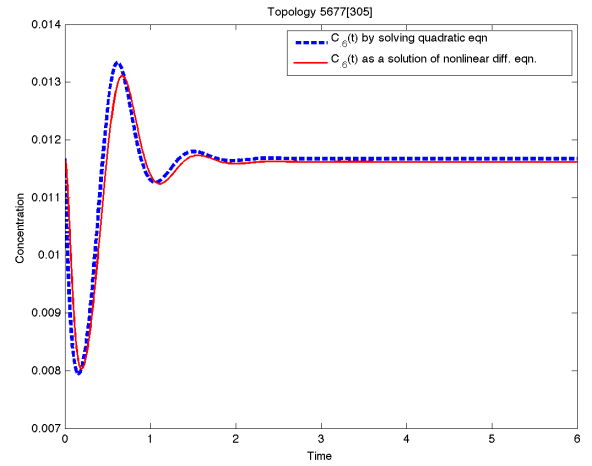
(a) Dynamics of A and B in linearized model



(b) Output from C nonlinear model



(c) Quadratic approx. and output of nonlinear system



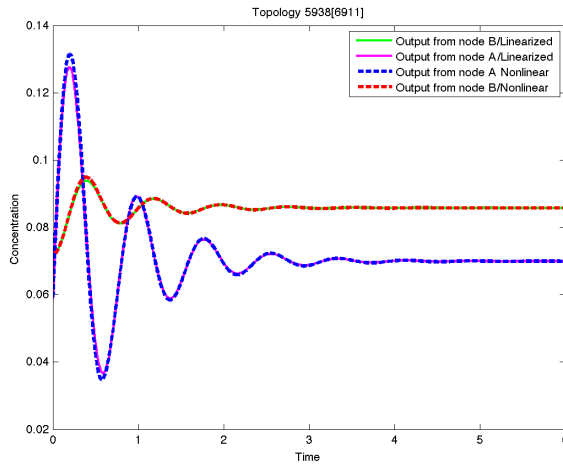
(d) Quadratic approx. and output of nonlinear system

Figure S12. Circuit 11.

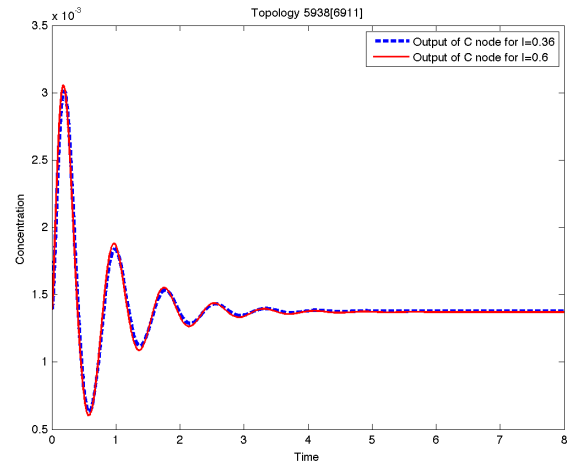
Circuit 12.

$$\begin{aligned}\dot{x}_A &= k_{uA}u\frac{\tilde{x}_A}{\tilde{x}_A + K_{uA}} - k_{BA}x_B\frac{x_A}{x_A + K_{BA}} + k_{CA}x_C\frac{\tilde{x}_A}{\tilde{x}_A + K_{CA}} \\ \dot{x}_B &= k_{AB}x_A\frac{\tilde{x}_B}{\tilde{x}_B + K_{AB}} + k_{CB}C\frac{\tilde{x}_B}{\tilde{x}_B + K_{CB}} - k_{F_B B}x_{F_B}\frac{x_B}{x_B + K_{F_B B}} \\ \dot{x}_C &= k_{AC}x_A\frac{\tilde{x}_C}{\tilde{x}_C + K_{AC}} - k_{BC}x_B\frac{x_C}{x_C + K_{BC}} - k_{CC}x_C\frac{x_C}{x_C + K_{CC}}\end{aligned}$$

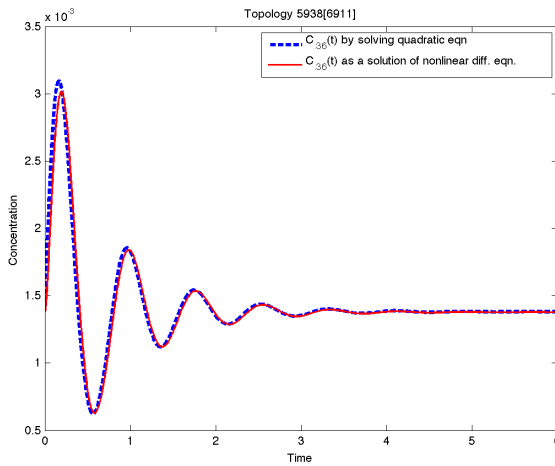
Parameters: $K_{uA} = 0.093918$; $k_{uA} = 11.447219$; $K_{BA} = 0.001688$; $k_{BA} = 44.802268$; $K_{CA} = 5.026318$; $k_{CA} = 45.803641$; $K_{AB} = 0.001191$; $k_{AB} = 1.466561$; $K_{F_B B} = 9.424319$; $k_{F_B B} = 22.745736$; $K_{AC} = 0.113697$; $k_{AC} = 1.211993$; $K_{BC} = 0.009891$; $k_{BC} = 7.239357$; $K_{CB} = 30.602013$; $k_{CB} = 3.811536$; $K_{CC} = 0.189125$; $k_{CC} = 17.910182$



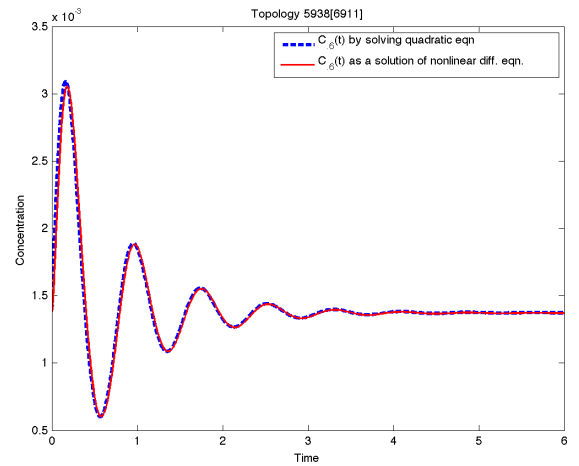
(a) Dynamics of A and B in linearized model



(b) Output from C nonlinear model



(c) Quadratic approx. and output of nonlinear system



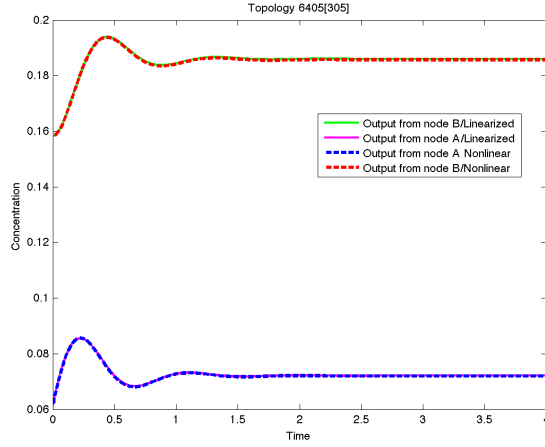
(d) Quadratic approx. and output of nonlinear system

Figure S13. Circuit 12.

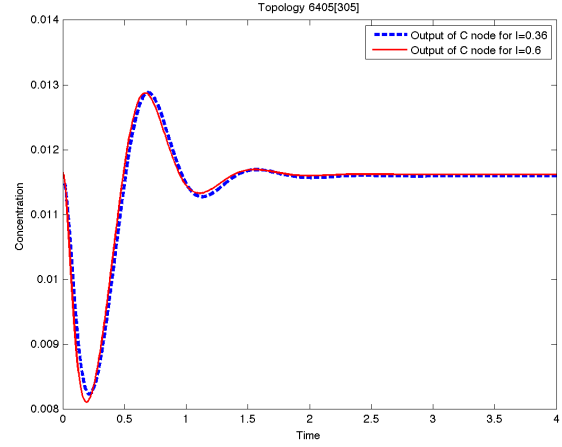
Circuit 13.

$$\begin{aligned}\dot{x}_A &= k_{uA}u\frac{\tilde{x}_A}{\tilde{x}_A + K_{uA}} - k_{BA}x_B\frac{x_A}{x_A + K_{BA}} - k_{AA}x_A\frac{x_A}{x_A + K_{AA}} + k_{CA}x_C\frac{\tilde{x}_A}{\tilde{x}_A + K_{CA}} \\ \dot{x}_B &= k_{AB}x_A\frac{\tilde{x}_B}{\tilde{x}_B + K_{AB}} + k_{CB}x_C\frac{\tilde{x}_B}{\tilde{x}_B + K_{CB}} - k_{BB}x_B\frac{x_B}{x_B + K_{BB}} \\ \dot{x}_C &= k_{BC}x_B\frac{\tilde{x}_C}{\tilde{x}_C + K_{BC}} - k_{AC}x_A\frac{x_C}{x_C + K_{AC}} - k_{CC}x_A\frac{x_C}{x_C + K_{CC}}\end{aligned}$$

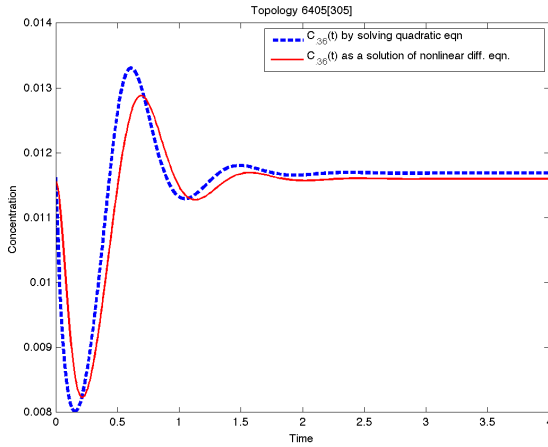
Parameters: $K_{AA} = 24.989065$; $k_{AA} = 53.174082$; $K_{AB} = 0.444375$; $k_{AB} = 12.053134$; $K_{FB} = 1.716920$; $k_{FB} = 11.601122$; $K_{AC} = 0.013988$; $k_{AC} = 8.521185$; $K_{BA} = 0.005461$; $k_{BA} = 7.103952$; $K_{BC} = 51.850148$; $k_{BC} = 80.408137$; $K_{CB} = 5.392001$; $k_{CB} = 3.086740$; $K_{CC} = 1.962230$; $k_{CC} = 17.382010$; $K_{uA} = 4.387832$; $k_{uA} = 19.638124$; $K_{CA} = 15.479253$; $k_{CA} = 4.903430$



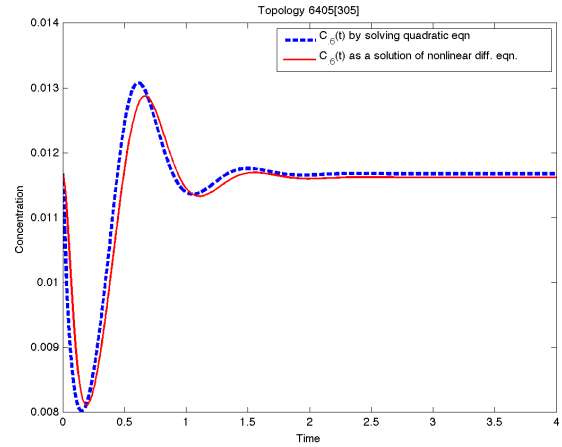
(a) Dynamics of A and B in linearized model



(b) Output from C nonlinear model



(c) Quadratic approx. and output of nonlinear system



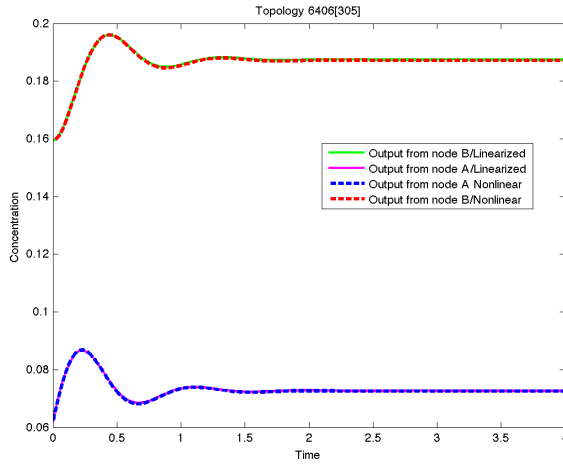
(d) Quadratic approx. and output of nonlinear system

Figure S14. Circuit 13.

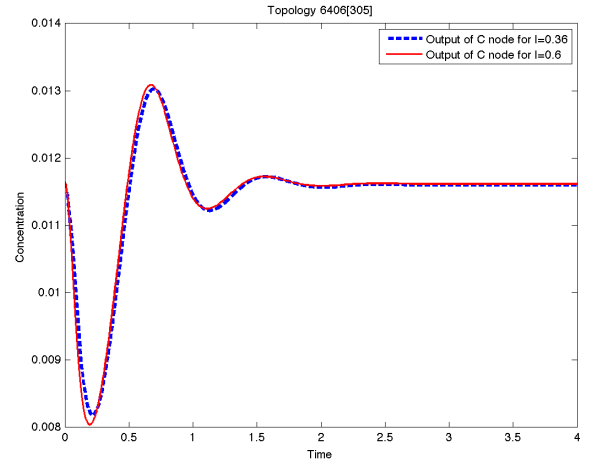
Circuit 14.

$$\begin{aligned}\dot{x}_A &= k_{uA}u\frac{\tilde{x}_A}{\tilde{x}_A + K_{uA}} - k_{BA}x_B\frac{x_A}{x_A + K_{BA}} + k_{CA}x_C\frac{\tilde{x}_A}{\tilde{x}_A + K_{CA}} \\ \dot{x}_B &= k_{AB}x_A\frac{\tilde{x}_B}{\tilde{x}_B + K_{AB}} + k_{CB}x_C\frac{\tilde{x}_B}{\tilde{x}_B + K_{CB}} - k_{BB}x_B\frac{x_B}{x_B + K_{BB}} \\ \dot{x}_C &= k_{BC}x_B\frac{\tilde{x}_C}{\tilde{x}_C + K_{BC}} - k_{AC}x_A\frac{x_C}{x_C + K_{AC}} - k_{CC}x_A\frac{x_C}{x_C + K_{CC}}\end{aligned}$$

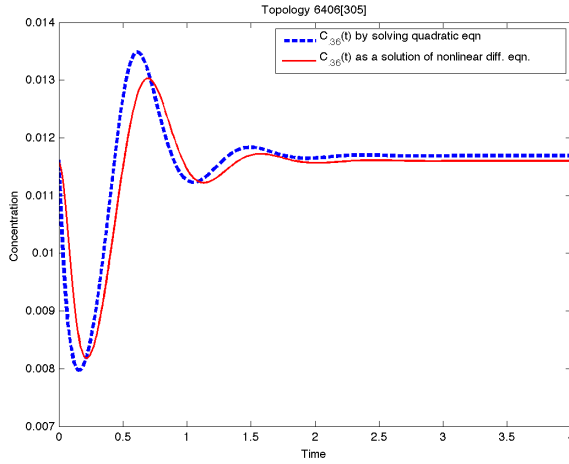
Parameters: $K_{AB} = 0.444375$; $k_{AB} = 12.053134$; $K_{FB} = 1.716920$; $k_{FB} = 11.601122$; $K_{AC} = 0.013988$; $k_{AC} = 8.521185$; $K_{BA} = 0.005461$; $k_{BA} = 7.103952$; $K_{BC} = 51.850148$; $k_{BC} = 80.408137$; $K_{CB} = 5.392001$; $k_{CB} = 3.086740$; $K_{CC} = 1.962230$; $k_{CC} = 17.382010$; $K_{uA} = 4.387832$; $k_{uA} = 19.638124$; $K_{CA} = 15.479253$; $k_{CA} = 4.903430$



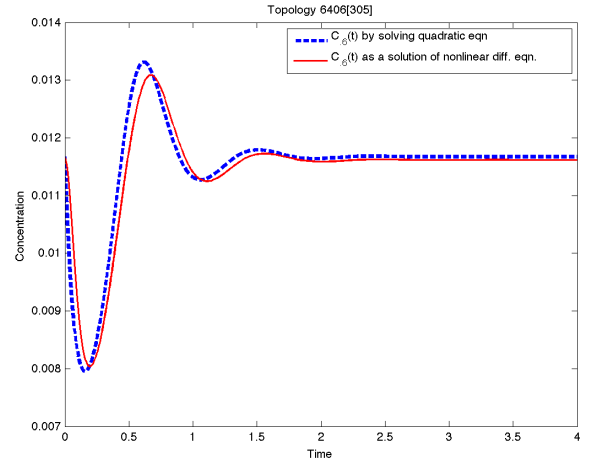
(a) Dynamics of A and B in linearized model



(b) Output from C nonlinear model



(c) Quadratic approx. and output of nonlinear system



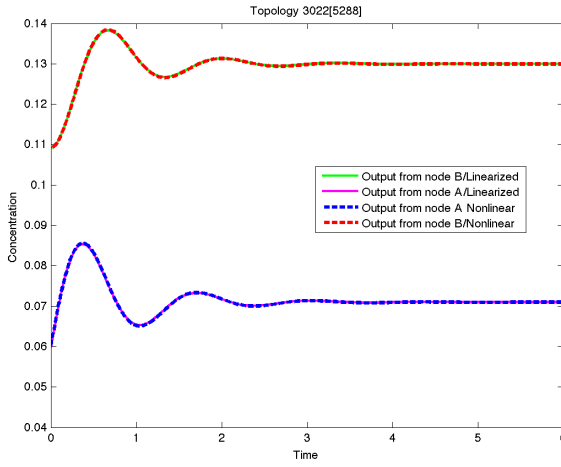
(d) Quadratic approx. and output of nonlinear system

Figure S15. Circuit 14.

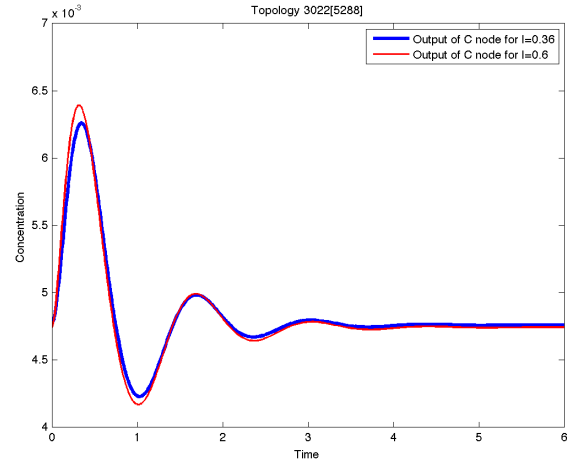
Circuit 15.

$$\begin{aligned}\dot{x}_A &= k_{uA}u\frac{\tilde{x}_A}{\tilde{x}_A + K_{uA}} - k_{BA}x_B\frac{x_A}{x_A + K_{BA}} \\ \dot{x}_B &= k_{AB}x_A\frac{\tilde{x}_B}{\tilde{x}_B + K_{AB}} - k_{FB}Bx_{FB}\frac{x_B}{x_B + K_{FB}} \\ \dot{x}_C &= k_{AC}x_A\frac{\tilde{x}_C}{\tilde{x}_C + K_{AC}} - k_{BC}x_B\frac{x_C}{x_C + K_{BC}} - k_{CC}x_A\frac{x_C}{x_C + K_{CC}}\end{aligned}$$

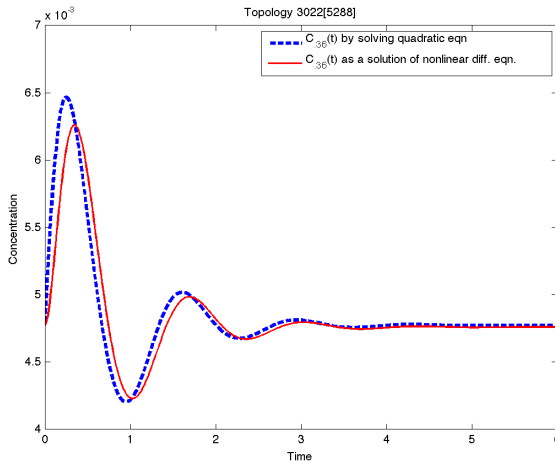
Parameters: $K_{AB} = 0.709169$; $k_{AB} = 7.445605$; $K_{FB} = 1.495375$; $k_{FB} = 7.282827$;
 $K_{AC} = 0.002566$; $k_{AC} = 1.115065$; $K_{BA} = 0.002522$; $k_{BA} = 5.753075$; $K_{BC} = 0.017051$;
 $k_{BC} = 2.777794$; $K_{CC} = 0.195997$; $k_{CC} = 1.480130$; $K_{uA} = 0.225814$; $k_{uA} = 2.492872$



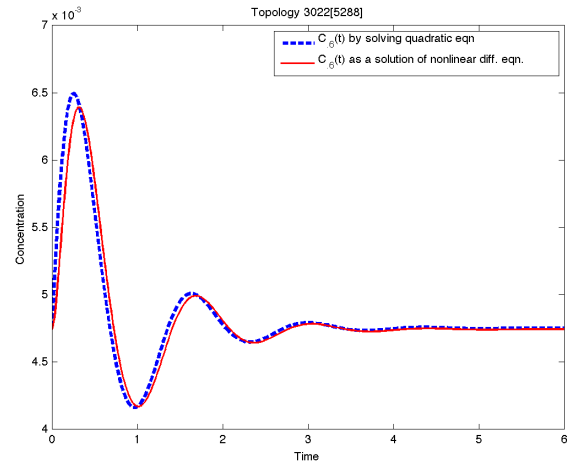
(a) Dynamics of A and B in linearized model



(b) Output from C nonlinear model



(c) Quadratic approx. and output of nonlinear system



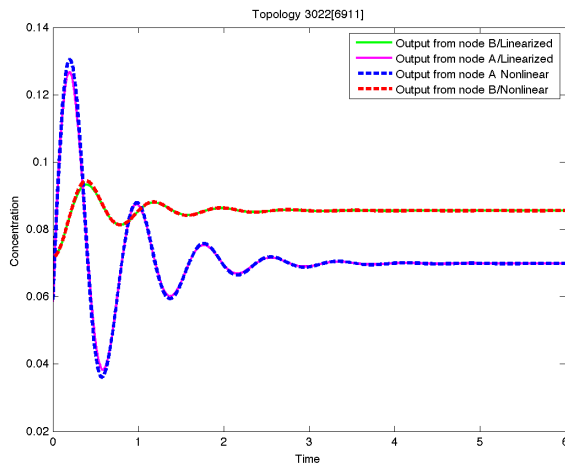
(d) Quadratic approx. and output of nonlinear system

Figure S16. Circuit 15.

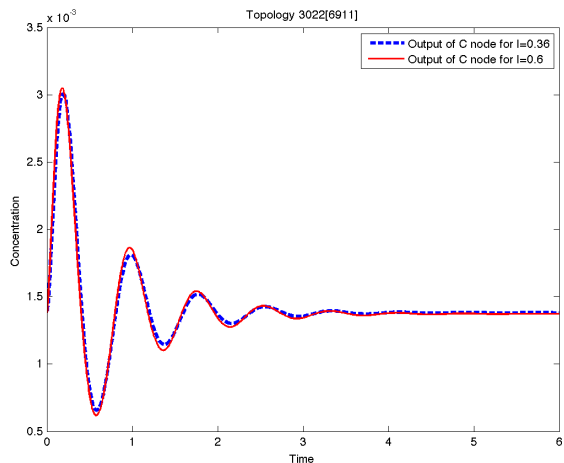
Circuit 16.

This is the same topology as in the previous case, only a different parameter set was used:

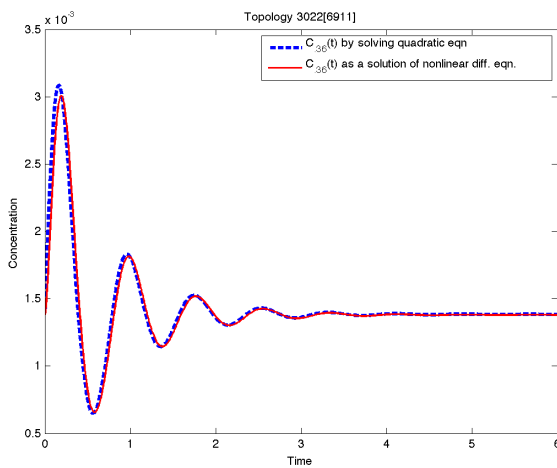
Parameters: $K_{AB} = 0.001191$; $k_{AB} = 1.466561$; $K_{FB} = 9.424319$; $k_{FB} = 22.745736$; $K_{AC} = 0.113697$; $k_{AC} = 1.211993$; $K_{BA} = 0.001688$; $k_{BA} = 44.802268$; $K_{BC} = 0.009891$; $k_{BC} = 7.239357$; $K_{CC} = 0.189125$; $k_{CC} = 17.910182$; $K_{uA} = 0.093918$; $k_{uA} = 11.447219$



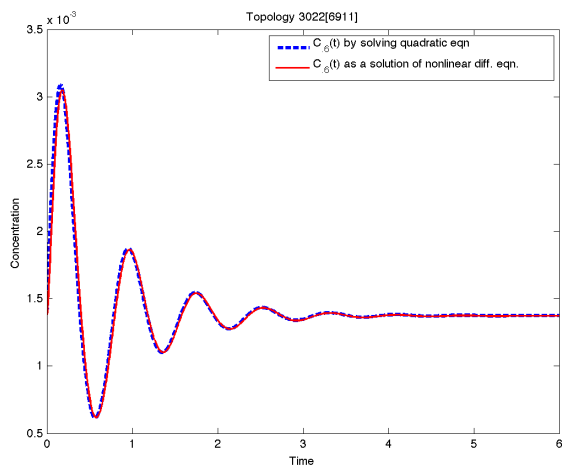
(a) Dynamics of A and B in linearized model



(b) Output from C nonlinear model



(c) Quadratic approx. and output of nonlinear system



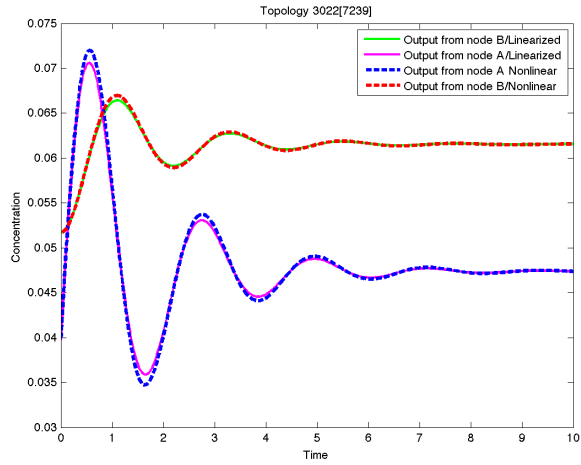
(d) Quadratic approx. and output of nonlinear system

Figure S17. Circuit 16.

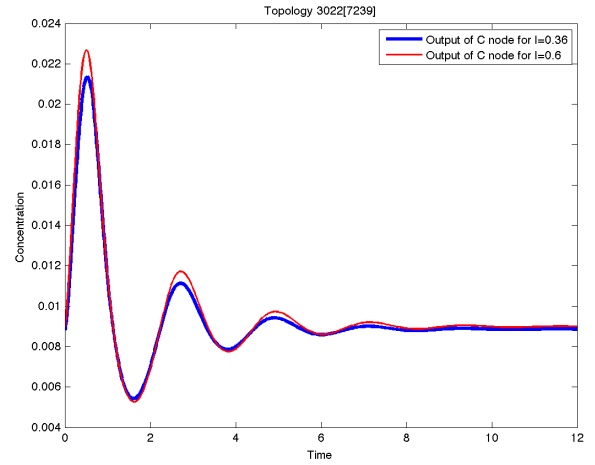
Circuit 17.

This is the same topology as in the previous case, only a different parameter set was used:

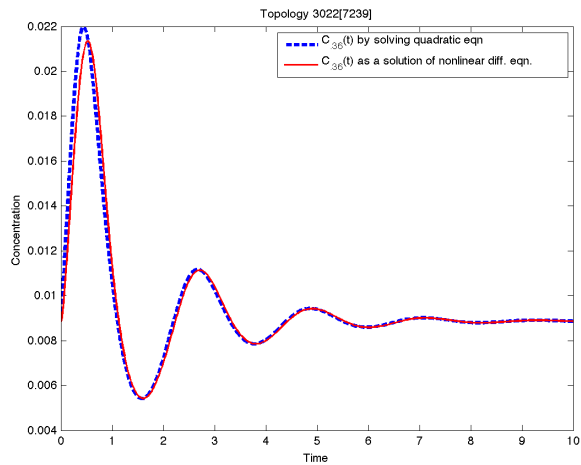
Parameters: $K_{AB} = 1.620877$; $k_{AB} = 2.306216$; $K_{FB} = 2.012565$; $k_{FB} = 2.700847$; $K_{AC} = 0.010933$; $k_{AC} = 8.968091$; $K_{BA} = 0.001812$; $k_{BA} = 10.039221$; $K_{BC} = 0.014199$; $k_{BC} = 17.762333$; $K_{CC} = 2.686891$; $k_{CC} = 4.139044$; $K_{uA} = 0.161715$; $k_{uA} = 1.933303$



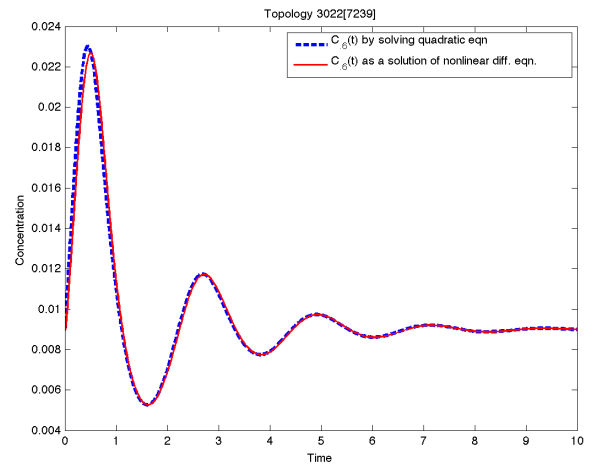
(a) Dynamics of A and B in linearized model



(b) Output from C nonlinear model



(c) Quadratic approx. and output of nonlinear system



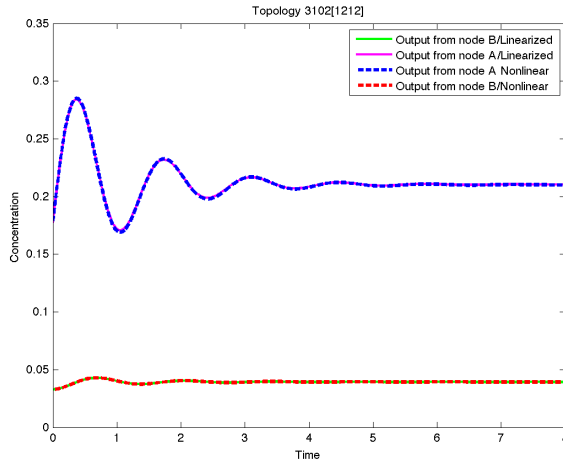
(d) Quadratic approx. and output of nonlinear system

Figure S18. Circuit 17.

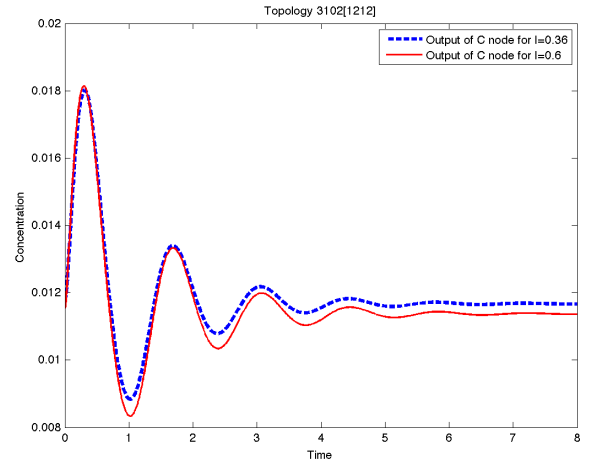
Circuit 18.

$$\begin{aligned}\dot{x}_A &= k_{uA}u\frac{\tilde{x}_A}{\tilde{x}_A + K_{uA}} - k_{BA}x_B\frac{x_A}{x_A + K_{BA}} - k_{AA}x_A\frac{x_A}{x_A + K_{AA}} \\ \dot{x}_B &= k_{AB}x_A\frac{\tilde{x}_B}{\tilde{x}_B + K_{AB}} + k_{BB}x_B\frac{\tilde{x}_B}{\tilde{x}_B + K_{BB}} - k_{F_B B}x_{F_B}\frac{x_B}{x_B + K_{F_B B}} \\ \dot{x}_C &= k_{AC}x_A\frac{\tilde{x}_C}{\tilde{x}_C + K_{AC}} - k_{BC}x_B\frac{x_C}{x_C + K_{BC}} - k_{CC}x_C\frac{x_C}{x_C + K_{CC}}\end{aligned}$$

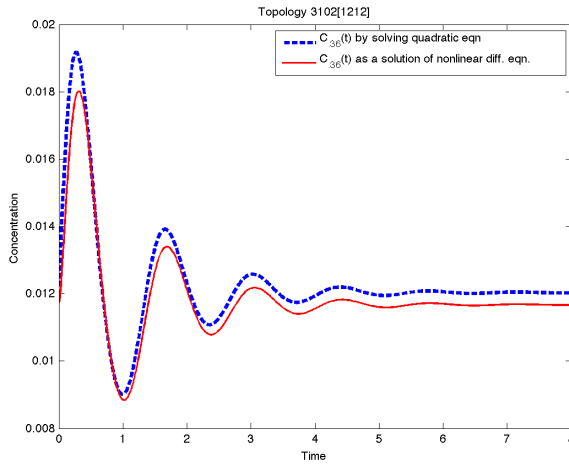
Parameters: $K_{AA} = 17.569120$; $k_{AA} = 2.198366$; $K_{AB} = 9.435176$; $k_{AB} = 3.134007$; $K_{F_B} = 0.469083$; $k_{F_B} = 1.934194$; $K_{AC} = 0.062914$; $k_{AC} = 2.742206$; $K_{BA} = 0.003245$; $k_{BA} = 75.352905$; $K_{BB} = 27.463128$; $k_{BB} = 10.551155$; $K_{BC} = 0.041615$; $k_{BC} = 61.333818$; $K_{CC} = 0.039332$; $k_{CC} = 4.756637$; $K_{uA} = 0.005167$; $k_{uA} = 8.186533$



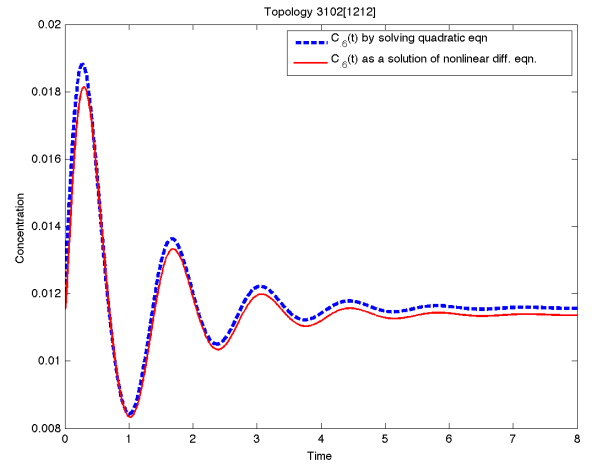
(a) Dynamics of A and B in linearized model



(b) Output from C nonlinear model



(c) Quadratic approx. and output of nonlinear system



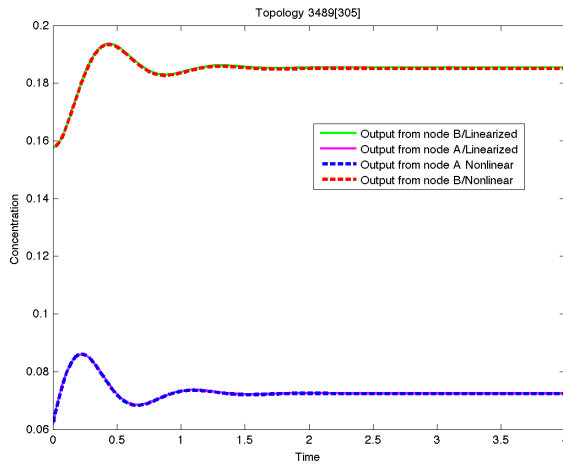
(d) Quadratic approx. and output of nonlinear system

Figure S19. Circuit 18.

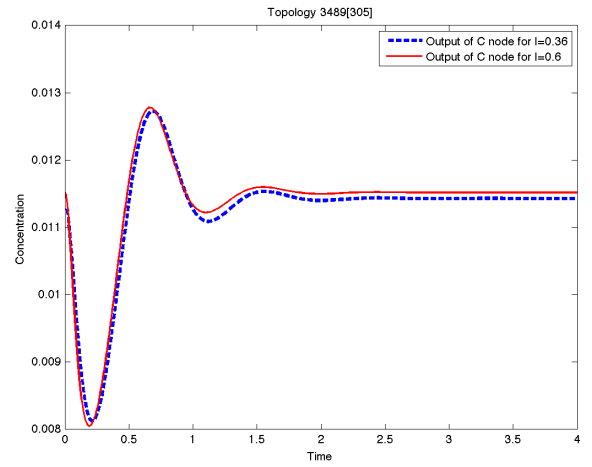
Circuit 19.

$$\begin{aligned}\dot{x}_A &= k_{uA}u\frac{\tilde{x}_A}{\tilde{x}_A + K_{uA}} - k_{BA}x_B\frac{x_A}{x_A + K_{BA}} - k_{AA}x_A\frac{x_A}{x_A + K_{AA}} \\ \dot{x}_B &= k_{AB}x_A\frac{\tilde{x}_B}{\tilde{x}_B + K_{AB}} - k_{F_B B}x_{F_B}\frac{x_B}{x_B + K_{F_B B}} \\ \dot{x}_C &= k_{BC}x_B\frac{\tilde{x}_C}{\tilde{x}_C + K_{BC}} - k_{AC}x_A\frac{x_C}{x_C + K_{AC}} - k_{CC}x_C\frac{x_C}{x_C + K_{CC}}\end{aligned}$$

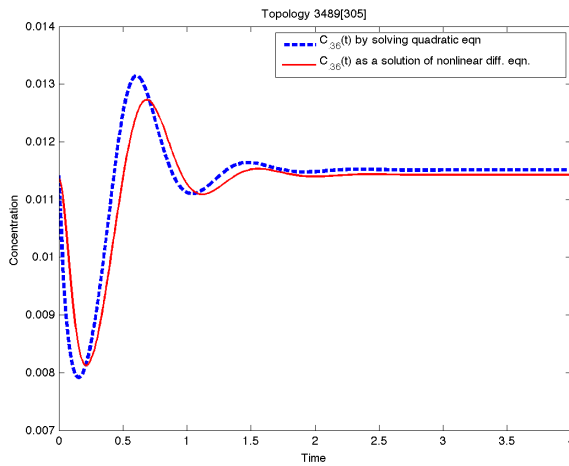
Parameters: $K_{uA} = 4.387832$; $k_{uA} = 19.638124$; $K_{BA} = 0.005461$; $k_{BA} = 7.103952$; $K_{AA} = 24.989065$; $k_{AA} = 53.174082$; $K_{AB} = 0.444375$; $k_{AB} = 12.053134$; $K_{F_B} = 1.716920$; $k_{F_B} = 11.601122$; $K_{BC} = 51.850148$; $k_{BC} = 80.408137$; $K_{AC} = 0.013988$; $k_{AC} = 8.521185$; $K_{CC} = 1.962230$; $k_{CC} = 17.382010$



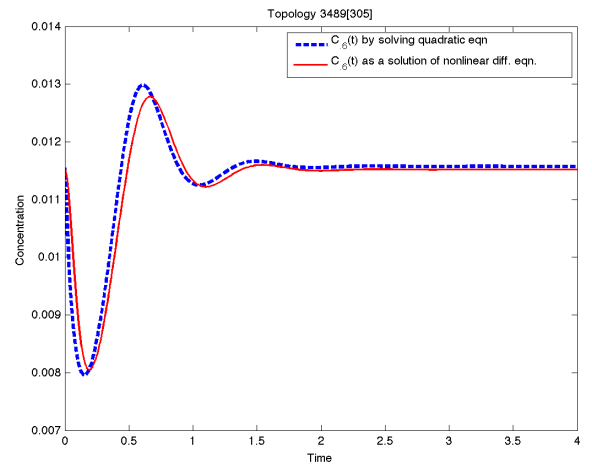
(a) Dynamics of A and B in linearized model



(b) Output from C nonlinear model



(c) Quadratic approx. and output of nonlinear system



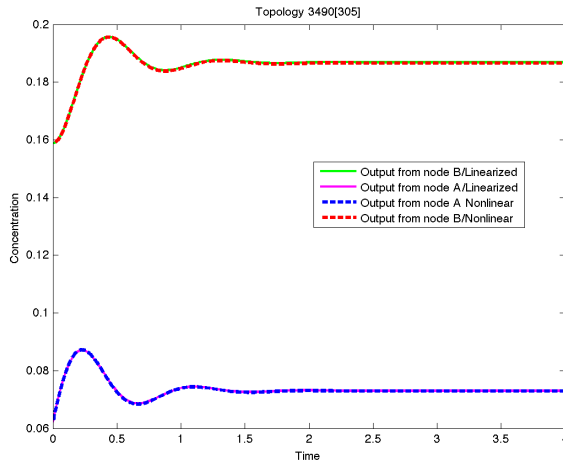
(d) Quadratic approx. and output of nonlinear system

Figure S20. Circuit 19.

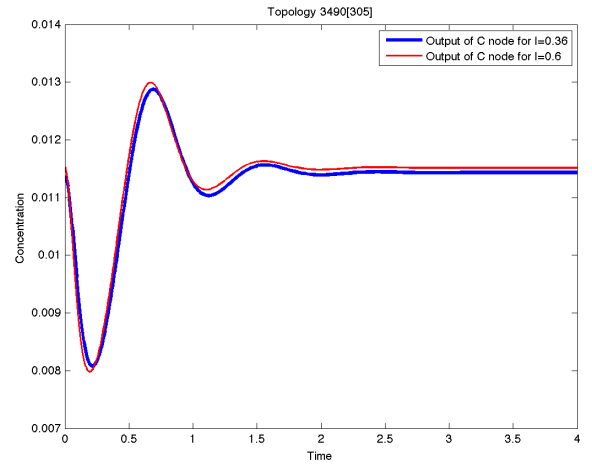
Circuit 20.

$$\begin{aligned}\dot{x}_A &= k_{uA}u\frac{\tilde{x}_A}{\tilde{x}_A + K_{uA}} - k_{BA}x_B\frac{x_A}{x_A + K_{BA}} \\ \dot{x}_B &= k_{AB}x_A\frac{\tilde{x}_B}{\tilde{x}_B + K_{AB}} - k_{FB}Bx_{FB}\frac{x_B}{x_B + K_{FB}} \\ \dot{x}_C &= k_{BC}x_B\frac{\tilde{x}_C}{\tilde{x}_C + K_{BC}} - k_{AC}x_A\frac{x_C}{x_C + K_{AC}} - k_{CC}x_C\frac{x_C}{x_C + K_{CC}}\end{aligned}$$

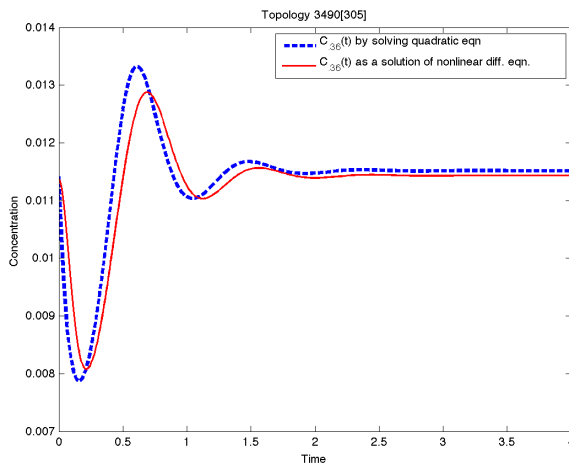
Parameters: $K_{uA} = 4.387832$; $k_{uA} = 19.638124$; $K_{BA} = 0.005461$; $k_{BA} = 7.103952$; $K_{AB} = 0.444375$; $k_{AB} = 12.053134$; $K_{FB} = 1.716920$; $k_{FB} = 11.601122$; $K_{BC} = 51.850148$; $k_{BC} = 80.408137$; $K_{AC} = 0.013988$; $k_{AC} = 8.521185$; $K_{CC} = 1.962230$; $k_{CC} = 17.382010$



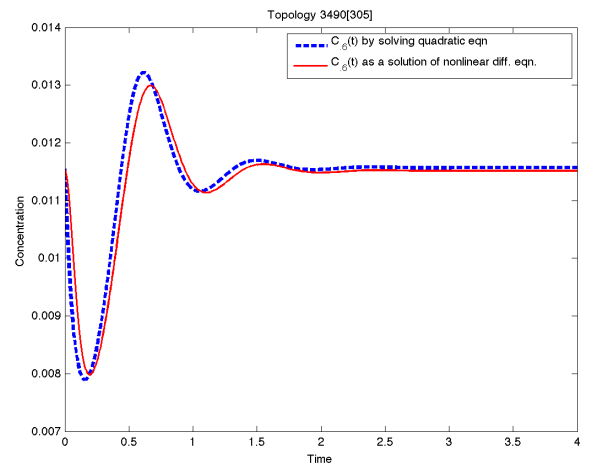
(a) Dynamics of A and B in linearized model



(b) Output from C nonlinear model



(c) Quadratic approx. and output of nonlinear system



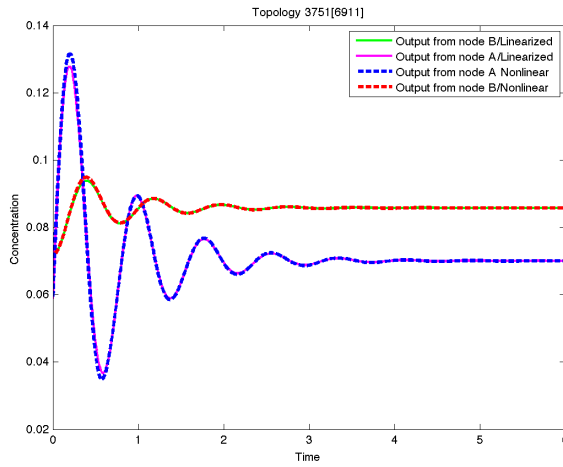
(d) Quadratic approx. and output of nonlinear system

Figure S21. Circuit 20.

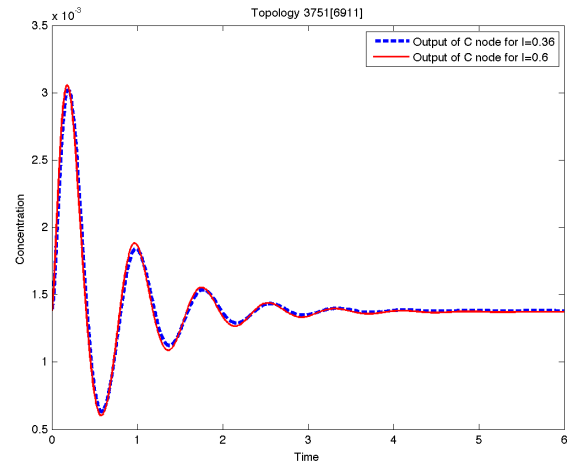
Circuit 21.

$$\begin{aligned}\dot{x}_A &= k_{uA}u\frac{\tilde{x}_A}{\tilde{x}_A + K_{uA}} - k_{BA}x_B\frac{x_A}{x_A + K_{BA}} + k_{CA}x_C\frac{\tilde{x}_A}{\tilde{x}_A + K_{CA}} \\ \dot{x}_B &= k_{AB}x_A\frac{\tilde{x}_B}{\tilde{x}_B + K_{AB}} - k_{FB}Bx_{FB}\frac{x_B}{x_B + K_{FB}} \\ \dot{x}_C &= k_{AC}x_A\frac{\tilde{x}_C}{\tilde{x}_C + K_{AC}} - k_{BC}x_B\frac{x_C}{x_C + K_{BC}} - k_{CC}x_C\frac{x_C}{x_C + K_{CC}}\end{aligned}$$

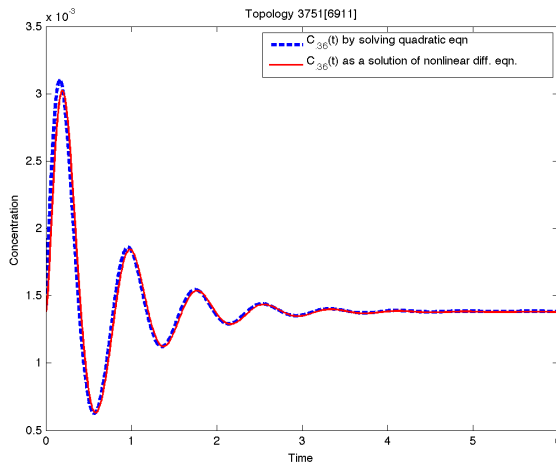
Parameters: $K_{uA} = 0.093918$; $k_{uA} = 11.447219$; $K_{BA} = 0.001688$; $k_{BA} = 44.802268$; $K_{CA} = 5.026318$; $k_{CA} = 45.803641$; $K_{AB} = 0.001191$; $k_{AB} = 1.466561$; $K_{FB} = 9.424319$; $k_{FB} = 22.745736$; $K_{AC} = 0.113697$; $k_{AC} = 1.211993$; $K_{BC} = 0.009891$; $k_{BC} = 7.239357$; $K_{CC} = 0.189125$; $k_{CC} = 17.910182$



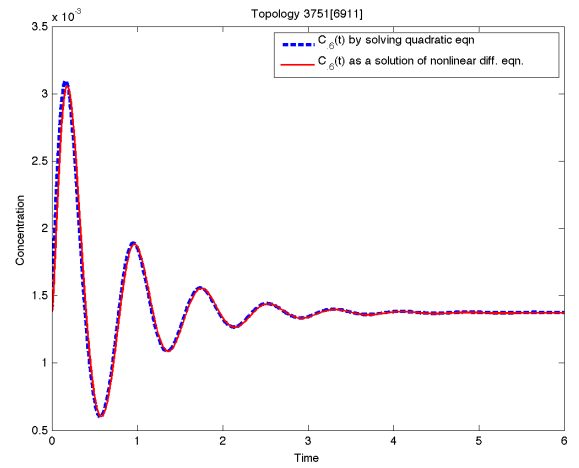
(a) Dynamics of A and B in linearized model



(b) Output from C nonlinear model



(c) Quadratic approx. and output of nonlinear system



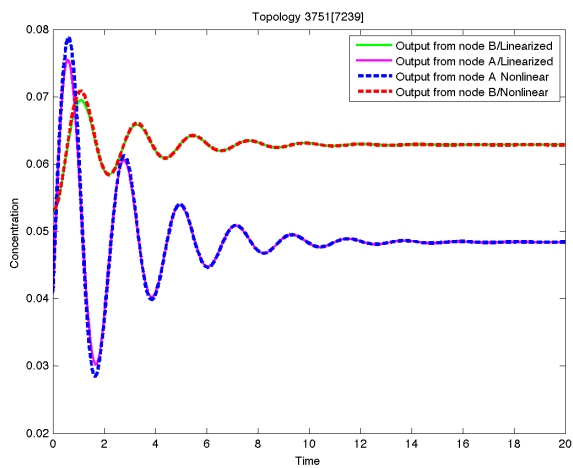
(d) Quadratic approx. and output of nonlinear system

Figure S22. Circuit 21.

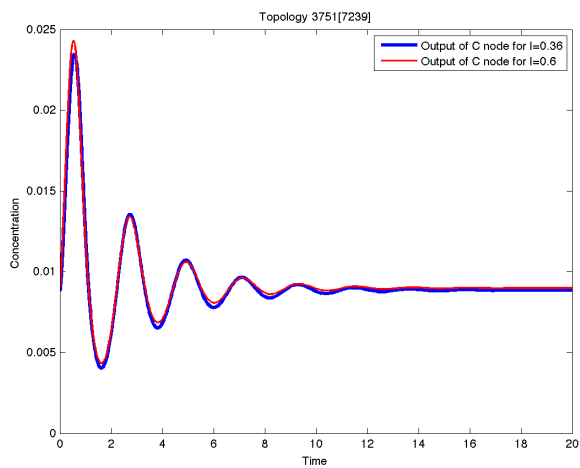
Circuit 22.

This is the same topology as in the previous case, only a different parameter set was used:

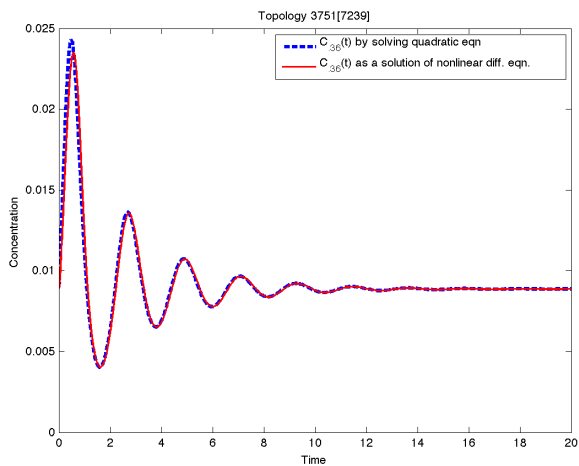
Parameters: $K_{AB} = 1.620877$; $k_{AB} = 2.306216$; $K_{FB} = 2.012565$; $k_{FB} = 2.700847$;
 $K_{AC} = 0.010933$; $k_{AC} = 8.968091$; $K_{BA} = 0.001812$; $k_{BA} = 10.039221$; $K_{BC} = 0.014199$;
 $k_{BC} = 17.762333$; $K_{CA} = 0.002690$; $k_{CA} = 1.506954$; $K_{CC} = 2.686891$; $k_{CC} = 4.139044$;
 $K_{uA} = 0.161715$; $k_{uA} = 1.933303$



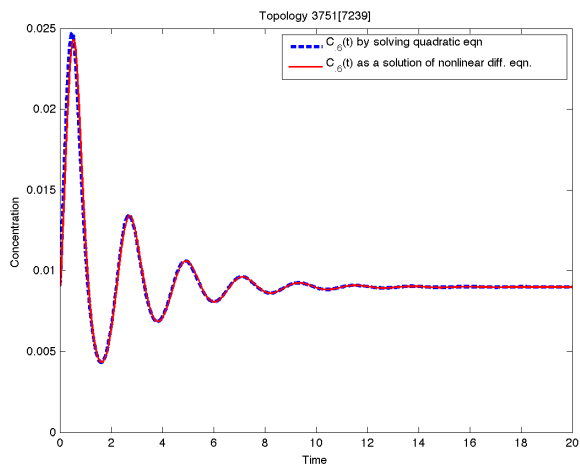
(a) Dynamics of A and B in linearized model



(b) Output from C nonlinear model



(c) Quadratic approx. and output of nonlinear system



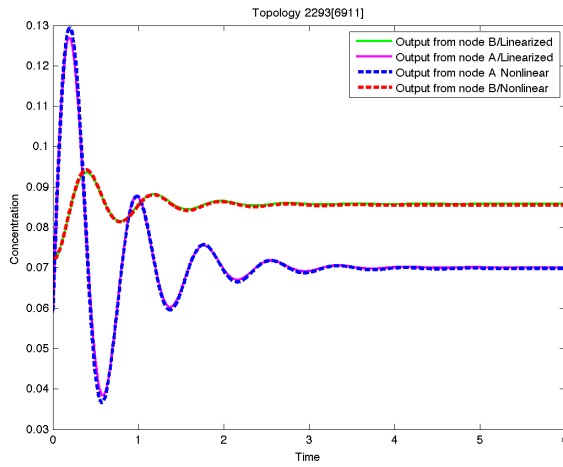
(d) Quadratic approx. and output of nonlinear system

Figure S23. Circuit 22.

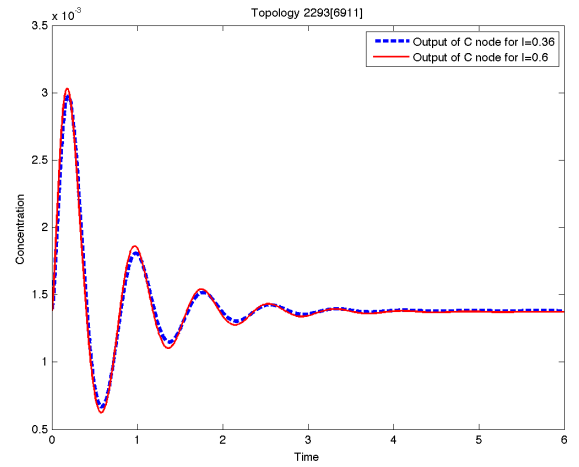
Circuit 23.

$$\begin{aligned}\dot{x}_A &= k_{uA}u\frac{\tilde{x}_A}{\tilde{x}_A + K_{uA}} - k_{BA}x_B\frac{x_A}{x_A + K_{BA}} - k_{CA}x_C\frac{x_A}{x_A + K_{CA}} \\ \dot{x}_B &= k_{AB}x_A\frac{\tilde{x}_B}{\tilde{x}_B + K_{AB}} - k_{FB}Bx_{FB}\frac{x_B}{x_B + K_{FB}} \\ \dot{x}_C &= k_{AC}x_A\frac{\tilde{x}_C}{\tilde{x}_C + K_{AC}} - k_{BC}x_B\frac{x_C}{x_C + K_{BC}} - k_{CC}x_C\frac{x_C}{x_C + K_{CC}}\end{aligned}$$

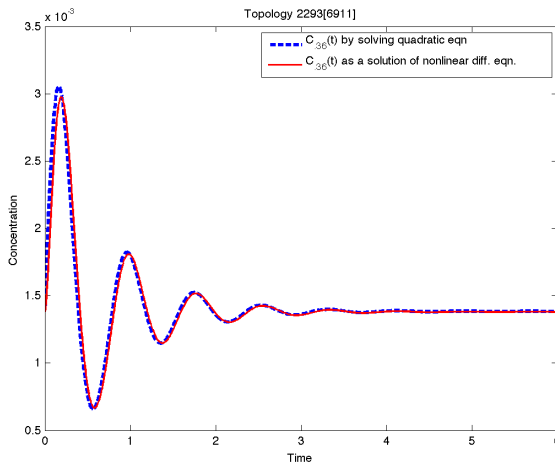
Parameters: $K_{uA} = 0.093918$; $k_{uA} = 11.447219$; $K_{BA} = 0.001688$; $k_{BA} = 44.802268$; $K_{CA} = 90.209027$; $k_{CA} = 96.671843$; $K_{AB} = 0.001191$; $k_{AB} = 1.466561$; $K_{FB} = 9.424319$; $k_{FB} = 22.745736$; $K_{AC} = 0.113697$; $k_{AC} = 1.211993$; $K_{BC} = 0.009891$; $k_{BC} = 7.239357$; $K_{CC} = 0.189125$; $k_{CC} = 17.910182$



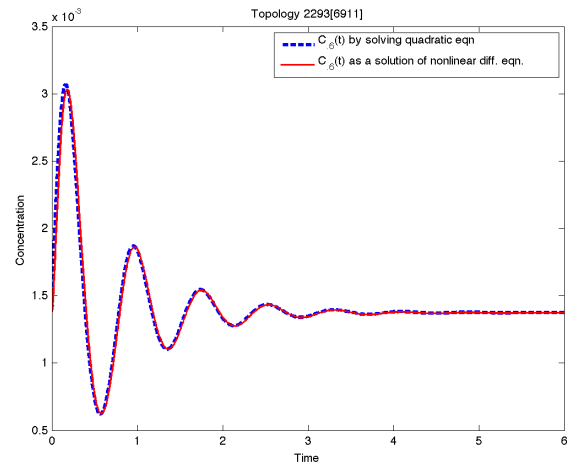
(a) Dynamics of A and B in linearized model



(b) Output from C nonlinear model



(c) Quadratic approx. and output of nonlinear system



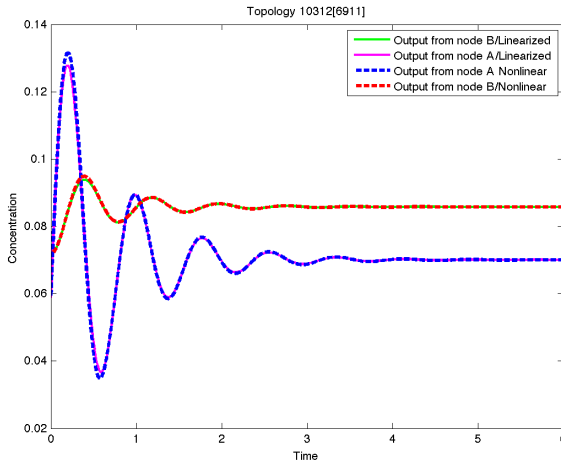
(d) Quadratic approx. and output of nonlinear system

Figure S24. Circuit 23.

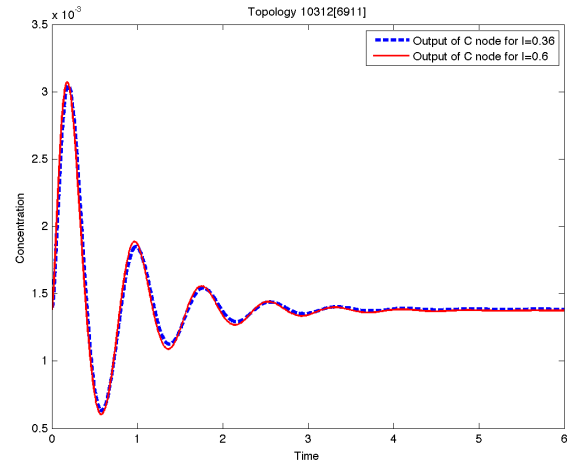
Circuit 24.

$$\begin{aligned}\dot{x}_A &= k_{uA}u\frac{\tilde{x}_A}{\tilde{x}_A + K_{uA}} - k_{BA}x_B\frac{x_A}{x_A + K_{BA}} + k_{CA}x_C\frac{\tilde{x}_A}{\tilde{x}_A + K_{CA}} \\ \dot{x}_B &= k_{AB}x_A\frac{\tilde{x}_B}{\tilde{x}_B + K_{AB}} - k_{F_B}x_{F_B}\frac{x_B}{x_B + K_{F_B}} \\ \dot{x}_C &= k_{AC}x_A\frac{\tilde{x}_C}{\tilde{x}_C + K_{AC}} - k_{BC}x_B\frac{x_C}{x_C + K_{BC}}\end{aligned}$$

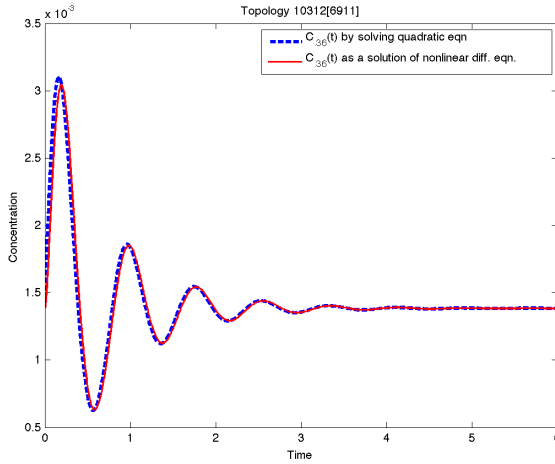
Parameters: $K_{uA} = 0.093918$; $k_{uA} = 11.447219$; $K_{BA} = 0.001688$; $k_{BA} = 44.802268$; $K_{CA} = 5.026318$; $k_{CA} = 45.803641$; $K_{AB} = 0.001191$; $k_{AB} = 1.466561$; $K_{F_B} = 9.424319$; $k_{F_B} = 22.745736$; $K_{AC} = 0.113697$; $k_{AC} = 1.211993$; $K_{BC} = 0.009891$; $k_{BC} = 7.239357$



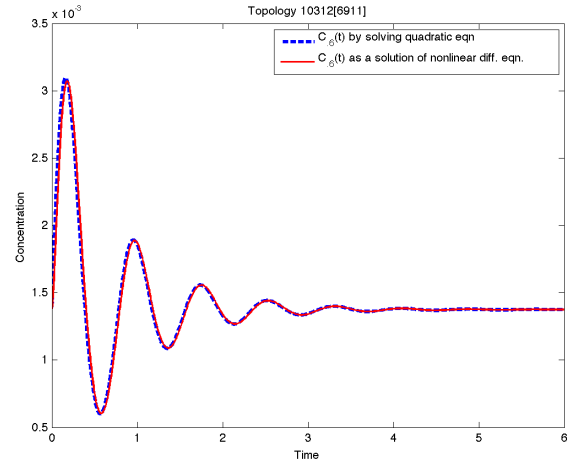
(a) Dynamics of A and B in linearized model



(b) Output from C nonlinear model



(c) Quadratic approx. and output of nonlinear system



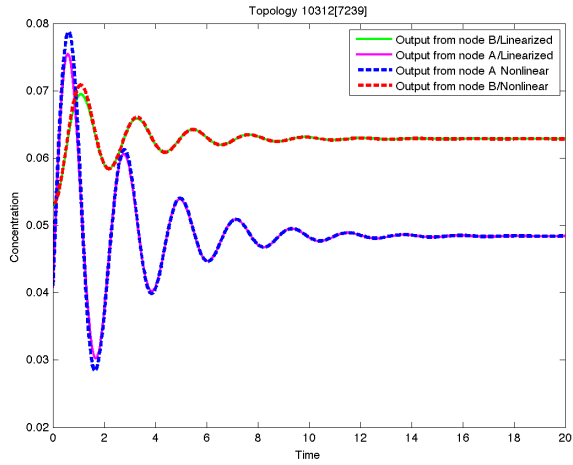
(d) Quadratic approx. and output of nonlinear system

Figure S25. Circuit 24.

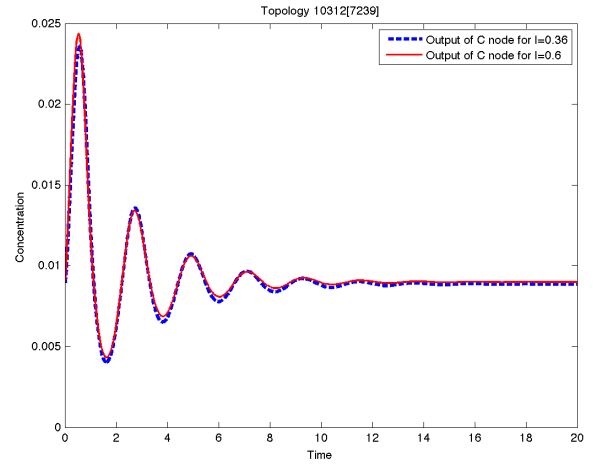
Circuit 25.

This is the same topology as in the previous case, only a different parameter set was used:

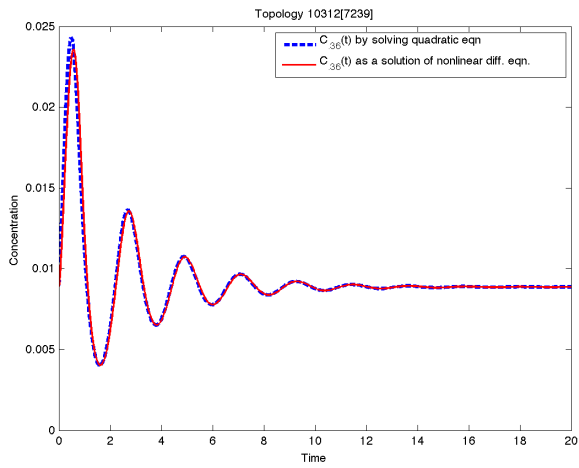
$$K_{AB} = 1.620877; k_{AB} = 2.306216; K_{FB} = 2.012565; k_{FB} = 2.700847; K_{AC} = 0.010933; k_{AC} = 8.968091; K_{BA} = 0.001812; k_{BA} = 10.039221; K_{BC} = 0.014199; k_{BC} = 17.762333; K_{CA} = 0.002690; k_{CA} = 1.506954; K_{uA} = 0.161715; k_{uA} = 1.93330$$



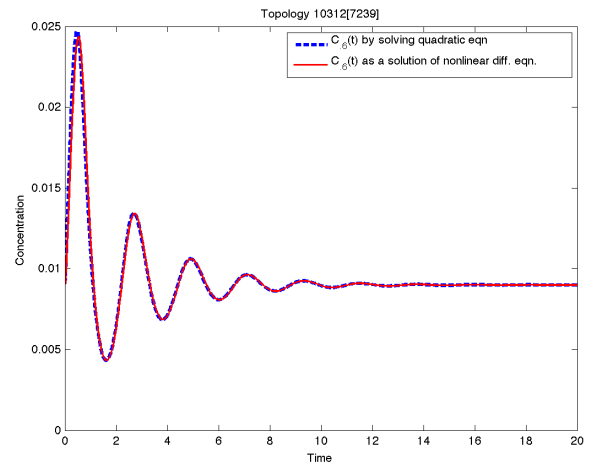
(a) Dynamics of A and B in linearized model



(b) Output from C nonlinear model



(c) Quadratic approx. and output of nonlinear system



(d) Quadratic approx. and output of nonlinear system

Figure S26. Circuit 25.

2 Ratios $x_A(t)/x_B(t)$

In this section, for each ASI circuit, we show that the ratio $x_A(t)/x_B(t)$ is approximately invariant when inputs are scaled, as discussed in the Main Text.

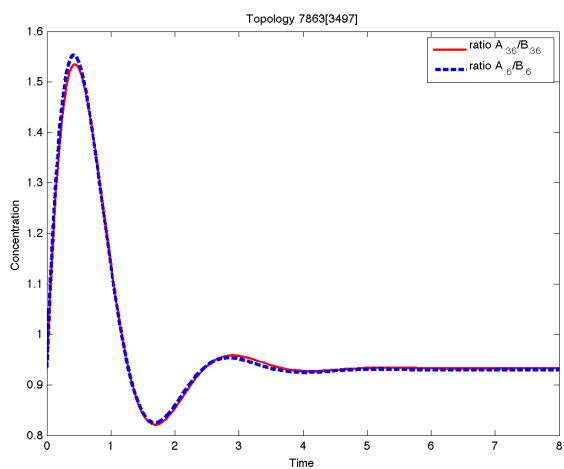
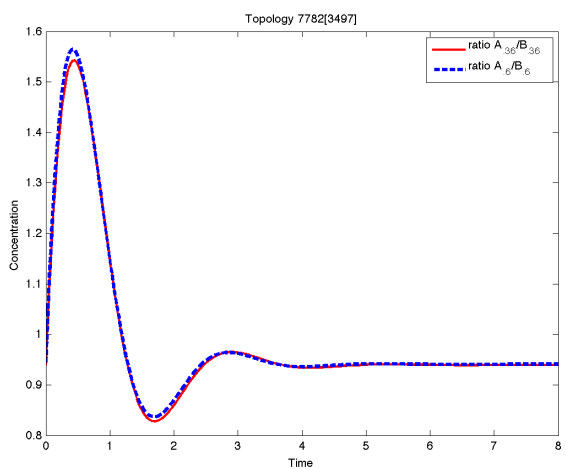
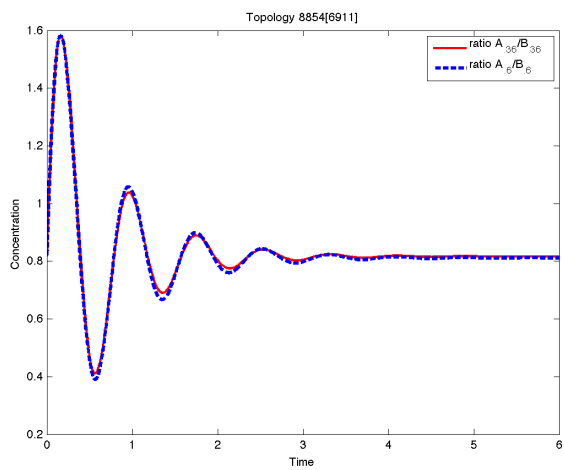
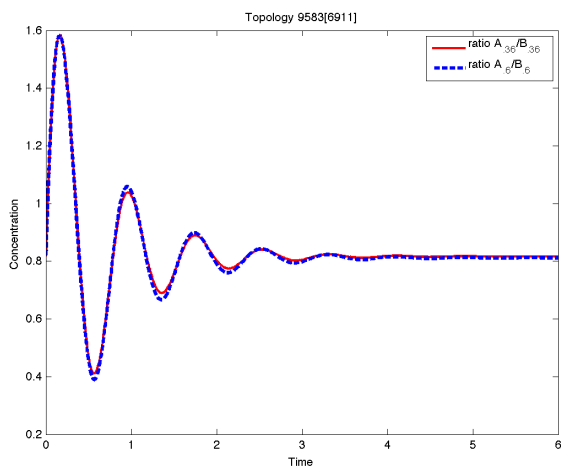


Figure S27. $x_A(t)/x_B(t)$ for Circuits 1-4

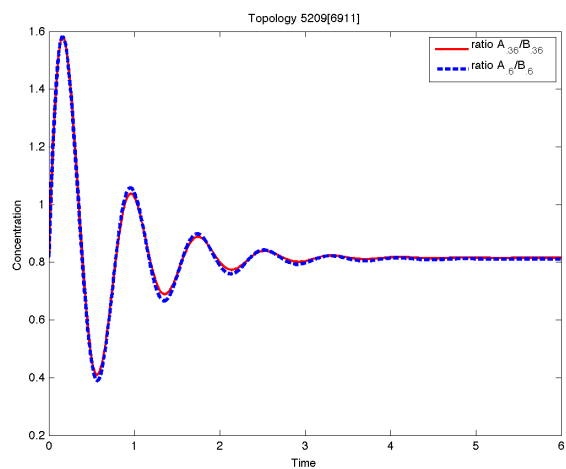
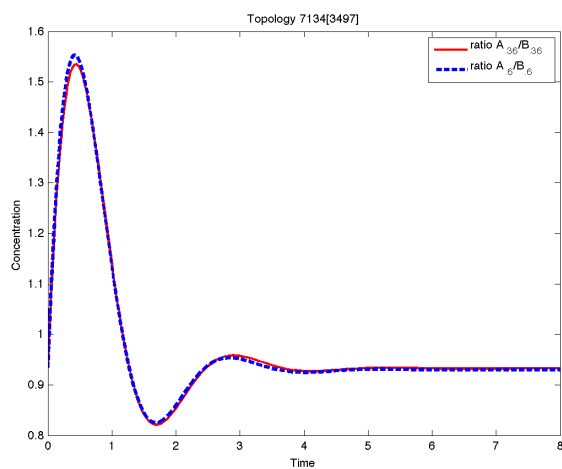
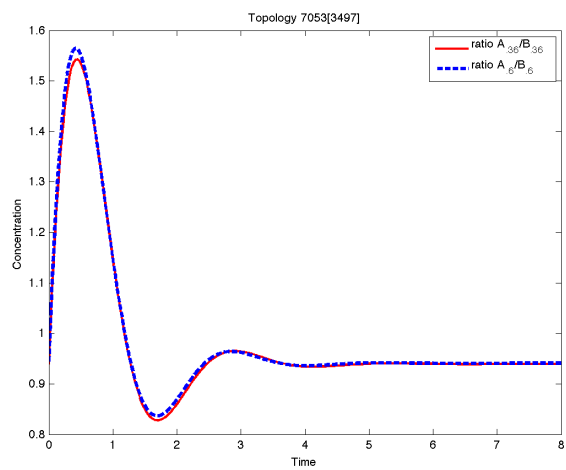
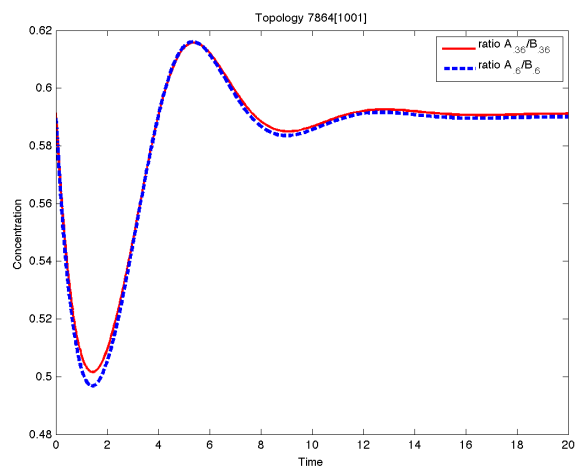


Figure S28. $x_A(t)/x_B(t)$ for Circuits 5-8

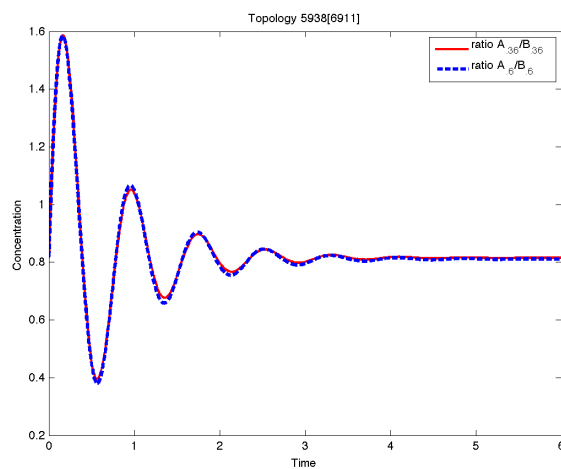
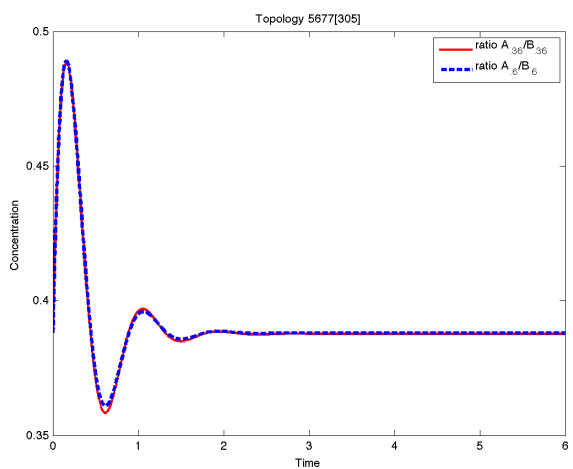
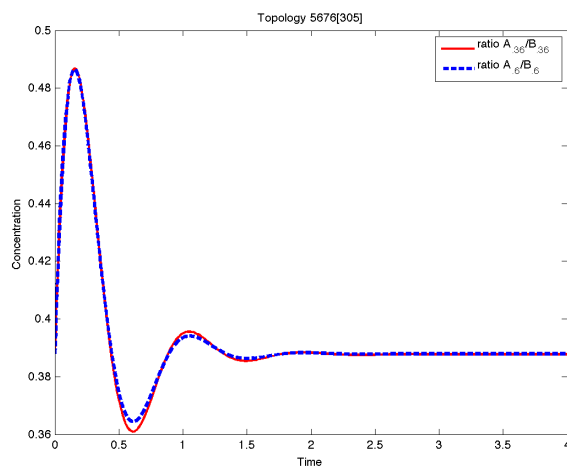
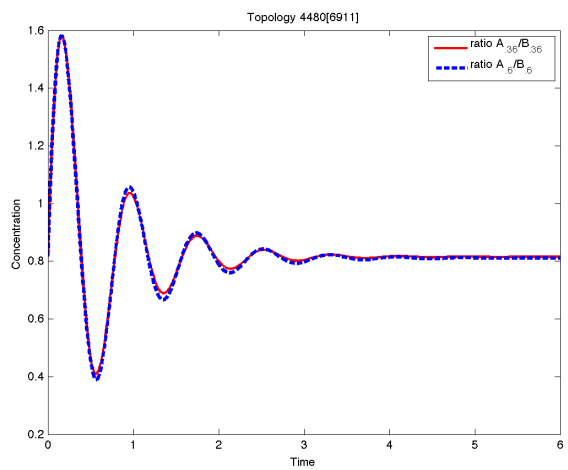


Figure S29. $x_A(t)/x_B(t)$ for Circuits 9-12

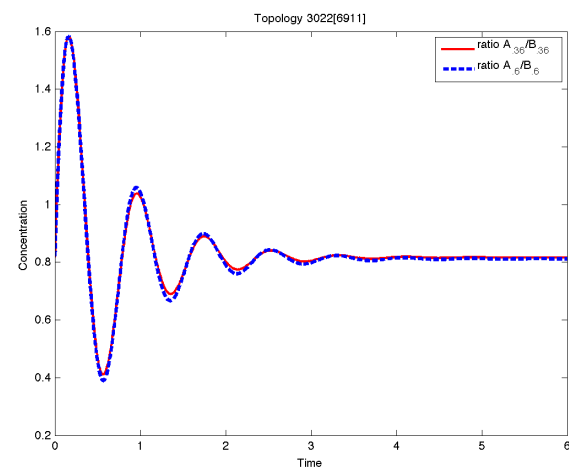
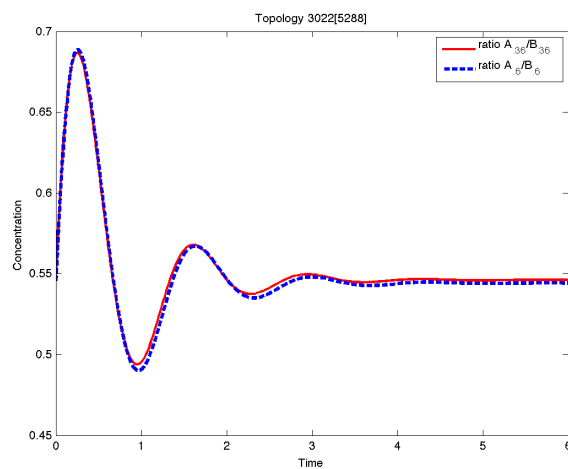
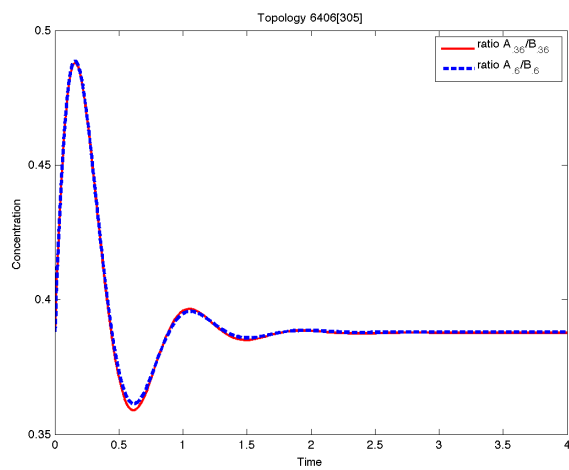
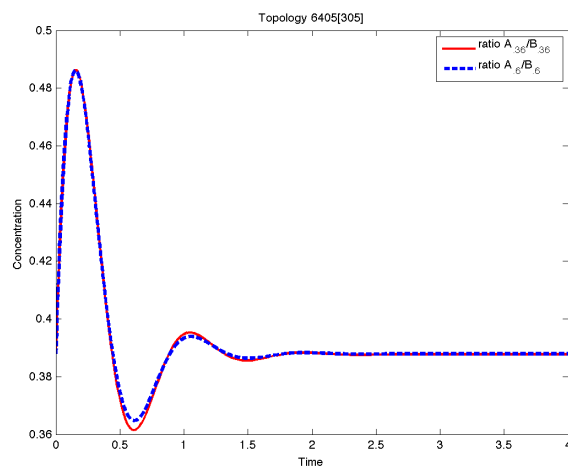


Figure S30. $x_A(t)/x_B(t)$ for Circuits 13-16

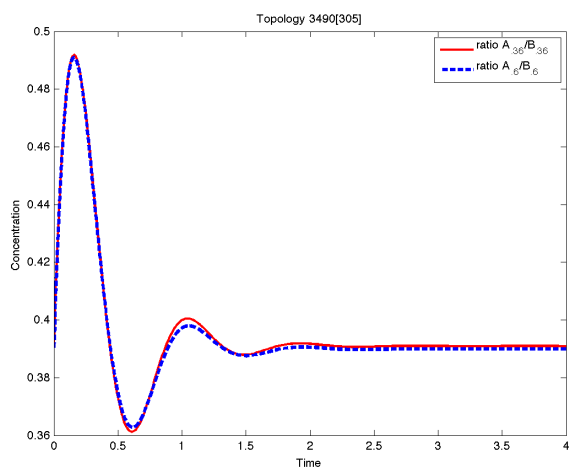
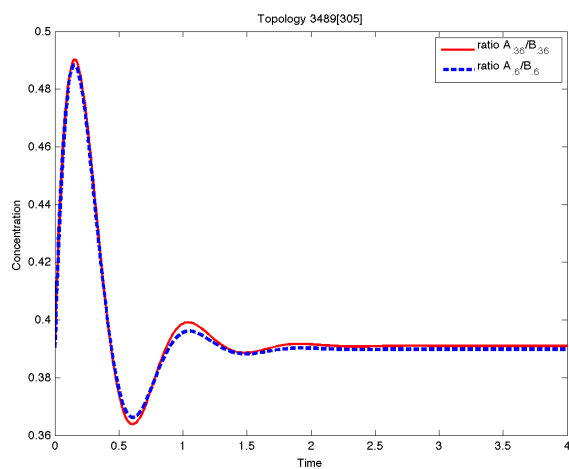
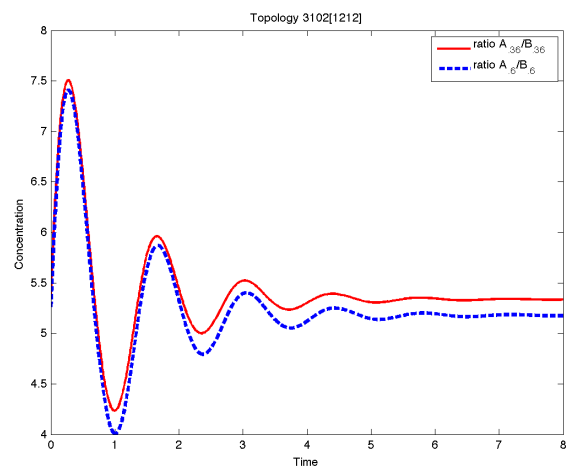
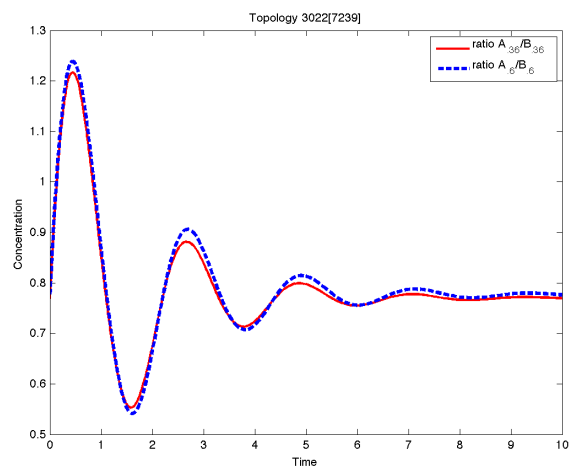


Figure S31. $x_A(t)/x_B(t)$ for Circuits 17-20

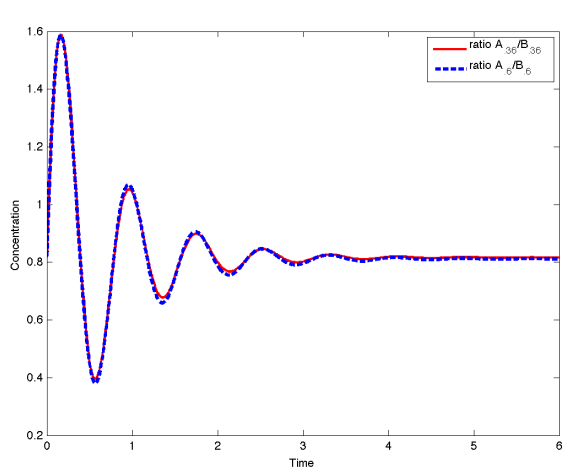
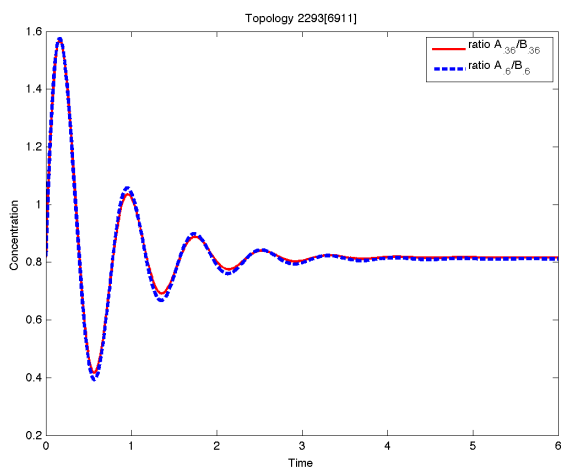
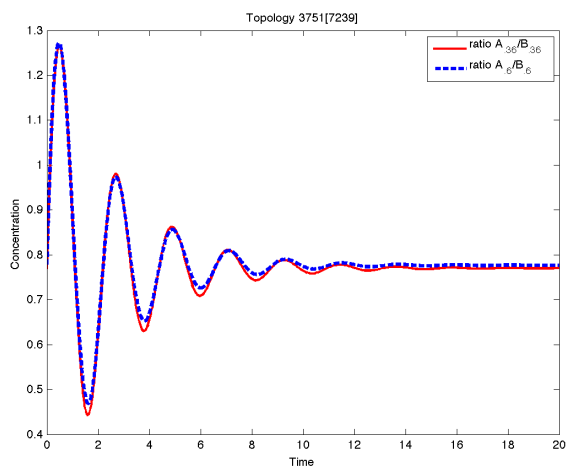
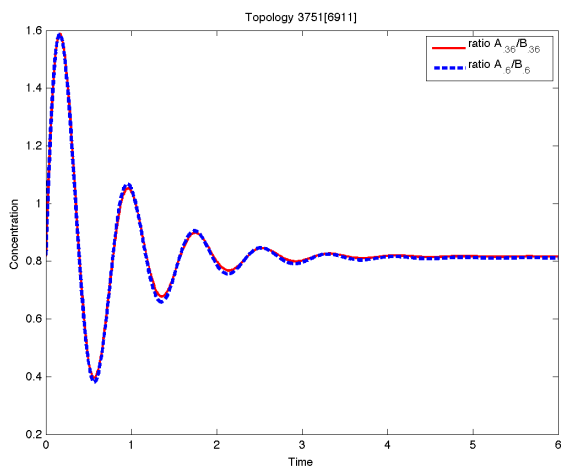


Figure S32. $x_A(t)/x_B(t)$ for Circuits 21-24

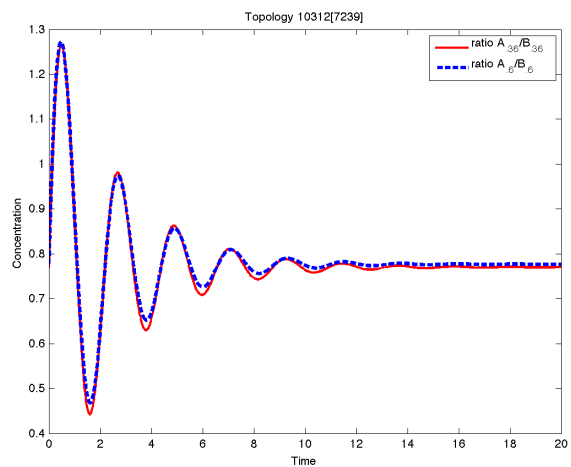


Figure S33. $x_A(t)/x_B(t)$ for Circuit 25.

3 Tables

In this section the following three tables for the 25 identified ASI circuits are shown:

- Table 1. Relative differences in linearization matrices corresponding to different linearizations, $\mathcal{A}_{0.3} = \mathcal{A}(0.3)$, $\mathcal{A}_{0.4} = \mathcal{A}(0.4)$, \dots , $\mathcal{B}_{0.6} = \mathcal{B}(0.6)$, rounded to 3 decimal places. The corresponding expressions are given by:

$$\mathcal{A}_{ij}^{\text{err}} = \sum_{u=0.3,0.4,0.5,0.6} \left| \frac{(\mathcal{A}_u)_{ij} - (\mathcal{A}_{0.45})_{ij}}{(\mathcal{A}_{0.45})_{ij}} \right|$$

and similarly for \mathcal{B}^{err} . These relative differences are very small. The entries in the table are of the following form: \mathcal{A}^{err} displayed as $[a_{11} \ a_{12}; a_{21} \ a_{22}]$ and \mathcal{B}^{err} displayed as $[b_1 \ b_2]^T$.

- Table 2. Relative error between original (nonlinear) system with an initial state $\xi = (x_A, x_B)$ corresponding to $u = 0.3$, and applied input $u = 0.36$, and the approximation is $\xi + z(t)$, where z solves the linear system with an initial condition of zero and a constant input of 0.06. Additionally, we provide relative errors between the original (nonlinear) system with an initial state corresponding to $u = 0.5$, and applied input of $u = 0.6$, and the approximation given by $\xi + z(t)$, where z solves the linear system with an initial condition of zero and a constant input of 0.1. The corresponding expressions are given by: $x_{Amax,u=0.36}^{\text{err}} = \max_{t \geq 0} \left| \frac{x_{A0.36}^L(t) - x_{A0.36}^N(t)}{x_{A0.36}^N(t)} \right|$,

$$x_{Amax,u=0.6}^{\text{err}} = \max_{t \geq 0} \left| \frac{x_{A0.6}^L(t) - x_{A0.6}^N(t)}{x_{A0.6}^N(t)} \right|,$$

where N denotes the nonlinear system, and L denotes the linear system.

We define similarly for $x_{Bmax,u=0.36}^{\text{err}}$ and $x_{Bmax,u=0.6}^{\text{err}}$.

- Table 3. Homogeneity property of the states x_A and x_B . For a constant input u , it holds that $\sigma(pu) \approx p\sigma(u)$, where $\sigma(u)$ is a unique steady state (x_A, x_B) .

Circuit	\mathcal{A}^{err}	\mathcal{B}^{err}
1	[0.069 0.004; 0 0.005]	[0.002 0] ^T
2	[0.084 0.006; 0.019 0.015]	[0.004 0] ^T
3	[0.069 0.004; 0 0.005]	[0.002 0] ^T
4	[0.114 0.007; 0.011 0.003]	[0.002 0] ^T
5	[0.045 0.003; 0.01 0.033]	[0 0] ^T
6	[0.075 0.012; 0.021 0.012]	[0.015 0] ^T
7	[0.057 0.012; 0.021 0.012]	[0.012 0] ^T
8	[0.055 0.012; 0.019 0.009]	[0.016 0] ^T
9	[0.069 0.004; 0 0.005]	[0.002 0] ^T
10	[0.037 0.022; 0.009 0.0707]	[0.002 0] ^T
11	[0.037 0.022; 0.007 0.009]	[0.002 0] ^T
12	[0.025 0.029; 0.007 0.006]	[0.012 0] ^T
13	[0.037 0.022; 0.009 0.007]	[0.002 0] ^T
14	[0.036 0.022; 0.007 0.009]	[0.002 0] ^T
15	[0.07 0.004; 0 0.005]	[0.002 0] ^T
16	[0.07 0.004; 0 0.005]	[0.002 0] ^T
17	[0.073 0.012; 0.017 0.009]	[0.015 0] ^T
18	[0.051 0.004; 0 0.005]	[0.002 0] ^T
19	[0.066 0.013; 0.018 0.009]	[0.015 0] ^T
20	[0.048 0.013; 0.018 0.009]	[0.016 0] ^T
21	[0.051 0.004; 0 0.005]	[0.002 0] ^T
22	[0.233 0; 0.011 0.003]	[0.002 0] ^T
23	[0.069 0.004; 0 0.005]	[0.002 0] ^T
24	[0.051 0.004; 0 0.005]	[0.002 0] ^T
25	[0.233 0; 0.011 0.003]	[0.002 0] ^T

Table S1. Relative error in linearization matrices

Circuit	$x_{A_{max},u=0.36}^{err}$	$x_{B_{max},u=0.36}^{err}$	$x_{A_{max},u=0.6}^{err}$	$x_{B_{max},u=0.6}^{err}$
1	0.055	0.011	0.028	0.005
2	0.008	0.007	0	0.002
3	0.055	0.010	0.028	0.005
4	0.03	0.007	0.012	0.004
5	0.031	0.006	0.003	0
6	0.015	0.016	0.011	0.005
7	0.023	0.021	0.005	0.004
8	0.023	0.021	0.004	0.004
9	0.055	0.01	0.028	0.005
10	0.097	0.020	0.081	0.016
11	0.010	0.020	0.084	0.016
12	0.033	0.021	0.024	0.010
13	0.097	0.020	0.081	0.016
14	0.010	0.02	0.084	0.016
15	0.056	0.010	0.028	0.005
16	0.056	0.010	0.028	0.005
17	0.027	0.022	0.004	0.004
18	0.047	0.010	0.028	0.006
19	0.027	0.023	0.005	0.004
20	0.023	0.021	0.005	0.004
21	0.04	0.009	0.034	0.004
22	0.116	0.027	0.05	0.013
23	0.055	0.010	0.028	0.005
24	0.045	0.01	0.027	0.005
25	0.117	0.03	0.05	0.013

Table S2. Relative error between nonlinear and linearized system

Circuit	$\sigma(u_{0.3})/0.3$	$\sigma(u_{0.4})/0.4$	$\sigma(u_{0.5})/0.5$	$\sigma(u_{0.6})/0.6$
1	(0.195, 0.239)	(0.193, 0.237)	(0.192, 0.236)	(0.19, 0.234)
2	(0.199, 0.364)	(0.197, 0.359)	(0.194, 0.356)	(0.192, 0.353)
3	(0.195, 0.239)	(0.193, 0.237)	(0.192, 0.236)	(0.191, 0.234)
4	(0.132, 0.172)	(0.131, 0.170)	(0.131, 0.169)	(0.13, 0.168)
5	(0.591, 0.11)	(0.58, 0.109)	(0.57, 0.109)	(0.561, 0.108)
6	(0.206, 0.526)	(0.198, 0.507)	(0.192, 0.493)	(0.188, 0.481)
7	(0.208, 0.529)	(0.2, 0.512)	(0.194, 0.498)	(0.19, 0.486)
8	(0.206, 0.530)	(0.199, 0.512)	(0.193, 0.499)	(0.189, 0.486)
9	(0.195, 0.239)	(0.194, 0.237)	(0.192, 0.236)	(0.190, 0.234)
10	(0.078, 0.083)	(0.075, 0.08)	(0.073, 0.078)	(0.071, 0.076)
11	(0.077, 0.083)	(0.074, 0.08)	(0.072, 0.078)	(0.071, 0.076)
12	(0.153, 0.09)	(0.145, 0.086)	(0.139, 0.082)	(0.135, 0.08)
13	(0.078, 0.083)	(0.075, 0.08)	(0.073, 0.078)	(0.071, 0.076)
14	(0.077, 0.083)	(0.074, 0.08)	(0.072, 0.078)	(0.071, 0.076)
15	(0.195, 0.239)	(0.193, 0.237)	(0.191, 0.235)	(0.190, 0.234)
16	(0.195, 0.239)	(0.193, 0.237)	(0.191, 0.236)	(0.19, 0.234)
17	(0.204, 0.526)	(0.197, 0.508)	(0.191, 0.494)	(0.186, 0.48)
18	(0.196, 0.24)	(0.193, 0.238)	(0.192, 0.236)	(0.19, 0.235)
19	(0.205, 0.528)	(0.197, 0.509)	(0.192, 0.494)	(0.187, 0.481)
20	(0.206, 0.532)	(0.199, 0.513)	(0.193, 0.5)	(0.189, 0.487)
21	(0.196, 0.24)	(0.194, 0.237)	(0.192, 0.236)	(0.191, 0.235)
22	(0.136, 0.177)	(0.134, 0.173)	(0.133, 0.171)	(0.132, 0.17)
23	(0.195, 0.239)	(0.193, 0.237)	(0.192, 0.236)	(0.191, 0.234)
24	(0.196, 0.240)	(0.194, 0.237)	(0.192, 0.236)	(0.190, 0.235)
25	(0.136, 0.178)	(0.134, 0.173)	(0.133, 0.171)	(0.132, 0.17)

Table S3. $\sigma(u)/u$ for constant inputs $u = 0.3, 0.4, 0.5, 0.6$